Assessing the persistence of emerging contaminants in wastewater treatment and surface waters

A Dissertation SUBMITTED TO THE FACULTY OF THE UNIVERSITY OF MINNESOTA BY

Priya Inge Hora

IN PARTIAL FULFILLMENT OF THE REQUIREMENTS FOR THE DEGREE OF DOCTOR OF PHILOSOPHY

William A. Arnold

June 2020

Acknowledgements

I would like to thank my advisor Dr. William Arnold for his support, encouragement, and patience throughout the PhD process. I learned incalculable lessons from Bill's incisive research guidance, thoughtful feedback on scientific writing and presentations, as well as from his dedication to the field and to advising.

I thank my committee, Dr. Lee Penn, Dr. Matt Simcik, and especially Dr. Paige Novak, for providing thorough and insightful comments, which improved the work presented in this dissertation. I am also grateful to Paige for her valuable input on research and advice on scientific practice.

I am indebted to many folks in the environmental program and the Arnold and Novak groups for their camaraderie, friendship, and help over the years. In particular, Sara BinAhmed-Menzies, Dr. Sarah Pati, Dr. Yiran Tong, Anndee Huff, Adel Soroush, Dr. Jill Kerrigan, Dr. Andrew McCabe, Dr. Hanna Temme, Dr. Ben Ma, Dr. Kuang Zhu, and Dr. Mehdi Karzar-Jeddi.

Thank you to my parents for their unwavering belief in me and to my Minnesota relatives for including me in numerous family gatherings filled with laughter and good food.

Last but certainly not least, to my adventurous band of friends: so long, and thanks for all the cake.

Dedication

To my parents.

Table of Contents

List of Tables

List of Figures

Chapter 1. Introduction

1.1 Objectives

Contaminants of emerging concern (CECs) are common household and industrial chemicals that have increasingly and frequently been detected in wastewater treatment plants and in wastewater effluent impacted water bodies. Pharmaceuticals, personal care products, and disinfectants are amongst the myriad potentially recalcitrant, unregulated organic contaminants that are detected in the environment and actively being studied to assess their fate and toxicity risk. The goals of this dissertation are to evaluate different attenuation mechanisms of select pharmaceutical compounds and cationic surfactants in: engineered systems (namely during ultraviolet light-based advanced oxidation processes) and natural systems (namely by sunlight photolysis and microbial transformation). The resulting information will allow for prediction of contaminant lifetimes in these various systems and identify relevant treatment and transformation phenomena.

1.2 Contaminants of emerging concern in the aquatic environment

In developed countries, municipal and industrial wastewater effluents are a major source of anthropogenic micropollutants or trace organic contaminants to the environment.[1] Many pharmaceuticals and personal care products are classified as trace contaminants or contaminants of emerging concern (CECs) because they are a group of compounds that can induce biological responses at minute concentrations and produce unintended ecological effects. Various studies have measured numerous compounds in the ng/L to μg/L range in freshwater, especially in densely populated areas.[1] The occurrence of CECs in treated wastewater and receiving water bodies signals that these

compounds are not effectively removed during the conventional treatment process and raises concerns about potential negative impacts to water resources and ecosystems.[2]

1.2.1 Pharmaceuticals

Certain pharmaceutical compounds are considered recalcitrant because removal during conventional wastewater treatment is limited and some like carbamazepine, an anticonvulsant, are known to not be susceptible to aerobic biodegradation.[3] Some of these compounds have also shown a degree of persistence in the environment with photolysis being identified over biodegradation and hydrolysis as an important loss mechanism in sunlight-exposed surface waters.[4] Additionally, research on removal of trace contaminants from synthetic wastewater and sludge supernatant via anaerobic treatment demonstrates varying degrees of contaminant loss in bench and pilot-scale experiments.[5–8] The relative risks of these compounds in the aquatic environment are an active area of research, but some of these compounds and/or their metabolites have been detected in fish and marine worms and linked to adverse effects in the organisms studied.[9–11] There is further concern that the presence of these compounds, in particular antibiotics, at sub-inhibitory concentrations can promote the spread of antibiotic resistance genes amongst bacteria.[12]

The human body metabolizes pharmaceuticals to differing extents after ingestion. The unaltered parent compound and metabolites are excreted and find their way into wastewater treatment plants. While the chemical properties of pharmaceuticals range widely, many contain polar functional moieties attached to a non-polar core and tend to be more polar than traditional contaminants.[13,14] They can also have acidic or basic functional groups.[13] Studies have shown that conventional wastewater and drinking water

treatment plants do not completely remove many pharmaceuticals.[2,15–20] Because pharmaceuticals as a class of compounds contain such variety in terms of chemical and physical properties, solubility, volatility, polarity, sorption ability, and biodegradability, removal efficiencies during treatment are uneven.[2,15,17,21] Thus, pharmaceuticals are ubiquitous in the aquatic environment, having been detected in surface and ground waters. Especially for endocrine-disrupting compounds, adverse ecological effects have been linked to pharmaceuticals at trace concentrations (i.e., <1 μg/L).[1,13] By and large, pharmaceuticals are unregulated environmental pollutants and as such there are very limited to nonexistent discharge requirements, and they vary by country.[21]

1.2.2 Quaternary ammonium compounds

Quaternary ammonium compounds (QACs or quats), also known as quaternary ammonium salts or quaternary amines or quaternary amine salts, are organic molecules that have been and are widely used in a variety of industrial and household consumer products for domestic, agricultural, industrial, and clinical applications since the late 1930s.[22–24] An extensive primary use and source of QACs are cationic surfactants in industrial and domestic applications.[25,26] QACs are commonly used chemicals in industrial and consumer applications as disinfectants, sanitizers, lytic biocides, fabric softeners, antistatics, phase transfer agents, food preservatives, herbicides, pesticides, corrosion inhibitors, clay stabilizers, and as active ingredients in pharmaceuticals, cosmetics, shampoos, and conditioners.[22,23,27–29]

The general structure of QACs is that they contain a central quaternary nitrogen atom that has a permanent positive charge independent of pH. This central nitrogen is covalently bonded to four carbon-containing "R"-substituents (R_4N^+).[27] The functional

groups tend to be at least one hydrophobic hydrocarbon chain and other alkyl groups that tend to be mostly short-chain substituents such as methyl or benzyl groups.[22,30] The general structure of QACs is shown in Figure 1-1[24] where R represents the carbon-containing functional groups (benzyl, methyl, or ester groups and at least one long-chained alkyl group) and X represents halide counter-ions (such as Cl^- and Br^-). QACs exhibit amphiphilic properties and are soluble in both polar and nonpolar liquids.[31,32] While highly water-soluble they will have a strong tendency to sorb to solids or surfaces based on electrostatic interactions and the presence of hydrophobic groups. The overall positive charge on QACs means that they have the tendency to readily sorb to predominately negatively charged surfaces. While soil, sediment, and sewage sludge have a distribution of surface charge, they tend to have a net negative charge and QAC sorption has been demonstrated by field studies.[23,28,33–36] The akyl chain groups of QACs also contribute to this strong tendency to sorb to hydrophobic compounds, indicating they are likely to be found associated with sediment and/or organic matter in water bodies.[23,28,31,37–41]

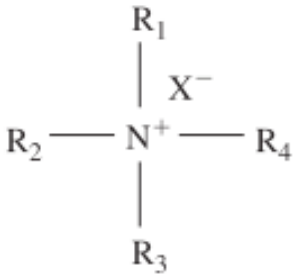

Figure 1-1. General chemical structure of a QAC

QACs exhibit greater hydrophobicity with increasing alkyl chain length.[25,42,43] Many biocides, including QACs, are short-lived or degradable through abiotic and biotic processes, but some may transform into more toxic or persistent compounds.[27]

There are three major classes of QACs: benzylalkyl dimethyl ammonium compounds (BACs), alkyltrimethyl ammonium compounds (ATMACs), and dialkyldimethyl ammonium compounds (DADMACs). Typically, DADMACs are divided into additional groups based on length of carbon chain. For those with shorter length carbon side chains with 8 to 10 carbon atoms, DADMACs are simply known as DADMACS. For longer carbon side chains with 12 or more carbon atoms, the compounds are known as ditallowdimethyl ammonium compounds (DTDMACs).[44] Incidentally, the three QAC classes most frequently detected in the environment are: DADMACs with alkyl chain lengths from C_8 to C_{18}, ATMACs with alkyl chain length from C_{12} to C_{18}, and BACs with alkyl chain lengths from C_{12} to C_{18}.[22] Compounds of the same class with different hydrocarbon chain length (and different number of carbons) are termed homologues of that particular class. BACs are one of the most commonly used QACs.

QACs are typically introduced into aquatic ecosystems through point source pollution and the discharge of effluent from wastewater treatment plants.[22,28,33,44–47] QACs are non-volatile thus atmospheric deposition is not an issue with transport of QACs.[44,48] QACs are ubiquitous pollutants detected in different environmental compartments including surface water and aquatic sediments and understanding the fate of QACs is important due to their high environmental concentration. Around 75% of QACs used annually are released into wastewater treatment systems and BAC is the most

frequently found QAC group worldwide in municipal wastewater.[43,46,49,50] The average concentration of QACs in domestic wastewater, treated effluent, sewage sludge and surface water has been reported to be around 0.5 mg/L, 0.05 mg/L, 5000 mg/kg dry weight, and 0.04 mg/L, respectively.[24,28,51] Additionally QACs are applied as herbicides in agricultural practices and can contaminate water bodies via runoff and soil erosion – in particular vineyard soils are some of the most prone, erodible agricultural soils.[37,47] QACs are classified as emerging pollutants because they are continuously released into the environment.[24,51] After application, QACs retain their biocidal properties, for they are not chemically transformed.[24]

Because QACs are extensively used in domestic, industrial, and medical applications primarily as disinfectants, there has been concern over their detection in non-target natural and engineered systems.[22,24,46,49,52–55] QACs have been implicated in the promotion and co-selection of antibiotic resistance in bacteria.[24,52,53,56]Antibiotic resistance of human pathogens and the horizontal transfer of resistance genes in the environment are of increasing public and environmental health concern and a global public health threat.[57,58] Additionally, QACs have been identified as precursors to the formation of carcinogenic disinfection byproducts during drinking water and wastewater disinfection processes.[28,59–61]

1.3 Wastewater treatment

Conventional biological wastewater treatment processes are energy intensive and focused on removal of bulk organics and nutrients (e.g., nitrogen). Conventional treatment processes are not designed to remove pharmaceuticals and surfactants; hence they are detected in surface waters. During activated sludge treatment, some

pharmaceuticals and QACs will be removed fully or partially by sorption to organic-rich substrates and biomass and/or biodegradation. Some pharmaceuticals, however, have a relatively low sorption affinity and QACs and pharmaceuticals may be resistant to biotransformation due to structure, concentration, or treatment conditions.

QACs in general, and BACs specifically, are also known to be degraded by certain microorganisms during aerobic biological treatment in wastewater treatment systems.[22,23,40,42,43,62–65] That being said, sorption of QACs occurs faster than aerobic biodegradation, which means that QACs end up being transferred to anaerobic and anoxic compartments like sewage sludge or biosolids.[14,22,28,35] BACs have largely been considered recalcitrant under anaerobic and anoxic conditions because there has been little experimental evidence that QACs containing alkyl and benzyl groups are mineralized under anaerobic conditions.[25,26,42,66–68]

Pharmaceutical removal can also occur through physically driven processes such as sorption or biologically mediated enzymatic reactions. Research has indicated the highest amount of pharmaceuticals discharged through secondary effluent includes beta-blockers and those that pose higher risk include antibiotics and some psychiatric drugs.[21]

1.4 Nitrite as a photosensitizer

The absorption spectra of NO_2^- is dominated by an intense $\pi \rightarrow \pi^*$ band at 205 nm ($\varepsilon = 5500\ M^{-1}cm^{-1}$) and has a weak $n \rightarrow \pi^*$ band reported at 360 ($\varepsilon = 22.5\ M^{-1}cm^{-1}$), 355, or 354 nm.[69–71] This means NO_2^- can absorb UV irradiation in the wavelength output range of medium pressure mercury vapor lamps – used in most commercial advanced oxidation operations – and solar radiation. Photolysis of NO_2^- causes fission of O-N bonds to generate reactive oxidizing species.[72] In aquatic systems at environmentally

relevant pH values, studies have shown that nitrite, upon absorption of actinic radiation produces hydroxyl radical (•OH; quantum yield = 0.024-0.078) and other reactive species.[27] In some natural waters, photolysis of nitrite (NO_2^-) is an important source of hydroxyl radical.[69,71,73–79] The production of reactive intermediates may contribute to the photochemical oxidation and transformation of organic contaminants in the environment.[72,76,80–84] The impact of nitrite on UV disinfection and advanced oxidation processes, however, has been minimally investigated.[69,85–87]

Photolysis of NO_2^- at $200 \leq \lambda \leq 400$ nm results in the formation of $NO^\bullet$, $O^{\bullet-}$, and eventually •OH (equations 1 – 3).[69,72]

$$NO_2^- + h\nu \rightarrow [NO_2^-]^* \quad (1)$$

$$[NO_2^-]^* \rightarrow NO^\bullet + O^{\bullet-} \quad (2)$$

$$O^{\bullet-} + H_2O \rightleftharpoons {}^\bullet OH + OH^- \quad (3)$$

$O^{\bullet-}$ will be protonated to •OH at pH < 11.9 (the pK_a of •OH). The rate of the forward reaction is $k_3 = 1.7 \times 10^6\ M^{-1}\ s^{-1}$ and the rate of the reverse reaction is $k_3 = 1.2 \times 10^{10}\ M^{-1}\ s^{-1}$ at pH = 11.[69,88] Additional reactions can occur resulting in the formation of another reactive nitrogen species $NO_2^\bullet$.[69,72,89] $NO^\bullet$ and •OH can recombine (equation 4) and •OH can react with NO_2^- (equation 5) at essentially diffusion-controlled rates, impacting the steady-state •OH concentration.[69]

$$NO^\bullet + {}^\bullet OH \rightarrow HNO_2 \quad (4)$$

$${}^\bullet OH + NO_2^- \rightarrow NO_2^\bullet + OH^- \quad (5)$$

Some research has suggested that NO_2^- photolysis could lead to reactions with organic pollutants and identified reactions with organic pollutants initiated by NO_2^- photolysis involve photonitration or photonitrosation (as well as hydroxylation or

hydroxynitration).[69,90] There has been research that nitration and nitrosation reactions with polycyclic aromatic hydrocarbons can lead to the formation of mutagenic and carcinogenic compounds and that N-nitrosodimethylamine can be photochemically generated by NO_2^- photolysis in the presence of dimethylamine.[69,90]

1.5 Paradigm shift

One situation where nitrite photolysis could be used is in the anaerobic ammonium oxidation (anammox) process. In efforts to reduce aeration costs for wastewater treatment, anaerobic biological nitrogen removal processes are being studied, piloted, and implemented at full scale. Anammox is one such method. During anammox, the anammox bacteria require nitrite as an electron acceptor to remove ammonia from wastewater streams.[91] Nitrite is produced from ammonia by aerobic autotrophic ammonia-oxidizing bacteria (AOB) in a process referred to as partial nitritation. Partial nitritation and anammox (PN/A) can be implemented either as a single-stage, in which PN/A occurs in a single reactor, or as two-stages, in which PN and A occur in separate reactors. Two-stage PN/A can allow for better suppression of competing nitrite oxidizing bacteria, separate process optimization and thus more complete utilization of anammox with enhanced AOB activity, simpler controls, and for easier retrofitting of existing infrastructure.[92–94] Furthermore, implementation of two-stage PN/A provides an opportunity in which the nitrite produced during partial nitritation could serve a dual purpose, creating a de-facto advanced oxidation process for contaminant removal with the installation of a UV step in between.

1.6 Natural attenuation and degradation mechanisms

As CECs like pharmaceuticals and QACs continue to make their way into terrestrial and aquatic systems due to incomplete or inefficient removal during wastewater treatment and discharge of effluent, uncontrolled and unintentional release, and even stormwater runoff, the fate of these compounds depends on a variety of environmental factors and processes. Natural attenuation involves physical, chemical, and biological transformation or immobilization processes that ideally transform contaminants to less toxic forms, retain them to reduce risk of transport and exposure, and/or decrease concentrations.[95] Photolysis, the light-induced chemical transformation of a compound, and biodegradation/biotransformation, the enzymatic breakdown of contaminants by bacterial populations, are known natural attenuation mechanisms and likely to be important in rivers and other surface waters.

1.6.1 Aquatic photochemistry: Indirect photolysis

Two photochemical processes occur in sunlit aquatic systems: direct photolysis and indirect photolysis. Target compounds such as contaminants undergo direct photolysis when they absorb photons resulting in bond cleavage. During indirect photolysis, a chromophore in the system – not the target compound – absorbs light and acts as a sensitizing species (Figure 1-2). All dissolved compounds are potentially subject to indirect photolysis even if they also absorb photons and undergo direct photolysis.[96]

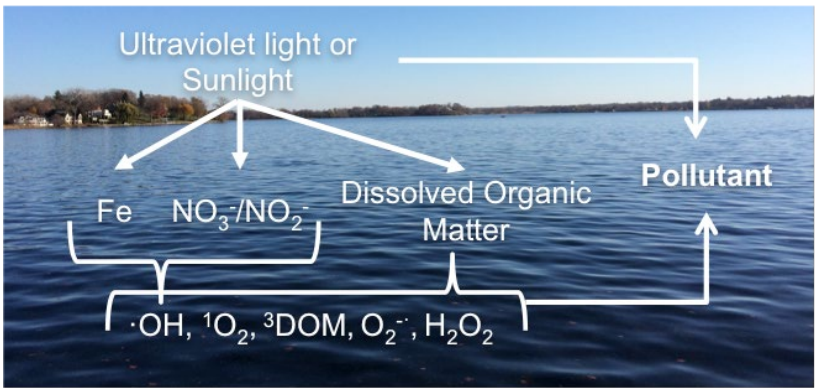

Figure 1-2. Schematic of Direct and Indirect Photolysis Reactions in Aquatic Systems

For organic environmental contaminants that exhibit poor absorption of sunlight (in the ultraviolet or visible light range) or are otherwise stable to reaction via direct photolysis, indirect photolysis processes will be more relevant in natural waters and could be an important attenuation mechanism. Indirect photolysis occurs when another chemical species, such as nitrate, nitrite, and chromophoric dissolved organic matter (CDOM) in natural waters, absorbs light energy, becomes electronically excited, and subsequently reacts with a contaminant directly through energy transfer or produces "photochemically produced reactive intermediates" (PPRIs) that are energetically capable of transforming target contaminants.[84,96] These constituents are sometimes referred to as photosensitizers.

Dissolved organic matter, a complex and heterogeneous mixture of organic molecules, is the principal light-absorbing substrate in natural waters.[96,97] CDOM acts as a photosensitizer, generating transient PPRIs upon absorption of light and subsequent electronic excitation.[84,98] The reaction mechanisms can differ based on the origin or type of DOM. Chromophores are light absorbing functional groups. In natural organic matter, major chromophores are conjugated π-electron bond structures, e.g., double bonds,

benzyl rings, carbonyl, carboxylate, nitro, and phenolate groups.[97] The chromophores in CDOM induce indirect photochemical transformation of organic pollutants after light absorption at wavelengths of 290 to 600 nm.[97] These PPRIs, including reactive oxygen species (ROS) – species in which oxygen atoms are important – like hydroxyl radical ($^{\bullet}OH$), singlet oxygen ($^1O_2$), peroxy radicals ($ROO^{\bullet}$), and superoxide anions ($O_2^{-\bullet}$), carbonate radical ($CO_3^{\bullet-}$), and non-ROS excited triplet states ($^3DOM^*$) and hydrated electrons, react with and transform contaminants in natural systems thus enhancing degradation and increasing phototransformation rates.[84,97,99–101] Other PPRIs that might be important reactive species in the transformation of organic pollutants are: hydrogen peroxide (H_2O_2), ozone (O_3), sulfate radical ($SO_4^{\bullet-}$), and nitrite radical, which is a nitrating agent that can yield nitroaromatic compounds.[97]

PPRIs tend to be present in the environment at low concentrations because of their high reactivity – they are scavenged, removed by physical processes like energy transfer, or eliminated by chemical processes.[97] The concentrations of PPRIs vary anywhere from 10^{-18} to 10^{-9} mol/L in natural waters. While PPRIs are present at substantially lower concentrations compared to other major chemical species, they are still important in the processing of dissolved species.[102] Compared to molecular oxygen ($^3O_2$), transient PPRIs are strong oxidants. Association with DOM then has a synergistic effect. DOM may also decrease indirect photolysis rates, however, by scavenging or quenching PPRIs or shielding contaminants.[103] While PPRIs are strong photooxidants and can have high second-order rate constants for reactions with various organic contaminants, the overall transformation rates however might be slow or not as significant due to relatively low steady-state concentrations.

Though photoexcited DOM is the main sensitizing species in natural systems, additional light-absorbing species can generate PPRIs. For example, nitrite and nitrate are also key photosensitizers in freshwaters. Nitrite and nitrate absorb actinic radiation including ultraviolet (UV) light and produce $^{\bullet}OH$ as the main transient species at environmentally relevant pH values, which can promote the degradation of contaminants in natural and engineered systems.[69,72,73,75,78,85,104–106] Nitrate has an absorption maximum at 305 nm in the UVB region. The maximum solar photon flux absorbed by nitrate is around 320 nm, decreasing to negligible greater than 340 nm, because the absorbance of nitrate decreases as the irradiance of sunlight increases at wavelengths > 305 nm.[107] Nitrite has a maximum absorbance reported around 355 nm in the UVA region and its absorption spectrum extends into the visible region.

Hydrogen peroxide (H_2O_2), which is commonly found in lakes, rivers, and the sea, can produce hydroxyl radical by direct photolysis.[108] The process is comparatively slow because H_2O_2 weakly absorbs solar radiation. In the photic zone, photolysis of ferric iron (Fe(III))-ligand complexes forms ferrous iron ($Fe(II)_{aq}$), which is thermodynamically unstable in the presence of dissolved oxygen. Subsequent oxidation of $Fe(II)_{aq}$ by O_2 produces superoxide anion radical. Hydroperoxyl radical (pK_a 4.8) is the conjugate acid of superoxide anion radical and can disproportionate or react with additional $Fe(II)_{aq}$ to generate H_2O_2. In turn, H_2O_2 can react with reduced transition metals, like Fe(II), to generate hydroxyl radical. This is known as the photo-Fenton reaction.[108,109]

PPRI reactivity and the specificity of the reaction vary depending on the PPRI itself and the chemical functional groups with which it reacts. Reaction rates of compounds are a function of the steady-state concentration of the PPRI in the system and

the second-order or bimolecular reaction rate constant. Free •OH is a non-selective, highly electrophilic reactive radical that reacts at diffusion-controlled rates to rapidly oxidize many organic contaminants, in particular those considered recalcitrant.[69,72,75,101,106,107] Hydroxyl radical is a non-specific oxidant that reacts by hydrogen bond abstraction from sp^3 hybridized C-H bonds or addition to C-C double bonds.[96] The photochemical formation of •OH by CDOM is not well understood. It has been proposed that irradiated CDOM produces $O_2^{-\bullet}$, which disproportionates into H_2O_2 and O_2, and the photoproduced H_2O_2 then yields •OH either by direct photolysis or via the Fenton reaction with aqueous Fe(II).[107] The aforementioned mechanism is attributed to about half of •OH photoproduction from CDOM while it is postulated that the photolysis of hydroxylated aromatic compounds as well as other processes account for the other half of •OH production.[107] Steady-state concentrations of hydroxyl radical in sunlit surface waters can range from 10^{-18} to 10^{-15} mol/L.[73,96]

Hydroxyl radical are consumed by chemical reactions with inorganic water constituents like HCO_3^- and CO_3^{2-}. In this case, the reaction may generate carbonate radical ($CO_3^{\bullet}$), which is less reactive than •OH but has a longer lifetime thus making it potentially important for transformation of pollutants.[97] Carbonate radical concentrations are estimated to be two orders of magnitude greater than steady-state •OH radical concentrations in sunlit waters.[97] Electron-rich compounds that are more easily oxidized, including anilines, phenols, and compounds with reduced sulfur, may react more readily with carbonate radical despite a slower reaction rate compared to that with •OH.[97]

Singlet oxygen, the first electronic excited state of ground state molecular oxygen, is present in sunlit surface waters at higher steady-state concentrations than hydroxyl

radical (10^{-15} to 10^{-12} mol/L) at the surface.[96,110] The formation of $^1O_2$ involves a sensitization process (Figure 1-3)[110]. First, energy is transferred to molecular oxygen (O_2) from the triplet-excited state of a photosensitizer (^{3}sens) like triplet CDOM. After energy transfer from ^{3}sens, ground state molecular oxygen, which is a triplet (it has two unpaired electrons in its valence shell), is then converted to $^1O_2$ or $^1\Delta_g$, which has 22.5 kcal mol^{-1} higher energy than the spin-unpaired ground state. While a more energetic singlet oxygen state ($^1\Sigma_g$) can be formed, it rapidly decays to $^1\Delta_g$.[110] The wavelength range for production of $^1O_2$ from CDOM is 290 to about 600 nm.[97]

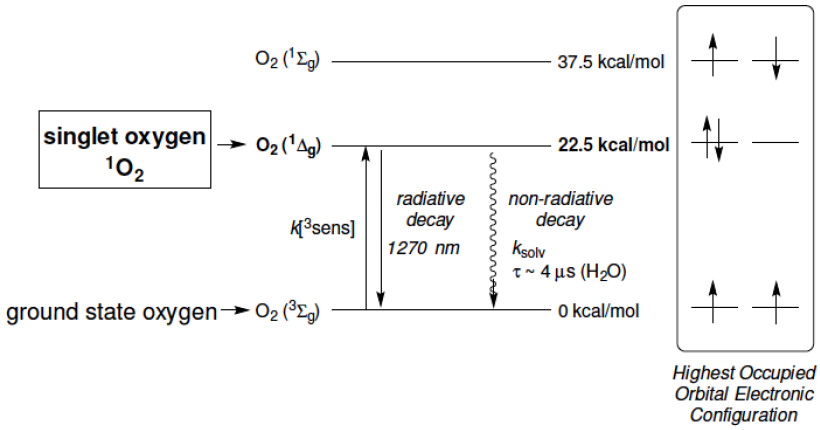

Figure 1-3. Physical Properties of Singlet Oxygen[110]

That being said, steady-state concentrations are relatively low due to the low quantum yield of $^1O_2$ production, rapid physical quenching by water, and some quenching by DOM moeties.[97,110] Singlet oxygen is a more selective oxidant than hydroxyl radical; it is an electrophile that reacts exclusively with specific electron-rich functional groups such as olefins/alkenes and aromatic compounds, phenolates, anilines, electron-rich phenols, furans, other electron-rich heterocycles, and sulfides.[96,110,111] For compounds containing these functional groups, reaction with singlet oxygen will be a dominant loss

mechanism given the higher steady-state concentration of singlet oxygen in natural waters.

Triplet CDOM is formed when CDOM is excited by light absorption to a short-lived singlet state CDOM ($^1CDOM^*$), which is quickly converted to the energetically lower and more stable triplet state ($^3CDOM^*$) via intersystem crossing.[97,103] Research using model triplet sensitizers, such as 4-carboxybenzophenone, has suggested that aromatic ketones are important precursors for $^3CDOM^*$.[112] The triplet state of CDOM can thusly undergo: 1) direct reaction and transformation of organic pollutants via electron or energy transfer, and 2) generation of PPRIs like H_2O_2, $^{\bullet}OH$, $^1O_2$, $O_2^{-\bullet}$, and peroxy radical ($ROO^{\bullet}$).[97,103] Reaction pathway 2 hinges on the fact that $^3CDOM^*$ is deactivated by energy transfer to molecular oxygen.[103,112]

1.6.2 Biodegradation in surface waters

Biodegradation and biotransformation in ecosystems occur when enzymes produced by native bacterial populations break down contaminants. Biodegradation can be considered distinct from biotransformation.[113] During biodegradation, bacteria use contaminants as food and an energy source for their growth. During biotransformation, breakdown of contaminants is co-metabolic as opposed to the contaminants serving as a substrate and bacteria produce metabolites without getting energy.[95] Microbial breakdown of contaminants depends on supportive conditions. Microbial habitats, catabolic potentials, and oxygenated zones will vary in surface waters. Microcosm or river die-away tests can be used to quantify transformation in surface waters.

The fate of pharmaceuticals in surface waters depends on physicochemical properties like solubility, hydrophobicity, and vapor pressure as well as environmental

and climate conditions (e.g., pH, temperature), and the presence of microbes that can degrade these compounds. Biodegradation by metabolic pathways means that microorganisms use the compound as a source of energy, carbon, nitrogen, or other nutrient.[113] Co-metabolism, in contrast, is the incidental breakdown of a compound of interest by an enzyme or cofactor produced during microbial metabolism of a different compound.[113] Degradation is also affected by concentration. High concentrations of certain pharmaceuticals can inhibit microbial activity. Though degradation rates can also be slowed due to low microbial biomass and thus low numbers of degrading microorganisms in comparison to higher substrate concentrations.[114] In the case of very low contaminant concentrations, co-metabolic processes might assist in degradation of contaminants as a result of bacterial consumption of other easily utilized carbon or nutrient sources.

Most research on the environmental fate and natural attenuation of QACs in the aquatic environment has focused on aerobic biodegradation of aqueous phase, bioavailable QACs. Further research has suggested that biodegradation of QACs under anaerobic or anoxic conditions is limited.[22,25] Besides aerobic biodegradation, sorption is the main dissipation pathway of QACs that has been studied extensively in literature. While biodegradation has been identified as a potential sink for QACs, sorption could reduce QAC availability to microorganisms that might degrade them.

Biotransformation of QACs has been known for decades.[65] While many studies have shown that QACs can be aerobically biodegraded, in particular in aerobic activated sludge treatment systems, the process is dependent on QAC concentration, structure, and types of microorganisms present.[22,30,42,50–52,62,115–118] If the concentration of QACs is too

high, the presence of QACs proves inhibitory to microbial activity and even detrimental to the microorganisms.[53,64,117,119] If the concentration of QACs is too low, the QAC may no longer serves as an attractive carbon source for the microorganisms.

1.7 Outline of Thesis

Chapter 2 presents the pros and cons of leveraging the presence of high concentrations of nitrite due to partial nitritation coupled with UV treatment in a de facto advanced oxidation process to remove pharmaceuticals from wastewater. Chapter 3 examines the photodegradation of QACs in sunlit surface waters and the influence of PPRIs generated from DOM. Chapter 4 evaluates the biotransformation of QACs in surface water and characterizes the microbial community and presence of antibiotic resistance genes. Chapter 5 summarizes the findings of the dissertation and provides concluding remarks and recommendations on areas for future research.

Chapter 2. Photodegradation of pharmaceutical compounds in partially nitritated wastewater during UV irradiation

P. I. Hora, P. J. Novak and W. A. Arnold, Photodegradation of pharmaceutical compounds in partially nitritated wastewater during UV irradiation, *Environ. Sci. Water Res. Technol.*, 2019, **5**, 897–909 - Reproduced with permission of The Royal Society of Chemistry.

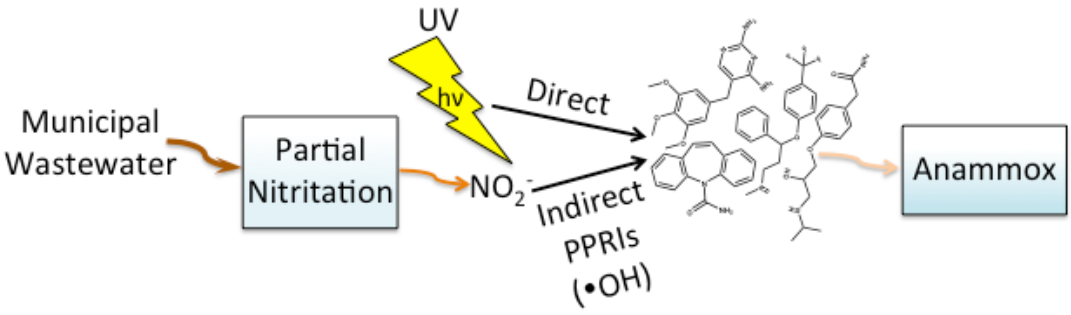

2.1 Preface

The first step of an anaerobic ammonia oxidation (anammox) system is typically the formation of nitrite (NO_2^-) via partial nitritation, which can generate hydroxyl radical ($^{\bullet}OH$) when irradiated with ultraviolet (UV) light. This study demonstrated that the presence of nitrite in buffer and wastewater matrices during medium-pressure UV irradiation (at $\lambda \geq 220$ or ≥ 280 nm) enhanced the degradation of select pharmaceutical compounds of different therapeutic classes (atenolol, carbamazepine, fluoxetine, and trimethoprim). Total pharmaceutical removals in a wastewater matrix irradiated at $\lambda \geq 280$ for 120 minutes were 47% for trimethoprim, 50% for carbamazepine, 60% for atenolol, and 57% for fluoxetine at fluences of 58.6 mEi m^{-2} (2033.1 mJ cm^{-2}). When irradiated at $\lambda \geq 220$ for 60 minutes, removals were 52% for trimethoprim, 56% for carbamazepine, 69% for atenolol, and 90% for fluoxetine at fluences of 634.7 mEi m^{-2} (23969.2 mJ cm^{-2}). Reaction with $^{\bullet}OH$ accounted for ~78 – 90% of pharmaceutical removal at $\lambda \geq 280$ nm. Although direct photolysis did contribute to target compound removal for irradiation with $\lambda \geq 220$ nm, much of the light was absorbed in the buffer and wastewater matrices, and reaction with $^{\bullet}OH$ accounted for ~70 – 93% of pharmaceutical removal. Quencher experiments with isopropanol confirmed the importance of reaction with $^{\bullet}OH$ as the main contributor to pharmaceutical removal. *para*-Chlorobenzoic acid was used as a probe to estimate steady-state $^{\bullet}OH$ concentrations, which averaged 8.58×10^{-15} M for both matrices at $\lambda \geq 280$ nm and 3.50×10^{-14} M for both matrices at $\lambda \geq 220$ nm. Nitrosamines were formed and accumulated during the UV treatment step, however, concomitant with their direct photochemical destruction. Presence of the

pharmaceutical micro-pollutants studied, such as the secondary-amine containing atenolol and fluoxetine, did not elevate nitrosamine formation.

2.2 Introduction

Contaminants of emerging concern (CECs) are common household and industrial chemicals that have been detected in wastewater treatment plant effluent and effluent-impacted water bodies.[15,17] In wastewater treatment, biological processes such as conventional activated sludge are commonly used, but were not specifically designed for the removal of CECs.[2,17] Pharmaceuticals and personal care products are amongst the myriad of potentially recalcitrant, unregulated CECs that are detected in effluent and the environment.[13,15] Of the pharmaceuticals detected in wastewater effluent and surface water, beta-blockers, antidepressants, antibiotics, and the antiepileptic carbamazepine are some of the most studied because they are highly prescribed, ubiquitous in wastewater influent, and exhibit variable susceptibility to biological removal, with carbamazepine considered particularly recalcitrant.[2,15,17,120] As a result, these compounds have been frequently detected in wastewater effluent at nanogram to microgram per liter concentrations.[1,2,15,17] Several pharmaceuticals, including carbamazepine and trimethoprim, have also shown a degree of persistence in the environment, with photolysis being identified over biodegradation and hydrolysis as an important loss mechanism in sunlight-exposed surface water.[4,76,121–123] Consequently, the use of photolysis for treatment of CECs has generated interest.[83,85,86,124–127]

Because conventional wastewater treatment processes are energy intensive, a shift is occurring towards energy neutral treatment and re-envisioning wastewater as a renewable resource with the potential for energy recovery.[128] One way in which this re-

envisioning is taking place is through the replacement of energy-intensive conventional biological nitrogen removal (BNR) (nitrification-denitrification) with partial-nitritation/anammox (PN/A), in which ammonia is first partially biologically oxidized to nitrite, followed by a second anaerobic biological ammonia oxidation step to nitrogen gas, in which ammonium serves as the electron donor and nitrite is the electron acceptor.[91,93,129,130] The use of PN/A leads to an estimated 25% to 60% reduction in aeration requirements, with resulting reductions in energy use.[92,93,128,130] There is evidence for biological removal of CECs during PN/A treatment,[6,8,131] but an opportunity might exist to combine PN/A with chemical treatment to provide more complete CEC removal.

In aqueous systems at environmentally relevant pH values, nitrite is known to absorb UV light in the 200 to 400 nm range and produce hydroxyl radical (•OH; quantum yield 0.024-0.078, compared to 0.007 – 0.014 for nitrate[98]), a non-selective and highly reactive species that oxidizes organic contaminants.[69,72,75,106] Many trace organic contaminants have been effectively removed by advanced oxidation processes (AOPs) that generate •OH.[86,127,132,133] For example, carbamazepine, atenolol, fluoxetine, and trimethoprim are all known to be degraded via reaction with •OH.[81,83,86,121,123,127] In systems containing nitrite, such as a system in which partial nitritation has taken place, a UV disinfection step could be leveraged to generate a de facto AOP using constituents in the wastewater[85] prior to the second anammox step, especially because nitrite is a more efficient producer of hydroxyl radical compared to nitrate.

While production of reactive radical species, such as hydroxyl radical, from nitrite and nitrate photolysis has been extensively studied in sunlit natural waters,[69,73–79]

much of the work investigating the relevance of this phenomenon to contaminant degradation with regard to water and wastewater treatment processes has focused on the impact of *nitrate* during UV or sunlight photolysis.[83,85,104,105,126,134] Many of the referenced studies looking at contaminant degradation in effluent have focused on *nitrified* wastewater. Rosario-Ortiz et al.[86] briefly touch on the influence of nitrite in their study of pharmaceutical oxidation in wastewater (by UV/H_2O_2), but only in terms of its hydroxyl radical scavenging capacity. Bahnmüller et al.[87] attribute a percentage of antibiotic transformation in effluents to hydroxyl radical generated by the photolysis of nitrite. Their experiments, however, were conducted using a solar simulator or a medium pressure mercury lamp transmitting $\lambda > 320$ nm. In their study on medium pressure UV disinfection of nitrified effluents, Keen et al.[85] determined both the quantum yield for $^{\bullet}OH$ formation from nitrite at $\lambda < 240$ nm and the steady-state hydroxyl radical concentrations produced because there is a synergistic effect wherein nitrate photolysis can generate nitrite, which photolyzes to produce additional $^{\bullet}OH$. It should also be noted that the NO_2^- concentrations in the aforementioned studies were below 1 mg/L-N. The study presented herein is the first to investigate the steady-state concentration of hydroxyl radical produced by nitrite and subsequent degradation of several organic contaminants in *nitritated* wastewater, that is water with appreciable levels of nitrite (e.g., around 20 mg/L-N), when irradiated by a medium pressure mercury vapor lamp at shorter wavelength ranges. The results of this study are all the more important because it was previously concluded that UV photolysis of NO_2^- would not be a viable advanced oxidation technology.[69]

Nevertheless, one concern with this strategy is formation of nitrosamines from nitrite or pharmaceutical compounds containing secondary amines.[90,135–138] Photonitrosation of natural organic matter can occur after medium pressure UV irradiation of nitrite.[139] One nitrosamine, N-nitrosodimethylamine (NDMA), reportedly forms photochemically in the presence of nitrite via nitrosation, though NDMA is also subsequently and rapidly degraded photochemically.[69,90,135,140–142] It has also been hypothesized that amine-containing pharmaceuticals can serve as important sources of NDMA precursors in domestic sewage.[135,137,140] There has been no work, however, identifying and attributing the relative importance of specific constituents for nitrosamine formation during UV treatment of wastewater effluent.

In this study, the prospect of implementing UV irradiation in between partial nitritation and anammox processes as a potential means for enhancing removal of pharmaceuticals was evaluated. The compounds selected for study, carbamazepine, trimethoprim, fluoxetine, and atenolol, are regularly prescribed and have been routinely detected in wastewater effluents, receiving water bodies, and drinking water supplies[16,18,19] and are neither readily biodegraded nor destroyed rapidly by solar direct photolysis. It was hypothesized that the nitrite in solution would efficiently generate $^{\bullet}OH$ and lead to transformation of contaminants via indirect photolysis. The possibility of photochemical nitrosamine formation from both nitrite and the pharmaceuticals themselves was assessed, and a kinetic model was developed that factored in both formation and destruction of NDMA by UV to evaluate nitrosamine concentration under different worst-case scenarios.

2.3 Materials and Methods

2.3.1 Chemicals and reagents

All pharmaceutical compounds used in this study were reagent or analytical grade (≥ 98% pure) and used as received: carbamazepine (Acros Organics), trimethoprim (Acros Organics), fluoxetine hydrochloride (TCI America), and atenolol (Sigma-Aldrich). Structures are shown in Table A-1. Aqueous stocks and solutions were prepared using ultrapure water (resistivity 18.2 MΩ-cm, Millipore Corp). *para*-Chlorobenzoic acid (pCBA; Acros Organics) was used as a hydroxyl radical probe.[143] Sodium nitrite (>95%, Fisher) and ammonium sulfate (≥99%, Sigma-Aldrich) salts were added to adjust the concentrations of desired nitrogen species in experimental solutions. Atrazine (99.8%, Fluka) was used as an actinometer.[144] High pressure liquid chromatography (HPLC) grade isopropanol (IPA; 99.9%, Fisher) was used as a radical quencher. HPLC grade acetonitrile (99.9%, Fisher) was used in HPLC eluents.

2.3.2 Reactor effluent collection and processing

Wastewater effluent was collected from a 5-L bench-scale biological sequencing batch reactor operated under conditions favorable to anammox, fed a synthetic nitrite- and ammonium-rich influent, and seeded with sludge from a full-scale DEMON system (York River wastewater treatment plant, Seaside, VA).[131] The effluent was collected in a clean plastic container over one complete pump-out cycle from the reactor and was stored overnight in the dark at 4 °C until further processing and analysis the following day. The effluent was transferred to four 250-mL sterile Corning centrifuge tubes and centrifuged at 5,000 rpm for 35 minutes at 2 °C. The supernatant was then vacuum filtered; first, through 0.7-μm pre-combusted glass fiber filters to remove larger solids and particulate

matter and then through a 0.2-μm Omnipore membrane filter (Millipore). The filtered effluent was subsequently analyzed for anions, ammonium, dissolved organic carbon (DOC), dissolved inorganic carbon (DIC), and pH, then stored at 4 °C in the dark until use. The reactor effluent water quality measurements are provided in Table A-2.

2.3.3 Experimental set-up

Photolysis Experiments. Photolysis experiments with individual compounds were performed in duplicate in ultrapure water and two nitrogen-containing matrices: (1) a carbon-free synthetic wastewater matrix containing sodium nitrite and ammonium sulfate at approximately 20 mg-N/L each (referred to as "synthetic nitrogen-containing matrix") and (2) the wastewater matrix to which additional sodium nitrite and ammonium sulfate were added to reach approximately 20 mg-N/L of each nitrogen species (referred to as "nitrogen-containing wastewater matrix"). These ammonium and nitrite concentration levels were selected as a reasonable amount to expect from an actual partial-nitritation preparatory step based on a range of ammonium values found in effluent from studies on anaerobic treatment of domestic wastewater (9 – 67 mg of N/L)[92] and typical partial nitritation stoichiometry.[94,129,145] The ultrapure water and "synthetic nitrogen-containing matrix" solutions were buffered (5 mM phosphate buffer, pH 7.5) to match the pH of the wastewater reactor effluent (reported in Table A-2).

The extent of pharmaceutical degradation in these systems was assessed by tracking loss of the parent compound under two UV irradiation conditions. Pharmaceuticals were amended from concentrated aqueous stock solutions (prepared in unbuffered ultrapure water) to achieve a concentration of approximately 1 μM. The initial pharmaceutical concentration was selected to be high enough to ensure adequate

detection and quantification during the course of the experiment and low enough so as not to contribute significantly to background radical scavenging or light screening.

Test solutions were irradiated in capped quartz test tubes (V=10 mL, i.d.= 1.1 cm, o.d.= 1.3 cm)[126,146] with a 450-W medium-pressure mercury vapor lamp (Ace Glass Inc., Vineland NJ) emitting polychromatic light. The lamp was situated in a quartz immersion well with tap water circulation. Samples were placed in a merry-go-round equipped with a fan for temperature control, which rotated around the lamp. The lamp was warmed up for at least 10 minutes prior to sample irradiation to ensure full, steady power output. Steady output was confirmed on two occasions using a broadband PMA2100 radiometer with PMA2110-WP (UVA) and PMA2106-WP (UVB) detectors. Either a quartz ($\lambda \geq 220$ nm) or Pyrex ($\lambda \geq 280$ nm) cutoff filter sleeve was used for experiments. Control experiments to account for direct photolysis consisted of spiking the pharmaceutical compounds into buffered ultrapure water without nitrite or ammonium. Control experiments to account for non-photochemical losses were also performed in which the test tubes were wrapped in aluminum foil. Sub-samples from all test tubes were withdrawn at regular time intervals using pre-combusted glass Pasteur pipettes and the concentration of the pharmaceuticals was measured.

Pseudo first-order reaction rate constants were derived from the slopes determined by linear regression of natural log concentration versus time plots of the data. The 95% confidence intervals for each rate constant were calculated by multiplying the standard error of the slope from Excel's LINEST function by the results of the two-tailed inverse of the Student's t-distribution (T.INV.2T function in Excel).

To test for nitrosamine formation, six 50-mL aliquots of the nitrogen-containing wastewater effluent with a molar concentration of approximately 9.92×10^{-4} M nitrite were apportioned out for total N-nitrosamine (TONO) formation experiments. Half of the aliquots were spiked with a cocktail of pharmaceuticals (1 μM of each). Duplicate samples were irradiated in borosilicate test tubes with the 280 nm cutoff in place or in quartz test tubes with the 220 nm cutoff. A dark control wrapped in aluminum foil was also irradiated for each condition. Samples were exposed for 2 hours with the aim of achieving pharmaceutical degradation to at least two half-lives. Samples were stored at 4 °C in glass bottles prior to being shipped on ice to Syracuse University.

Lamp fluence measurement. Chemical actinometry was used to characterize the UV dose or fluence of the lamp. The incident photon fluence rate value or incident photon irradiance, E_p^0, in the wavelength intervals from 220 nm or 280 nm to 405 nm (because nitrite absorbs deep UV (λ<240 nm) as well as wavelengths up to 400 nm[85]) was determined at low optical density using 9 μM aqueous atrazine, buffered at pH 7.0 in 10 mM phosphate buffer, as an actinometer[144,147,148]. Identical geometry and similar solution volumes were used as in the photolysis experiments. Per Canonica et al.,[144] using the spectral energy distribution of radiated mercury lines provided by the lamp manufacturer, and assuming negligible light absorbance or attenuation over the depth of the solution, the fluence was calculated according to:

$$E_{p\,(\lambda_1-405\ nm)}^0 = \frac{k_{p,atr}}{2.303\phi_{atr}\sum_{\lambda_1}^{405\ nm}(f_{p,\lambda}\varepsilon_{atr,\lambda})} \quad (6)$$

where $\lambda_1 = 220\ or\ 280\ nm,\ k_{p,atr}$ is the pseudo first-order rate of atrazine degradation, ϕ_{atr} is the quantum yield of atrazine degradation ($0.046\ mol\ Ei^{-1}$) assuming wavelength independence, $f_{p,\lambda}$ is the photon flux-based emission spectrum of the lamp

normalized over the wavelength interval, and $\varepsilon_{atr,\lambda}$ is the molar absorption coefficient of atrazine. Because the experiment was performed in buffered Milli-Q water, and the solute concentration was relatively low, it was assumed that negligible light absorption (i.e., $\alpha \times z < 0.02$, where α is the light attenuation coefficient and z is solution depth) occurred, allowing the use of the near-surface approximation. The incident photon fluence rate values (E_p^0) were determined to be 176.3 $\mu Ei\ m^{-2}s^{-1}$ (6.7 $mJ\ cm^{-2}s^{-1}$) and 8.1 $\mu Ei\ m^{-2}s^{-1}$ (0.3 $mJ\ cm^{-2}s^{-1}$) for 220 – 405 nm and 280 – 405 nm, respectively. UV fluence values reported below are calculated by using the appropriate E_p^0 value multiplied by the exposure time.

Quantification of hydroxyl radical concentrations. The steady-state hydroxyl radical concentration ($[^{\bullet}OH]_{ss}$) was calculated from the disappearance of 5 μM of the radical-specific molecular probe compound pCBA in the nitrogen-containing matrices irradiated under the same conditions as the pharmaceuticals. It is also possible that reactive nitrogen species such as $NH_2^{\bullet}$, $NO^{\bullet}$, and $NO_2^{\bullet}$ could form in these systems.[69,72,89] Evidence suggests, however, that these species are less potent oxidants than hydroxyl radical. Reactivity between pCBA or benzoate ion has not been reported for $NO_2^{\bullet}$ or $NO^{\bullet}$. $NH_2^{\bullet}$ does not appear to react quickly with benzoate ion (k <1x10^5 M^{-1} s^{-1} at pH 11.2).[149]

A direct photolysis control of the probe compound in buffered ultrapure water was also performed. If pCBA concentration is sufficiently low so as not to affect $[^{\bullet}OH]_{ss}$, the rate of pCBA loss is proportional to the $^{\bullet}OH$ concentration, and follows pseudo first-order kinetics:

$$\frac{d[pCBA]}{dt} = -k'_{pCBA}[pCBA] \quad (7)$$

$$k'_{pCBA} = k_{\cdot OH,pCBA}[\cdot OH]_{ss} \quad (8)$$

Rate constants (k') were determined as described above. The second-order scavenging rate constant for reaction of pCBA with •OH is $k_{\cdot OH,pCBA} = 5 \times 10^9$ $M^{-1}s^{-1}$.[88] Thus, $[^{\bullet}OH]_{ss} = k'_{pCBA}/k_{\cdot OH,pCBA}$. For $\lambda \geq 280$ nm, direct photolysis rates were subtracted to ascertain the indirect contribution. The overall pseudo first-order photolysis rate constant for compound loss in the nitrogen-containing matrices is $k'_{nitrogen-containing}$ and the indirect photolysis pseudo first-order rate constant is $k'_{indirect,280} = k'_{nitrogen-containing} - k'_{direct}$, where k'_{direct} is the direct photolysis pseudo first-order rate constant of the compound in buffer.

To assess and account for any direct photochemical losses of pCBA in the nitrite-containing matrices for $\lambda \geq 220$ nm, 1% IPA, a •OH quencher,[83,126,146] was added to determine the role of indirect versus direct photolysis of the probe. If IPA dramatically suppresses the reaction, it would indicate that direct photolysis reactions are limited due to light screening by the nitrite or other matrix components, and loss of pCBA in the unquenched samples was due to interaction with •OH. Thus, the decrease in the pseudo first-order rate constant resulting from the quenching of •OH in the nitrogen-containing synthetic and wastewater matrices would be equivalent to the contribution of •OH to overall photolysis of the probe (i.e., $k'_{indirect,220} = k'_{nitrogen-containing} - k'_{nitrogen-containing,IPA}$) as distinct from direct photolysis, allowing for an upper bound estimate of steady-state hydroxyl radical concentration. Equation 9 shows the calculation for steady-state hydroxyl radical concentration for $\lambda \geq 220$ nm.

$$[\cdot OH]_{ss,220} = k'_{indirect,220}/k_{\cdot OH,pCBA} \quad (9)$$

Experimental bimolecular rate constants for reaction of each pharmaceutical with •OH could be determined using the calculated steady-state •OH concentrations and the pseudo first-order rate constants for pharmaceutical loss, as shown in equation 10:

$$k_{OH,Pharm} = \frac{k'_{indirect}}{[\cdot OH]_{ss}} \quad (10)$$

Indirect photolysis contribution to pharmaceutical loss. The indirect photolysis contribution in the two nitrogen-containing matrices was estimated using equation 11 and the respective $k'_{indirect}$ values for each pharmaceutical at $\lambda \geq 220$ nm and 280 nm.

$$\%\ indirect = \frac{k'_{indirect}}{k'_{nitrogen-containing}} \times 100 \quad (11)$$

2.3.4 Analytical methods

Water quality parameters. Anions (nitrate and nitrite) were measured by ion chromatography using a Metrohm Compact ion chromatograph. Combined nitrite and nitrate standards made with sodium salts were also run to generate calibration curves. Ammonium (measured as ammonia) was measured colorimetrically using a Hach Test 'N Tube™ kit (AmVer™ High Range Ammonia Reagent Set 2606945, Method 10031, Hach Corporation) and a Hach DR 900 colorimeter. Dissolved organic carbon (DOC), as non-purgeable organic carbon, and dissolved inorganic carbon (DIC) were measured with a Shimadzu TOC-L total organic carbon analyzer. Calibration curves were generated using potassium hydrogen phthalate for DOC and anhydrous sodium carbonate and sodium bicarbonate for DIC. Reactor effluent pH was measured using a calibrated Thermo Orion pH probe and Thermo Orion DUAL STAR pH/ISE meter (pH 4, 7, and 10 standard solutions from BDH VWR Analytical).

Absorption spectra. Light absorbance of the matrices and buffered aqueous pharmaceutical, pCBA, and actinometer solutions at the same concentration used in experiments (1-9 μM) were measured with a Shimadzu UV-1601PC spectrophotometer using 1 cm quartz cuvettes (Figure A-1).

Measurement of pharmaceutical compounds, pCBA, and atrazine. Sub-samples were dispensed into 200 μL HPLC vial inserts. Losses of the pharmaceutical compounds, atrazine, and pCBA were measured using an Agilent 1100 HPLC equipped with a UV absorbance detector. Isocratic HPLC methods are summarized in the Electronic Supplementary Information (Table A-3).

Nitrosamine quantification. TONO analysis followed protocols described previously.[137,150,151] Details are provided in the ESI.

2.4 Results and Discussion

2.4.1 Reactions driven by •OH in nitrogen-containing wastewater matrices at λ ≥ 280 nm

pCBA degradation was used to determine the steady state concentration of •OH produced from the photolysis of the nitrogen-containing matrices at λ ≥ 280 nm. pCBA degradation was pseudo first-order for $\lambda \geq 280$ conditions (Figure 2-1A), demonstrating that •OH formed in the nitrogen-containing matrices at fluences up to 73.2 mEi m^{-2}. The kinetics in both the nitrogen-containing synthetic matrix and wastewater were very similar (Table A-4), suggesting that nitrite was responsible for •OH production. The calculated steady-state •OH concentrations are reported in Table 2-1, and were similar to those measured by Keen et al.,[85] despite significantly higher nitrite concentrations in our system (20 mg/L as N compared to ~0.6 mg/L as N resulting in an $[^{\bullet}OH]_{ss} \approx 3.25\times10^{-14}$

M[85]). Carbonate species, DOC, and ammonium in the wastewater likely consumed a portion of the •OH produced.[73,85,88] It is likely that nitrite not only produced, but also scavenged the •OH (k = 1.1 x 10^{10} $M^{-1}s^{-1}$).[74,85]

Table 2-1. Steady-state Hydroxyl Radical Concentrations[a]

Nitrogen-containing Matrix	**$[^{\bullet}OH]_{ss,\ 280}$ (M)**	**$[^{\bullet}OH]_{ss,\ 220}$ (M)**
Synthetic	$8.48\pm0.27 \times 10^{-15}$	$3.76\pm0.85 \times 10^{-14}$
Wastewater	$8.69\pm0.30 \times 10^{-15}$	$3.24\pm0.84 \times 10^{-14}$

[a]Errors are 95% confidence intervals

Pharmaceutical compounds were photolyzed at $\lambda \geq 280$, under conditions where direct photolysis was limited and indirect processes dominated (Figure 2-1). The degradation of the pharmaceuticals was enhanced in the two nitrogen-containing matrices relative to the buffer control (Figure 2-1; pseudo first order rate constants in Table A-4). The indirect photolysis contribution in the two nitrogen-containing matrices was estimated (Equation 11); it was determined that indirect photolysis was responsible for approximately 76% (synthetic) to 80% (wastewater) of the fluoxetine loss; 90% of the carbamazepine loss (both matrices); 84% (wastewater) to 85% (synthetic) of the trimethoprim loss; and 87% (synthetic) to 91% (wastewater) of the atenolol loss.

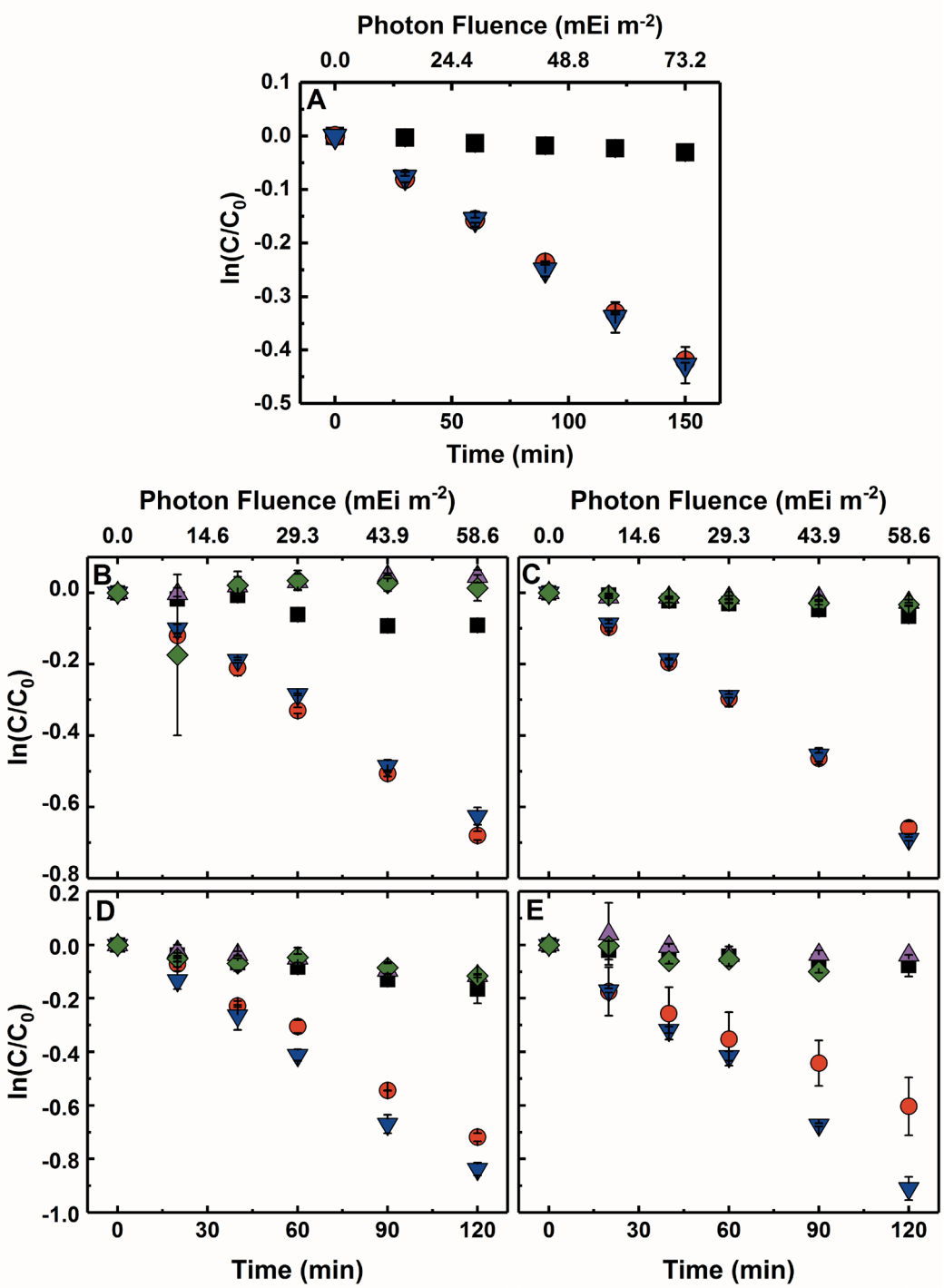

Figure 2-1. *para*-Chlorobenzoic acid (pCBA) and pharmaceutical compound photodegradation at $\lambda \geq 280$ nm as a function of time and corresponding UV fluence in buffer (black, ■), synthetic nitrogen-containing matrix (red, ●), synthetic nitrogen-containing matrix with IPA added (purple, ▲), nitrogen-containing wastewater matrix (blue, ▼), and nitrogen-containing wastewater matrix with IPA (green, ◆). Panels are: (A) pCBA, (B) trimethoprim, (C) carbamazepine, (D) fluoxetine, and (E) atenolol. Error bars represent one standard deviation of duplicates.

Reaction by indirect photolysis is attributed to reactions between •OH and the pharmaceuticals. As seen in Figure 2-1, the addition of IPA (a •OH (and $CO_3^{\bullet-}$) quencher) to the nitrogen-containing matrices significantly slowed the reaction kinetics. This indicates that much of the loss seen beyond direct photolysis (observed in the buffer control) was a result of •OH production/reaction. For fluoxetine and atenolol, degradation rates were faster in the wastewater compared to the synthetic nitrogen-containing matrix, but the addition of IPA to both matrices decreased the rate of pharmaceutical degradation to about that observed in the buffer control. Lam et al.[121] found that $CO_3^{\bullet-}$ could play a role in fluoxetine degradation, though oxidation with •OH was likely dominant. Research on the indirect photolysis of atenolol has suggested that reactions can occur with $CO_3^{\bullet-}$, albeit at slower rates compared to those with •OH.[83] Conversely, others suggested that •OH was not a major sink for atenolol, whereas reactions with singlet oxygen and triplet excited states were important.[81,152] Our results, however, support the importance of •OH reactions with fluoxetine and atenolol in these nitrite-containing matrices.[123] Experimental bimolecular rate constants for reaction of each pharmaceutical with •OH were determined and are presented in Table 2-2. The calculated second order rate constants are consistent with a range of literature values collected under various conditions,[76,86,121,124,125,127,153,154] again indicating that •OH was the primary reactive species in the system.

Table 2-2. Second-order rate constants for reaction with hydroxyl radical in the nitrogen-containing synthetic matrix and wastewater[a]

	$\lambda \geq 280$ nm		$\lambda \geq 220$ nm		
	Synthetic matrix	Wastewater	Synthetic matrix	Wastewater	
Compound	$k_{\bullet OH}$ ($M^{-1}s^{-1}$)	$k_{\bullet OH}$ ($M^{-1}s^{-1}$)	$k_{\bullet OH}$ ($M^{-1}s^{-1}$)	$k_{\bullet OH}$ ($M^{-1}s^{-1}$)	Literature values ($M^{-1}s^{-1}$)
Carbamazepine	$9.34\pm 0.60\times10^{9}$	$9.23\pm1.01\times10^{9}$	$6.20\pm1.41\times10^{9}$	$7.05\pm1.83\times10^{9}$	$3 - 10\times10^{9}$ [76,124,125,127,153]
Trimethoprim	$9.39\pm0.60\times10^{9}$	$8.32\pm0.73\times10^{9}$	$5.46\pm1.28\times10^{9}$	$6.04\pm1.62\times10^{9}$	$6 - 8\times10^{9}$ [86,127]
Fluoxetine	$8.68\pm0.99\times10^{9}$	$1.08\pm0.07\times10^{10}$	N/A	N/A	$8 - 10\times10^{9}$ [121,127]
Atenolol	$8.94\pm1.37\times10^{9}$	$1.31\pm0.08\times10^{10}$	$3.53\pm1.30\times10^{9}$	$6.83\pm1.78\times10^{9}$	$7 - 8\times10^{9}$ [86,127,154]

[a]Errors are 95% confidence intervals

2.4.2 Photolysis reactions in nitrogen-containing wastewater matrices at λ ≥220 nm

As with the experiments at $\lambda \geq 280$ nm, pCBA degradation was assessed at $\lambda \geq 220$ nm to clarify the roles of direct and indirect photolysis, light screening, and •OH in the nitrogen-containing matrices. The degradation of pCBA exhibited pseudo first-order kinetics for $\lambda \geq 220$ experiments. Direct photolysis of pCBA occurred as a result of light absorption by pCBA between 220 and 260 nm (Figure A-1). The rate of pCBA photolysis at wavelengths above 220 nm in buffer was faster than that observed in matrices containing nitrite, however, indicating light screening, and a subsequent slowing of direct photolysis by constituents in the nitrogen-containing matrices occurred (Figure 2-2, Table A-5). pCBA photolysis was also performed with 1% IPA amendment to assess the role of •OH in the system. Because IPA might also quench the direct photolysis process of pCBA if a radical intermediate is involved, a buffer control with IPA and pCBA was also run. Results (Figure 2-2A) showed that IPA reduced the direct photolysis rate constant of pCBA by 37% ($2.96 \pm 0.16 \times 10^{-2}$ min^{-1}) in the buffer control, which could indicate quenching of a radical back to the parent compound. The pseudo first-order rate constant for pCBA degradation in buffer with IPA, after correcting for screening (following previously established methods[84,100] described in the ESI), were comparable to the values observed in the nitrogen-containing matrices, suggesting that direct photochemical degradation could account for some of the pCBA loss observed in the nitrogen-containing matrices under the tested conditions. When IPA was added to the nitrogen-containing matrices, however, the reaction slowed dramatically (Figure 2-2A), with the pseudo first-order rate of pCBA loss in the IPA-quenched experiment ($5.10 \pm 2.50 \times 10^{-3}$ min^{-1}) about 69% lower than in the unquenched analogue (Table A-5). Taken together, these results

corroborate that direct photolysis was effectively screened in the nitrogen-containing matrices, with screening factor calculations (Table A-6) suggesting that the matrices screen more than half of light (Figure 2-2, Table A-5). Loss of pCBA in the nitrogen-containing matrices, therefore, is treated as a reaction with predominantly •OH, with direct photolysis minimal in these matrices due to light screening, and the $[^{\bullet}OH]_{ss}$ reported in Table 2-1 is an upper bound estimate in the system.

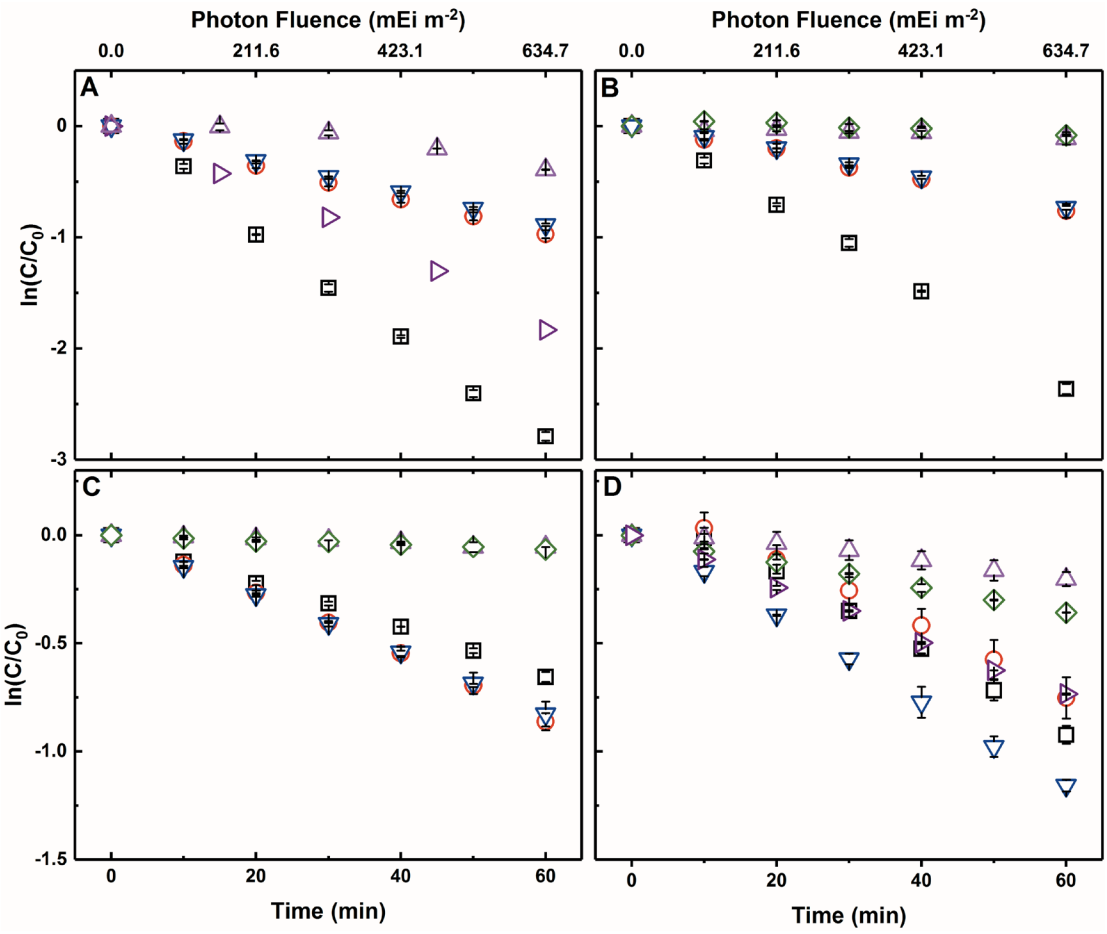

Figure 2-2. pCBA and pharmaceutical compound photodegradation at $\lambda \geq 220$ nm as a function of time and corresponding UV fluence in buffer (black, □), buffer with IPA (dark purple, ▷), synthetic nitrogen-containing matrix (red, ○), synthetic nitrogen-containing matrix with IPA (purple, △), nitrogen-containing wastewater (blue, ▽), and nitrogen-containing wastewater with IPA (green, ◇). Panels are: (A) pCBA, (B) trimethoprim, (C) carbamazepine, and (D) atenolol. Photolysis of fluoxetine occurred rapidly with complete disappearance within a few minutes; therefore, the data is not shown. Error bars represent one standard deviation of duplicates.

In the case of the pharmaceuticals, both direct and indirect photolysis were also observed, with the degradation of each pharmaceutical faster by an order of magnitude or more when photolyzed under $\lambda \geq 220$ nm conditions (Table A-5). Indeed, at these lower wavelengths the pharmaceuticals experienced significantly enhanced direct photolysis in the solutions without nitrogen. For example, photolysis of fluoxetine under $\lambda \geq 220$ conditions occurred so rapidly that complete disappearance was observed within a few minutes (data not shown). Trimethoprim exhibited substantial direct photolysis in buffer, and the reaction occurred faster than in the nitrogen-containing matrices, even after accounting for screening. Similar to pCBA, estimated screening factors indicated light screening occurred in the nitrogen-containing matrices, limiting the direct photolysis. IPA quenched the reactions in these matrices, almost completely so for carbamazepine and trimethoprim and approximately 69-72% for atenolol (Figure 2-2). Thus, like for pCBA, light was absorbed by nitrite and other constituents in the synthetic and wastewater matrices, and direct photolysis was inhibited by light screening in these nitrogen-containing matrices.

Bimolecular rate constants for reaction of carbamazepine and trimethoprim with $^{\bullet}OH$ were again estimated (Table 2-2) as described previously in equation 10, with the exception that k'_{direct} was considered negligible (due to screening as outlined above) and thus $k'_{indirect} = k'_{nitrogen-containing}$. Calculation of bimolecular rate constants for atenolol was more complex. As discussed for the 280 nm conditions, atenolol is known to react with transient oxidants other than $^{\bullet}OH$, such as $CO_3^{\bullet-}$, singlet oxygen, and triplet state organic matter. The experimental results presented herein, however, indicated that while other processes are occurring that are responsible for the partial sensitized

degradation of atenolol, •OH is the major oxidant in the matrices. To better estimate the rate of indirect photolysis due to •OH in the nitrogen-containing matrices, the pseudo first-order rate constants for the IPA spiked experiments were subtracted from the pseudo first-order rate constants of atenolol loss in the respective matrix (i.e., $k'_{indirect,OH} = k'_{nitrogen-containing} - k'_{nitrogen-containing,IPA}$). Overall, the estimates of rate constants for reaction with •OH at $\lambda \geq 220$ nm (Table 2-2) are within approximately a factor of 2 of the values calculated at $\lambda \geq 280$ nm and consistent with literature values, indicating an important role for □OH in the $\lambda \geq 220$ nm experiments. Thus, while there is inherent error in these calculations due to the uncertainties associated with the steady-state [•OH] estimate and assumptions made based on quencher experiment results, the values appear to be reasonable. We suspect the generally lower values of the second-order rate constants calculated for $\lambda \geq 220$ compared to the experiments at $\lambda \geq 280$ nm and literature values are due to these assumptions.

2.4.3 N-Nitrosamine formation potential

TONO were detected in the nitrogen-containing wastewater at average concentrations ranging from 467.2±31.8 ng/L as NDMA for $\lambda \geq 220$ to 3332.0±72.7 ng/L as NDMA for $\lambda \geq 280$ (Figure 2-3) at corresponding fluences of 1269.3 $mEi\ m^{-2}$ (47938.3 $mJ\ cm^{-2}$) to 58.6 $mEi\ m^{-2}$ (2033.1 $mJ\ cm^{-2}$), respectively. The trace levels of pharmaceuticals studied in these experiments (1 μM of each of the four compounds), some of which contain secondary amine groups, did not increase TONO concentration (349.1±15.4 and 3310.6±14.6 ng/L as NDMA for $\lambda \geq 220$ nm and $\lambda \geq 280$ nm, respectively). TONO concentrations in the dark controls were below the LOQ (10 ng/L as NDMA). The significantly lower TONO concentrations in the nitrogen-containing

wastewater irradiated at $\lambda \geq 220$ nm was attributed to greater subsequent photolytic removal of nitrosamines via direct photolysis compared to $\lambda \geq 280$ nm. Due to the relatively high nitrite concentrations and possible microbiologically-derived organic nitrogen in the reactor effluent, the measured TONO concentrations were comparable to, or higher than, levels measured in raw (403-963 ng/L as NDMA), chloraminated (889-2110 ng/L as NDMA), and ozonated (910-2980 ng/L as NDMA) conventional (i.e., no nutrient removal) wastewater effluents.[138]

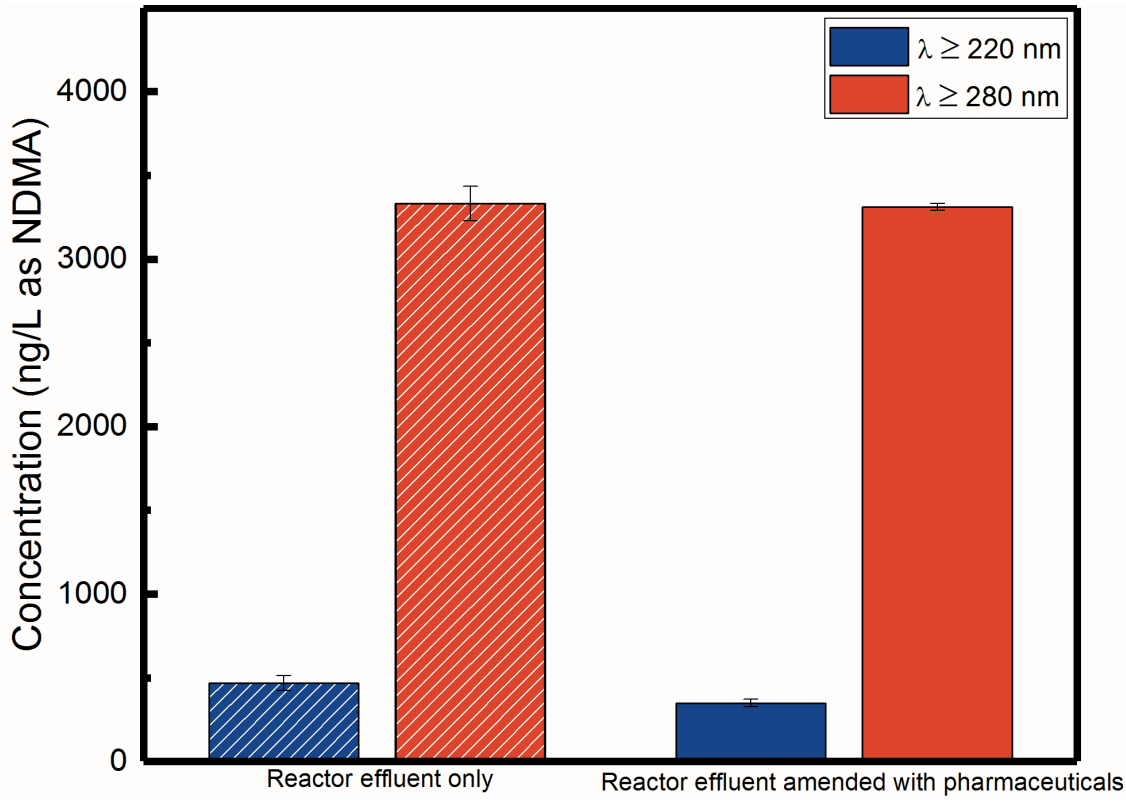

Figure 2-3. Total nitrosamines in amended reactor effluent samples (n=2) without and with the addition of all four pharmaceutical compounds (1 μM of each) irradiated with the 220 or 280 nm cut-off filter. Error bars represent one standard deviation.

While NDMA is only a fraction of TONO measured in wastewaters,[151,155] for the purposes of modeling a "worst-case" scenario, it is assumed that all nitrosamines formed are NDMA. A first-order linear ordinary differential equation (12) was used to model NDMA concentration as a function of time throughout the reaction vessel. The rate of formation (R_{NDMA}) was based on the photochemical formation of NDMA as a function of dimethylamine and nitrite ion photolysis,[90] minus the rate of subsequent NDMA destruction by direct UV photolysis (k_{loss}).

$$\frac{dC_{NDMA}}{dt} = k_{form}[NO_2^-][DMA] - \phi I_\lambda \varepsilon C_{NDMA} \quad (12)$$

$$\frac{dC_{NDMA}}{dt} = R_{NDMA} - k_{loss} C_{NDMA} \quad (13)$$

$$C_{NDMA}(t) = \frac{R_{NDMA}}{k_{loss}} + \alpha e^{-k_{loss}t} \quad (14)$$

The term α is a constant of integration found using the initial condition $C_{NDMA}(t = 0) = 0$, as shown in equation 14, and is calculated for each model scenario (equation 15).

$$\alpha = \frac{-R_{NDMA}}{k_{loss}} \quad (15)$$

Past research has shown that $^{\bullet}$OH does not enhance the photodegradation of NDMA under polychromatic irradiation and that AOPs generating $^{\bullet}$OH are less efficient compared to UV photolysis due to moderate second order rate constants.[142,156] Furthermore, research has suggested that direct photolysis of NDMA dominated under natural sunlight in a wetland system.[83] Subsequently, NDMA loss as a result of reaction with $^{\bullet}$OH was not included in this model for $\lambda \geq 280$ nm and $\lambda \geq 220$ nm conditions.

Eight scenarios were modeled with R_{NDMA} values derived from results reported by Lee and Yoon[90] during the photolysis of 1 mM NO_2^- with either 1 or 4 mM of DMA (i.e., R_{NDMA} for scenario 1 is for 1 mM DMA, R_{NDMA} for scenario 2 is for 4 mM DMA,

and so on). It was determined that within the first 60 minutes of UV-A (300-400 nm) irradiation with a measured incident photon intensity of 1.4×10^{-5} Einstein $L^{-1}s^{-1}$, 1.26×10^4 ng/L (1.7×10^{-7} M) and 4.59×10^4 ng/L (6.2×10^{-7} M) of NDMA formed with 1 and 4 mM DMA present, respectively.[90] For each scenario, k_{loss} varied and was based on data collected from the TONO measurements in the system presented above (Figure 2-3) and literature values. The rate of NDMA loss was calculated for scenarios 1-6 using equation 16 and assuming that a steady-state concentration of NDMA ($C_{NDMA,SS}$) would be reached in the system, based on literature observations[90].

$$k_{loss} = \frac{R_{NDMA}}{C_{NDMA,SS}} \quad (16)$$

In scenarios 1 and 2, k_{loss} was derived using the approximate $C_{NDMA,SS}$ from Lee and Yoon; approximate steady-state concentrations of NDMA at 180 minutes were estimated to be 1.11×10^4 ng/L (1.5×10^{-7} M) and 4.44×10^4 ng/L (6.0×10^{-7} M) for 1 and 4 mM DMA respectively. In scenarios 3 – 6, measured TONO concentrations in reactor samples irradiated under conditions of $\lambda \geq 220$ nm and $\lambda \geq 280$ nm were used to estimate k_{loss} values in our system. Because the measurements were made after 120 minutes of irradiation, it was assumed the concentration of TONO had reached steady state, and that concentration was treated as the equivalent steady state NDMA concentration. In scenarios 7 and 8, a time-based, average $k_{loss} (= 0.36\ min^{-1})$ from Sharpless and Linden[142] for direct photochemical reaction between 200 and 300 nm was used.

UV fluences above 500 mJ cm^{-2} were used for NDMA removal[142] and a fluence of ~1000 mJ cm^{-2} was required for a log order reduction in NDMA[135]. For all scenarios modeled (Figure 2-4) significant steady-state concentrations of NDMA formed over 120 minutes, assuming minimal destruction of nitrosamine precursors throughout irradiation.

For scenarios 5 and 6, which exhibited the lowest steady-state concentrations, even with polychromatic light irradiation at λ≥ 220 nm for 30 minutes – an equivalent fluence of 317.3 $mEi\ m^{-2}$ (11984.6 $mJ\ cm^{-2}$), the model predicted NDMA concentrations reaching about 467 ng/L as NDMA.

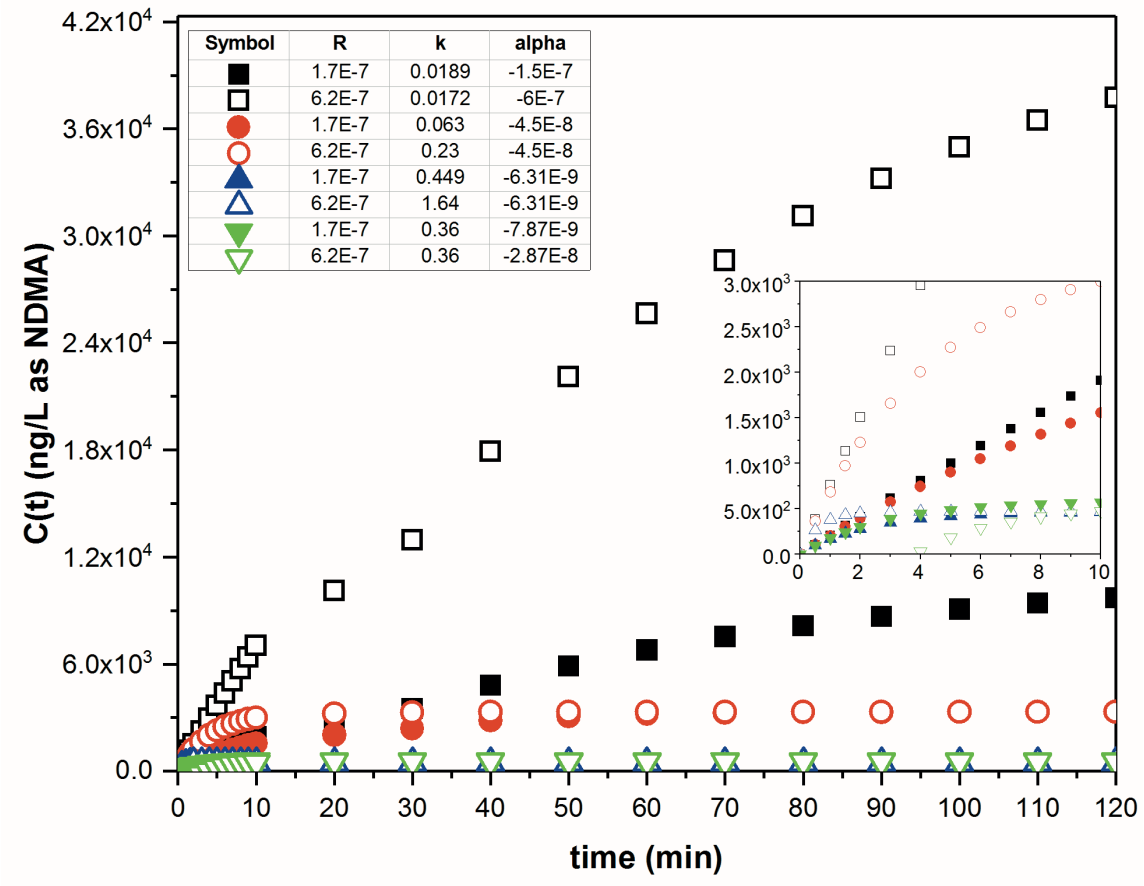

Figure 2-4. Model of NDMA concentrations over time for 8 scenarios. Symbols and corresponding model variables, rate of formation (*R*, M min^{-1}), rate constant of loss (*k,* min^{-1}), and constant of integration (*alpha*), are summarized in the inset table in the left corner of the figure. Rates of formation are a function of either 4 mM (indicated by open symbols) or 1 mM DMA (indicated by closed symbols) and 1 mM nitrite for λ = 300-400 nm. Scenarios 1 and 2 are represented by squares (□,■) with rates of loss calculated from Lee and Yoon 2007[90] for λ = 300-400 nm; scenarios 3 and 4 are represented by circles (○,●) with rates of loss calculated from reactor effluent λ ≥ 280 nm TONO measurements (**Figure 2-3**); scenarios 5 and 6 are represented by triangles (△,▲) with rates of loss calculated from reactor effluent λ ≥ 220 nm TONO measurements (**Figure 2-3**); scenarios 7 and 8 are represented by upside down triangles (▼,▽) with the rate of loss constant determined by Sharpless and Linden 2003[142].

2.5 Conclusions

In a partially nitritated wastewater stream containing high levels of nitrite, trace pharmaceutical compounds could undergo photolytic degradation when exposed to UV. The results of this study also suggest that if nitritated effluents were exposed to solar light (for example, in a treatment wetland or lagoon), trace organic contaminants would also be degraded by solar photolysis. Oxidation by •OH was responsible for much of the degradation observed. This process could increase removal of organic contaminants found in municipal wastewater, in particular, compounds that are considered recalcitrant because they are not readily biodegraded or completely removed by conventional or anaerobic treatment and may have low direct photolysis quantum yields. Previous research has shown that some recalcitrant pharmaceuticals, such as carbamazepine, and their products can undergo enhanced biotransformation and mineralization after UV/H_2O_2 AOP treatment and antibiotics like trimethoprim can have no antibacterially active transformation products.[3,12,157] Therefore, transformation of these compounds by reaction with •OH could increase the susceptibility of products to biodegradation, which would make an intermediate UV process even more promising to further remove these trace organic compounds, especially those that already demonstrate some propensity to biodegrade.[3,5,6,8,158,159] Nevertheless, a foreseeable downside is that significant total N-nitrosamine formation could occur from nitrite photolysis. Because nitrosamines are also subject to photolytic degradation, more research is needed to determine how to operate such a system to facilitate nitrosamine loss in addition to pharmaceutical destruction.

Conflicts of Interest

The authors declare no conflicts of interest.

Acknowledgements

The authors acknowledge funding provided by the University of Minnesota, NSF Sustainability Research Networks grant (1444745), and the Environment and Natural Resources Trust Fund as recommended by the Legislative Citizen Commission on Minnesota Resources. We would like to thank Kira Peterson and J. Cesar Bezares-Cruz for help with reactor set-up, operation, and maintenance, Teng Zeng and Chancheng Pu at Syracuse University for performing the TONO analyses, and Griffin Dempsey for assistance with laboratory work.

Chapter 3. Photochemical Fate of Quaternary Ammonium Compounds in River Water

P. I. Hora and W. A. Arnold, Photochemical Fate of Quaternary Ammonium Compounds in River Water, *Environ. Sci. Process. Impacts*, 2020, DOI:10.1039/D0EM00086H. - Reproduced with permission of The Royal Society of Chemistry.

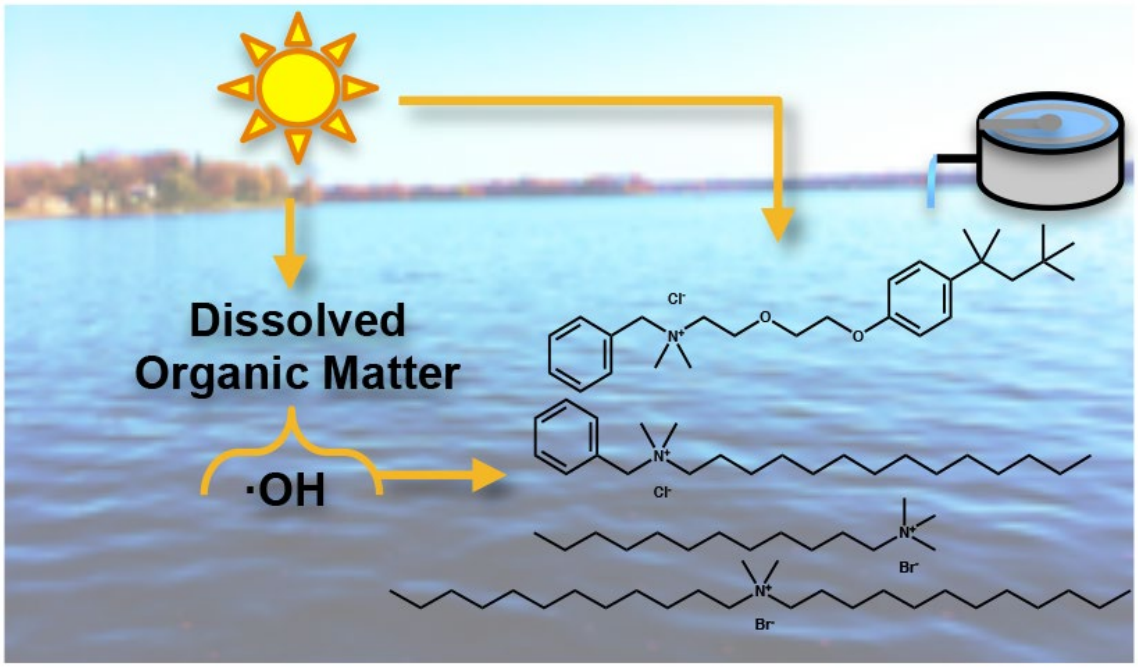

The photochemical fate of quaternary ammonium compounds in surface water is largely influenced by reaction with hydroxyl radical.

3.1 Preface

Quaternary ammonium compounds (QACs) are not completely removed during wastewater treatment and are frequently detected in surface waters and sediments. Photochemical transformation of QACs has not been thoroughly investigated as a potential degradation pathway affecting their fate in the environment. Kinetic studies of common QACs with and without aromatic groups under simulated and natural sunlight conditions were performed with model sensitizers and dissolved organic matter to estimate photochemical half-lives in the aquatic environment. All QACs investigated react with hydroxyl radical at diffusion-controlled rates (~2.9×10^9 to 1.2×10^{10} M^{-1} s^{-1}). Benzethonium reacted via direct photolysis ($\Phi_{BZT,outdoor} = 1.7 \times 10^{-2}$ (mol Ei^{-1})). Benzethonium also reacted with the triplet excited state model sensitizer 2-acetylnaphthalene, but evidence suggests this reaction pathway is unimportant in natural waters due to faster quenching of the triplet 2-acetylnapthalene by oxygen. Reactivity with singlet oxygen for the QACs was minimal. Overall, reactions with hydroxyl radical will dominate over direct photolysis due to limited spectral overlap of sunlight emission and QAC absorbance. Photolysis half-lives are predicted to be 12 to 94 days, indicating slow abiotic degradation in surface water.

3.2 Introduction

Since the late 1930s, quaternary ammonium compounds (QACs) have been a widely used class of chemicals, chemical mixtures, and additives in a variety of industrial, agricultural, clinical, and consumer products and applications.[22–24] Some QACs are designated by the U.S. Environmental Protection Agency and the Organization for Economic Cooperation and Development as high production volume chemicals (≥1

million pounds per year imported or manufactured). An extensive primary use of QACs is as cationic surfactants.[25,26] QACs are used in fabric softeners, antistatic agents, commercial disinfectants, sanitizers, antimicrobials, biocides, herbicides, pesticides, food preservatives, detergents, phase transfer agents, and active ingredients in pharmaceuticals, cosmetics, and personal care products such as shampoos and antibacterial soaps.[22,23,27,28] QACs are also used as lytic biocides, corrosion inhibitors, and clay stabilizers in hydraulic fracturing.[27,48,160,161]

QACs contain at least one hydrophobic hydrocarbon chain bonded to a positively charged quaternary nitrogen atom and have other alkyl groups that tend to be mostly short-chain substituents such as methyl or benzyl functional groups.[22,30] The central nitrogen is covalently bonded to four carbon-containing "R"-substituents (R_4N^+).[27] There are three major classes of QACs: benzylalkyl dimethyl ammonium compounds (BACs), alkyltrimethyl ammonium compounds (ATMACs), and dialkyldimethyl ammonium compounds (DADMACs).

QACs are introduced into aquatic ecosystems through point source pollution and the discharge of effluent from wastewater treatment plants and are considered emerging pollutants.[22,23,28,33,44–47] QACs have been detected in environmental compartments ranging from surface water to sediment and may be found in septic and sewage impacted areas.[28,34,48,162,163] Worldwide average concentration of QACs in domestic wastewater, treated effluent, and surface water has been reported to be approximately 500 µg/L, 50 µg/L, and 40 µg/L, respectively.[24,28,45] The three QAC classes most frequently detected in the environment are: DADMACs with alkyl chain lengths from C_8 to C_{18}, ATMACs with alkyl chain length from C_{12} to C_{18}, and BACs with alkyl chain lengths from C_{12} to C_{18}.[22]

Approximately 75% of QACs used annually are released into wastewater treatment systems and BAC is the most frequently found QAC group worldwide in municipal wastewater effluent at concentrations ranging from 20 to 300 μg/L.[43,46,49,50,163] Although a large fraction of QACs are removed during the wastewater treatment process, QACs are still detected in aquatic environments, especially at higher concentrations in locations downstream of wastewater effluent discharge.[28,34,35,45,160,162,164,165]

Understanding the fate of QACs is important because an estimated 32.5% of QACs produced worldwide are released to the environment,[24] and they retain their biocidal properties after application.[24,54,56] QACs are known to be aerobically biodegradable, but the extent of biodegradation is variable.[25,40,42,48,166] Based on laboratory studies, rates can vary from hours to months and depend on factors such as QAC structure, concentration, and microbial acclimation.[51,62,167,168] Results from some of these studies suggest that biodegradation rates decrease with increasing hydrophobic alkyl chain length. Additionally, the data indicate that QACs with a benzyl group have decreased biodegradation.[48] Moreover, while water-soluble, QACs have a strong tendency to sorb to organic matter in water bodies due to favorable hydrophobic and electrostatic interactions,[28,34,39,162] which might reduce bioavailability and inhibit biodegradation. QACs have been detected in sediments at concentrations higher than in the aqueous phase,[28,34,35,163,169] suggesting QACs are environmentally persistent[48] and their transport and fate are dependent upon association with organic matter in surface waters.[169]

Ecotoxicological effective concentrations (EC_{50}) of QACs reported for various fish, algae, crustacean, daphnia, rotifer, bacterial, and protozoan species range from tens of μg

L^{-1} to mg L^{-1}.[22,23,42,116,170] While QACs generally have not been considered acutely toxic to aquatic organisms based on reported surface water concentrations below many EC_{50} values, more research is needed.[23,28,170] QACs might still pose cumulative chronic effects. Concerns about the detection of QACs in the environment stem from the possibility that prolonged exposure to sub-inhibitory QAC concentrations co-selects for antibiotic resistant bacteria.[24,56,171–175]

The photochemical behavior of QACs in natural environments is still not well understood. BACs are considered stable to direct photodegradation.[27,176] Direct photolysis occurs when a contaminant undergoes transformation, such as breaking of bonds, resulting from directly absorbing light energy.[84] Many QACs lack chromophoric functional groups or exhibit poor absorption of light in the visible spectrum; thus, direct photolysis processes may be limited in natural waters. Indirect photolysis, facilitated by QAC association with dissolved organic matter (DOM), could be an important and under-studied attenuation mechanism. Indirect photolysis occurs when a photosensitizer such as organic matter in natural waters absorbs light energy, becomes electronically excited, and subsequently reacts with a contaminant or produces transient photochemically produced reactive intermediates (PPRIs) that are energetically capable of transforming target contaminants.[84] PPRIs, including reactive oxygen species (ROS), including hydroxyl radical ($^{\bullet}OH$) and singlet oxygen ($^1O_2$), and non-ROS excited triplet states of DOM ($^3DOM^*$), react with contaminants in natural systems thus enhancing degradation and increasing phototransformation rates.[84,99–101] QACs may sorb to DOM, which is ubiquitous in natural waters, and this interaction affects their distribution, transformation, and bioavailability. In aquatic systems, DOM may act as a sink for QACs and as a photosensitizer. For some

hydrophobic compounds, attachment to DOM can expose the pollutant to heterogeneous microenvironments with high concentrations of PPRIs[177] that accelerate degradation, or alternatively, this association could shield compounds from light, inhibiting reactions.

This study examines the photochemical fate of 5 QACs in surface waters and addresses gaps in knowledge on biocide degradation.[27] By conducting experiments in buffered ultrapure water using sensitizers and radical quenchers and in Mississippi River water, the relative contributions of direct and indirect photolysis for each QAC are determined. Kinetic studies allow for calculation of second-order reaction rate constants in radical-mediated processes, estimation of quantum yields where relevant, and estimation of environmental half-lives in natural waters.

3.3 Materials and methods

3.3.1 Chemicals and reagents

The quaternary ammonium compounds used in this study were: benzyldimethyl-n-dodecylammonium chloride (C_{12}-BAC, 98%, Alfa Aesar), benzyldimethyltetradecyl-ammonium chloride hydrate (C_{14}-BAC, 99%, TCI America), benzethonium chloride (BZT, 99%, TCI America), didodecyldimethylammonium bromide (C_{12}-DADMA, 99.9%, Santa Cruz Biotechnology), and didodecyltrimethyl ammonium bromide (C_{12}-ATMA, 99%, Acros Organics). Structures are shown in Electronic Supplementary Information (ESI) Table B-1, and these compounds were selected because they represent high use molecules in different QAC classes. Experimental aqueous stocks, solutions, and buffers were prepared using ultrapure water (resistivity 18.2 MΩ-cm, EMD Millipore Corp.). Hydrogen peroxide (H_2O_2, 30%, Fisher) was used as a $^{\bullet}OH$ sensitizer, Rose Bengal (RB, dye content 95%, Sigma-Aldrich) and 2-acetylnaphthalene (2-AN, 99%,

Alfa Aesar), were used as $^1O_2$ sensitizers, para-chlorobenzoic acid (pCBA, 98%, Acros Organics) was used as a $^{\bullet}OH$ probe, furfuryl alcohol (FFA, 98%, Sigma-Aldrich) was used as a $^1O_2$ probe, HPLC grade 2-propanol (IPA, 99.9%, Fisher) was used as a $^{\bullet}OH$ quencher, L-Histidine (His, 99%, Sigma Aldrich) was used as a $^1O_2$ quencher, and sorbic acid (99%, Alfa Aesar) was used as a quenching agent for triplet excited states. p-Nitroacetophenone and pyridine (PNAP-PYR) were used as an actinometer.[178,179] Tetraoctylammonium bromide (C_8-TAA, 98%, Sigma Aldrich) and tetrapentylammonium bromide (C_5-TAA, 99%, Sigma Aldrich) were used as internal standards for mass spectrometry analysis. Sodium phosphate monobasic monohydrate (98%, Fisher), sodium phosphate dibasic anhydrous (99%, J.T. Baker), ammonium acetate (97%, Macron), sodium hydroxide (98%, Macron), hydrochloric acid (35%, TraceMetal Grade, Fisher), o-phosphoric acid (85%, HPLC Grade, Fisher), glacial acetic acid (99%, ACS Grade, BDH) and formic acid (88%, ACS Grade, Fisher) were used to prepare buffers for experiments and high-pressure liquid chromatography (HPLC) analysis. HPLC grade methanol (99.9%, Fisher) and HPLC grade acetonitrile (99.9%, Fisher or J.T. Baker) were used in HPLC eluents. Optima LC/MS grade (Fisher Scientific) acetonitrile, water, formic acid, and ammonium acetate were used in eluents for mass spectrometry.

3.3.2 River water sample collection and analysis

Mississippi River water (MRW) grab samples were collected in Minneapolis, MN in clean (soaked in Alcanox overnight and rinsed 3× with tap water, deionized water, and ultrapure water), combusted (5 hours at 550 °C) Pyrex glass media bottles at Saint Anthony Falls Laboratory (February 27, 2019) and the University of Minnesota

Boathouse dock (June 5, 2018). Whole water samples were immediately vacuum filtered through a combusted 0.7 μm glass fiber filter followed by a sterile 0.2 μm Omnipore membrane filter (Millipore) and then stored at 4 °C in the dark prior to photolysis experiments.

River water samples were characterized immediately before conducting photolysis experiments. Nitrate and nitrite were measured by ion chromatography using a Metrohm Compact ion chromatograph model 930. Calibration curves were generated with ACS grade sodium salts and detection limits were 0.1 mg L^{-1} as N for both NO_3^- and NO_2^-. Dissolved organic carbon (DOC), as non-purgeable organic carbon, and dissolved inorganic carbon (DIC) were measured with a Shimadzu TOC-L total organic carbon analyzer. Calibration curves were generated using potassium hydrogen phthalate (≥99.95%, Sigma-Aldrich) for DOC and anhydrous sodium carbonate (ACS grade, Fisher) and sodium bicarbonate (99.7–100.3%, Sigma-Aldrich) for DIC. River water pH was measured using a Thermo Scientific Orion pH probe (calibrated with pH 4, 7, and 10 standard solutions from Fisher). This information is tabulated in Table B-2.

3.3.3 Absorption spectra

Ultraviolet-visible absorbance of river water as well as aqueous QAC, probe, and actinometer solutions were measured with a Shimadzu UV-1601PC spectrophotometer using 1 cm quartz cuvettes. The light absorption properties of the chemicals are shown in the Figure B-1.

3.3.4 Analytical methods

Concentrations of QAC with an aromatic group (C_{12}-BAC, C_{14}-BAC, BZT), the actinometer, and probe compounds were determined by HPLC using an Agilent 1100 LC with a variable wavelength detector. HPLC methods are summarized in Table B-3. C_{12}-DADMA and C_{12}-ATMA were quantified on a Thermo Dionex UltiMate 3000 RSLCnano system equipped with a Thermo TSQ Vantage triple quadrupole tandem mass spectrometer (LC-MS/MS) in positive electrospray ionization mode at the University of Minnesota Masonic Cancer Center using the following parameters: heated electrospray ionization, spray voltage of 2.6 kV, vaporizer temperature 250 °C, sheath gas pressure of 25 psi, aux gas pressure of 20 psi, capillary temperature of 300 °C, SRM scan width (m/z) of 0.1 and scan time (s) of 0.25. Separation was performed on a Waters XSelect CSH C18 (3.5 µm, 130 Å, 50×2.1mm) column. Flow rate was maintained at 250 µL/min, sample temperature was 10 °C, the column was kept at room temperature, and 4 µL was injected on the column. 10 minute isocratic methods of mobile phases A: 2 mM ammonium acetate with 0.1% formic acid in water, B: 0.1% formic acid in acetonitrile, and C: isopropanol were used (65% A, 20% B, and 15% C for C_{12}-ATMA and 37% A, 33% B, and 30% C for C_{12}-DADMA). Flow was diverted to waste from 0 to 4.5 minutes. For C_{12}-ATMA the m/z values monitored were 228.26 and 60.15 and the retention time was 6.1 min, and for C_{12}-DADMA they were 382.44, 214.28, and 5.6 min.

3.3.5 Model sensitizer photochemical experiments

Experiments were performed to determine the reactivity of QACs with $^{\bullet}OH$s using H_2O_2 and with $^1O_2$ using RB and 2-acetylnaphthalene. Duplicate experiments were run in sealed quartz test tubes in an Atlas Suntest CPS+ solar simulator equipped with a

1500 W xenon arc lamp and 290 nm cutoff filter, though it has previously been reported there is some light transmission <290 nm,[100] at a light intensity over 300-800 nm of 765 Wm^{-2} for $^{\bullet}OH$ experiments, at 350 Wm^{-2} for $^1O_2$ experiments with RB, and at 765 Wm^{-2} for $^1O_2$ experiments with 2-AN. The different light intensities were used to control the time over which the reaction occurred. During $^{\bullet}OH$ experiments, QACs (C_{12} and C_{14}-BAC, BZT) and pCBA were spiked from concentrated aqueous stock solutions prepared in unbuffered ultrapure water to achieve an initial concentration of approximately 10 µM in 6-8 mL of phosphate buffer (10 mM, pH 7.0) with 1 mM H_2O_2. Sub-samples of 200 or 500 µL were withdrawn at regular time intervals using combusted glass Pasteur pipettes and dispensed into 1.5 mL amber glass HPLC vials with crimp caps. Equivalent experiments with C_{12}-DADMA and C_{12}-ATMA had initial QAC concentrations of 1 µM and a pCBA concentration of 5 µM. Sub-samples of 900 µL were dispensed into screw top HPLC vials with 100 µL internal standard mix in acetonitrile (C_8-TAA for C_{12}-DADMA and C_5-TAA for C_{12}-ATMA) for LC-MS/MS analysis and 500 µL samples were withdrawn for pCBA analysis via HPLC. Control experiments to account for direct photochemical and non-photochemical losses were performed. Direct controls were run in buffer with the QAC and probe. Dark controls containing the QAC, sensitizer, and probe compound were wrapped in aluminum foil. A quenched control spiked with 1% IPA was also simultaneously run.

Singlet oxygen experiments were conducted in a similar fashion with test tubes containing 8 mL of phosphate buffer (10 mM, pH 7.0), 1-2 µM RB (ground-state reduction potential, E^o (S/S^-) = -0.54 V_{SHE}; triplet energy, E_T = 171 kJ mol^{-1}; triplet state reduction potential, E^{o*} ($^3S^*/S^-$) = 1.23 V_{SHE}; $^1O_2$ quantum yield Φ_Δ = 0.75)[112], 40 µM

FFA, and 10 μM BZT or C_{12}-BAC. L-Histidine (20 mM) was used as a $^1O_2$ quencher. To explore the role of $^1O_2$ and triplet states, experiments with deoxygenated (i.e., nitrogen-sparged) solutions were carried out. Additional experiments were conducted for BZT with 16 μM 2-AN (ground-state reduction potential, E^o (S/S^-) = -1.48 V_{SHE}; triplet energy, E_T = 249 kJ mol^{-1}; triplet state reduction potential, E^{o*} ($^3S^*/S^-$) = 1.10 V_{SHE}; $^1O_2$ quantum yield Φ_Δ = 0.71).[112] Deoxygenated solutions were prepared in an anaerobic glove bag (97% N_2/3% H_2, Pd catalyst, Coy Laboratory Products Inc.) by spiking aqueous stocks (in deoxygenated ultrapure water) of BZT, 2-AN, and FFA in deoxygenated pH7 10 mM phosphate buffer, which was sparged with N_2 gas for 2 hours. The solution was placed into quartz test tubes and further bubbled with N_2 outside of the glove bag for 5-10 minutes prior to being sealed with foil and rubber septa caps. The deoxygenated tubes were sampled sacrificially at 20 and 50 minutes. Another experiment with BZT in deoxygenated phosphate buffer was run with 1 mM sorbic acid to quench triplets.[180,181] Sorbic acid was stirred overnight on a heated stir plate and then sonicated and degassed with application of vacuum for 10 - 20 minutes at 30 – 40 °C before being brought into the glove bag. Other solutions were prepared as above, and all sample solutions were bubbled with N_2 outside the glove bag for 30 minutes prior to being dispensed into test tubes under a nitrogen blanket and sealed with foil and rubber septa caps. Tubes were sampled sacrificially after 10, 20, 30, 40, and 50 minutes.

Steady-state concentrations of hydroxyl radical ($[^{\bullet}OH]_{ss}$) and singlet oxygen ($[^1O_2]_{ss}$ were calculated from the ratio of the measured pseudo-first-order rate constant (k_{obs}), determined via linear regression, and the bimolecular reaction rate constant of pCBA with $^{\bullet}OH$ ($k_{\bullet OH,pCBA} = 5 \times 10^9$ $M^{-1}s^{-1}$) [88] and FFA with $^1O_2$ ($k_{1O2,FFA} = 1.17 \times 10^8$

$M^{-1}s^{-1}$ at 30 °C).[111] Direct photolysis losses of the probes were negligible. Assuming a first-order kinetic dependence on each QAC and pCBA and that the reactions proceed independently, bimolecular reaction rate constants of QACs with •OH ($k_{\cdot OH,QAC}$) were derived using competition kinetics according to equation 17.

$$\ln\left(\frac{[QAC]}{[QAC_0]}\right) = \ln\left(\frac{[pCBA]}{[pCBA_0]}\right)\frac{k_{\cdot OH,QAC}}{k_{\cdot OH,pCBA}} \quad (17)$$

The rate constants for respective QACs were obtained from linear regressions of logarithmic plots of normalized QAC versus pCBA concentrations in the same tube.

3.3.6 Simulated and outdoor photochemical experiments in river water

QAC photolysis experiments were performed in Mississippi River water and phosphate buffer under simulated and natural sunlight to assess the relative importance of direct photolysis and indirect photochemical transformation due to PPRIs. The radical-specific probe pCBA was used for the quantification of •OH steady-state concentrations in the same tube. Direct photolysis controls were performed for all QACs and pCBA in phosphate buffer solutions (10 mM, pH 7.0), and dark control experiments for QACs and pCBA in river water were performed in tubes wrapped with aluminum foil. River water solutions spiked with 1% IPA as a radical quencher were concurrently irradiated to evaluate the importance of indirect photolysis processes involving •OH. Time resolved samples of 200 or 500 µL were removed for HPLC analysis to determine reaction kinetics.

For simulated sunlight experiments, C_{12} and C_{14}-BAC and BZT were photolyzed in filtered Mississippi River water using the solar simulator. The light intensity was set to 765 $Wm^{-2,}$ and samples were taken every 5 hours. All experiments were run in duplicate. For outdoor natural sunlight experiments, C_{12} and C_{14}-BAC and BZT were photolyzed in

filtered Mississippi River water collected on June 5, 2018 over a total of 26.8 hours from June 28, 2018 to July 6, 2018 (Table B-4 summarizes the exposures) on the rooftop of the University of Minnesota Mechanical Engineering building (latitude: 44°58'30"N, longitude: 93°14'1"W, elevation: 860 ft, azimuth: 218°SW).

Aliquots of 6-8 mL initial volume reaction solutions in 10 mL quartz test tubes (13 mm o.d., 11 mm i.d.) were sealed with pre-combusted aluminum foil squares and then rubber septa caps. Test tubes were irradiated at a 30° angle from horizontal. Initial QAC and probe concentrations were nominally 10 μM, allowing for direct monitoring of reactant and probe compound concentrations and minimization of light screening.

The chemical actinometer PNAP-PYR was simultaneously irradiated during simulated and natural sunlight river water experiments to estimate the spectral irradiance of the light source, calculate direct photolysis quantum yields for QACs at low optical density, and plot long duration experimental data by dose via actinometer loss to compare laboratory and outdoor experiments. The PNAP-PYR actinometer was chosen because the half-life of the QACs was expected to be greater than 4 hours based on preliminary experiments. The concentrations of pyridine were set using relationships in Leifer [178] such that the actinometer loss rate would occur over the same time scale as QAC loss. The spectral irradiance of the solar simulator at wavelengths 276-400 nm was estimated using a bimolecular solution of 47.2 mM pyridine added to 10.7 μM p-nitroacetophenone for a desired half-life of 17 hours in river water experiments. For rooftop experiments, a 11.4 μM PNAP/52.3 mM pyridine solution was used. The molar absorptivity of PNAP (ε_{PNAP}) was calculated by linear regression of absorbance measurements of 3 analytical standards (concentrations 5, 10, and 15 μM) prepared in Milli-Q with trace acetonitrile.

The SMARTS 2.9.5 model[182–184] was used to calculate the solar spectral irradiance (Figure B-1) over the time course of outdoor experiments. Salient inputs are summarized in SI Table B-5. Global tilted irradiances were calculated for each solar hour in an experimental day, summed, and divided by the total exposure hours for each day. The daily irradiances were then averaged for quantum yield calculations.

Direct photolysis quantum yields were calculated following the methods outlined in Dulin and Mill[179] and Leifer[178] with the updated PNAP-PYR quantum yield relationship published by Laszakovits et al.,[185] summarized by equation 18.

$$\phi_{dc} = \frac{k_{dc}}{k_{da}} \frac{\sum_{\lambda}(I_{\lambda}\varepsilon_{\lambda a})}{\sum_{\lambda}(I_{\lambda}\varepsilon_{\lambda c})} \phi_{da} \quad (18)$$

I_{λ} = the irradiance (intensity) of incident light in einsteins m^{-2} s^{-1} at a fixed wavelength λ. ε_{λ}= the decadic molar absorption coefficient of the actinometer (a) or the compound (c) in M^{-1} m^{-1}. The molar absorptivity of the QAC cation was determined by measuring the absorption spectra of a 100 μM solution in buffer and subtracting the absorption of an equivalent concentration of the counter anion (100 μM NaCl or NaBr) as a blank.

$\phi_{da} = \phi_{PNAP} = 0.0074[pyr] + 1.1 \times 10^{-5}$.[185] $\frac{k_{dc}}{k_{da}}$ = the slope of the logarithmic plot of direct photodegradation of the compound versus actinometer determined by linear regression. The wavelength range was 276 to 400 nm for the solar simulator and 280 to 400 nm for outdoor experiments.

3.3.7 Data Analysis

Data points from replicate experiments were plotted individually. The slope of the regression lines and their standard error were used to calculate the required slopes/reaction rate constants and the associated 95% confidence intervals, respectively. Linear fits and generation of rate constants, standard errors of slopes, and 95%

confidence intervals were performed with Origin, Version 2017 (OriginLab Corporation, Northampton, MA, USA).

3.4 Results and discussion

3.4.1 Reactivity of QACs with •OH from H_2O_2 sensitizer experiments

Based on previous work with ionic liquids,[82] •OH was hypothesized to be an important PPRI for the indirect photochemical transformation of QACs. Competition kinetics experiments were conducted with H_2O_2 and pCBA to determine bimolecular reaction rate constants between QACs and •OH ($k_{\cdot OH,QAC}$). Figure 3-1 shows the natural log of the ratio of concentration normalized by the initial concentration of QACs during a solar simulator irradiation experiment with H_2O_2 producing •OH. The C_{12}-ATMA H_2O_2 40 minute data points (Figure 3-1D) were treated as outliers due to anomalous instrumental measurements, indicated by open symbols, and excluded from ensuing regression and analysis. For all the compounds studied, photolysis in the presence of •OH follows pseudo-first order kinetics ($r^2 \geq 0.83$). Dark controls dosed with H_2O_2 showed no significant change in QAC concentration. Quantification of steady-state •OH concentrations was done using pCBA (Figure B-2 and Table B-6).

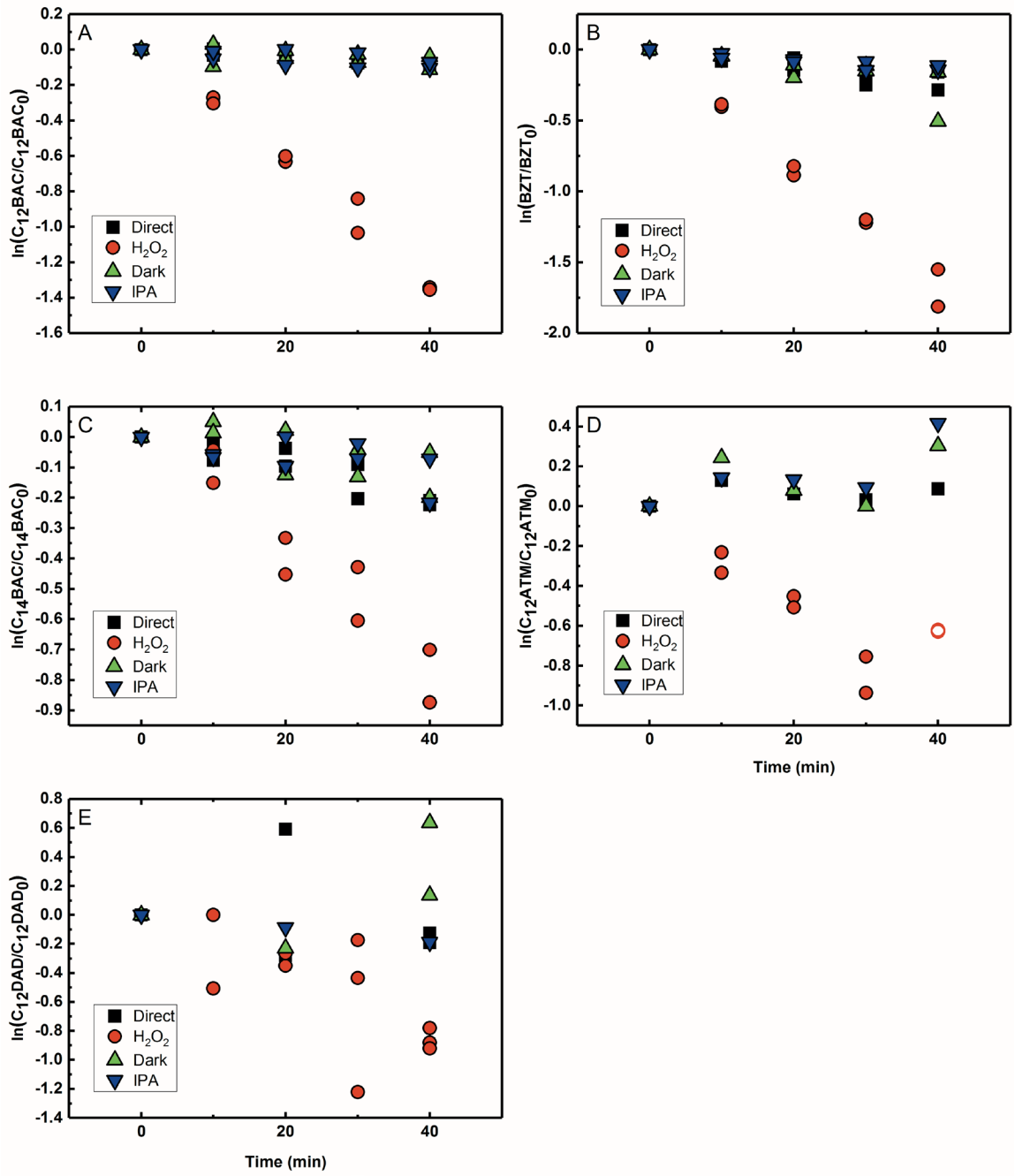

Figure 3-1. Phototransformation over time of: C_{12}-BAC (A), BZT (B), C_{14}-BAC (C), C_{12}-ATMA (D), C_{12}-DADMA (E) in the presence of pCBA under simulated sunlight in phosphate buffer (Direct, black squares), with 1 mM hydrogen peroxide (H_2O_2, red circles), H_2O_2 dark control (Dark, green triangle), H_2O_2 with 1% isopropanol (IPA, blue upside down triangle). Open symbols denote outliers.

Figure 3-2 shows the log-log plot of concentrations of the 5 QACs versus that of pCBA. Using the slopes of the linear regressions in Figure 3-2 and the bimolecular reaction rate constant of pCBA with •OH, $k_{\cdot OH,QAC}$ values were calculated for the QACs using equation 17 (Table 3-1).

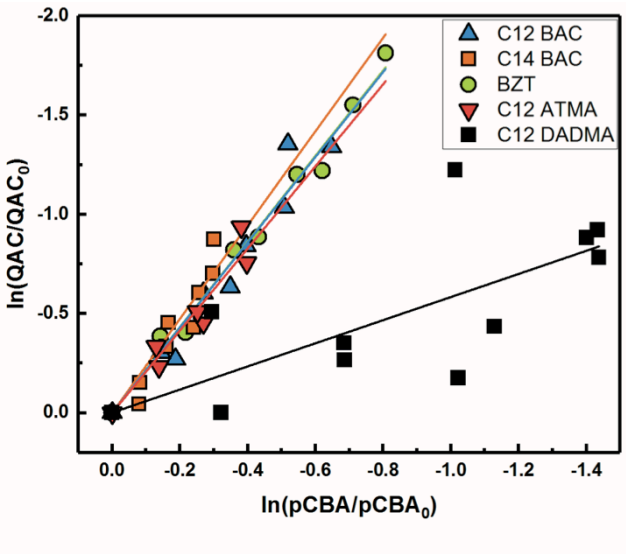

Figure 3-2. Log-log concentrations of QACs versus para-chlorobenzoic acid from solar simulator irradiation experiments with hydrogen peroxide. Solid lines represent linear regressions.

Table 3-1. Bimolecular reaction rate constants of QACs with hydroxyl radical, $k_{\cdot OH,QAC}$ (M^{-1} s^{-1}), determined using hydrogen peroxide as a sensitizer as well as those determined in Mississippi River water under simulated and natural sunlight.[a]

QAC	Hydrogen Peroxide	Solar Simulator, River Water		Outdoors, River Water	
	$k_{\cdot OH,QAC}$ (M^{-1} s^{-1})	$[\cdot OH]_{ss}$ (M)	$k_{\cdot OH,QAC}$ (M^{-1} s^{-1})	$[\cdot OH]_{ss}$ (M)	$k_{\cdot OH,QAC}$ (M^{-1} s^{-1}),
C_{12}-BAC	$(1.1 \pm 0.1) \times 10^{10}$	$(7.0 \pm 0.2) \times 10^{-16}$	$(1.1 \pm 0.2) \times 10^{10}$	$(3.8 \pm 0.3) \times 10^{-16}$	$(1.2 \pm 0.1) \times 10^{10}$
C_{14}-BAC	$(1.2 \pm 0.2) \times 10^{10}$	$(6.7 \pm 0.1) \times 10^{-16}$	$(1.2 \pm 0.3) \times 10^{10}$	$(3.8 \pm 0.3) \times 10^{-16}$	$(1.2 \pm 0.3) \times 10^{10}$
BZT	$(1.08 \pm 0.05) \times 10^{10}$	$(6.1 \pm 0.4) \times 10^{-16}$	$(9.3 \pm 1.3) \times 10^{9}$	$(3.9 \pm 0.4) \times 10^{-16}$	$(9.4 \pm 3.2) \times 10^{9}$
C_{12}-ATMA	$(1.03 \pm 0.14) \times 10^{10}$				
C_{12}-DADMA	$(2.9 \pm 1.0) \times 10^{9}$				

[a]Errors represent 95% confidence intervals associated with the regression slopes in Figure 3-2.

The results demonstrate that the QACs studied react with •OH at or near the diffusion-controlled limit (i.e., $k_{\cdot OH,c} = 5 \times 10^9 - 10^{10}\ M^{-1}s^{-1}$), which is the case for many organic contaminants.[88,97] Hydroxyl radical reacts unselectively with most organic compounds and reactions occur at different functional groups. Typically, •OH behaves as an electrophile and reacts with organic pollutants in two ways: 1) OH group addition to an aromatic ring or a double bond and 2) hydrogen atom abstraction from aliphatic carbon-hydrogen bonds.[88,97] The structural differences of the studied QACs did not significantly affect the bimolecular rate constant, except the reaction between DADMA and •OH is about an order of magnitude lower than for the other compounds.

Similar for imidazolium cations,[82] there was a slight trend seen for increasing $k_{\cdot OH,QAC}$ with the increasing side-chain length of C_{12} and C_{14}-BAC though the values are within error. For C_{12}-DADMA, where reaction with •OH only occurs via H atom abstraction at C-H bonds in the side-chains, rates were smaller than for the BACs and BZT, and C_{12}-ATMA. The exchange of a methyl group (ATMA) for a 12 carbon alkyl chain (DADMA) noticeably slows the reaction kinetics. The alkoxy groups in BZT have both inductive electron withdrawing and resonance electron-donating effects. Hydroxyl radical reacts rapidly with compounds containing aromatic rings with electron-donating substituents and addition reactions still occur at appreciable rates in the presence of electron-withdrawing groups.[97] The coincidence in rates for the BACs, BZT, and C_{12}-ATMA suggests that H atom abstraction at C-H bonds in the side-chain contributes to the overall reaction of BACs and BZT with •OH in addition to any reaction at the ring.

3.4.2 Assessing reactivity with other PPRIs

To further explore the role of specific PPRIs in QAC degradation in the presence of DOM and more definitively rule out additional pathways, sensitizer experiments were conducted to assess reactivity with $^1O_2$ and triplet excited states. Because $^1O_2$ is a selective electrophile preferentially reacting with electron-rich functional groups like sulfides, phenols, alkenes and aromatic compounds, anilines, furans, and other electron-rich heterocycles,[96,110,111] it was hypothesized QACs would have limited interaction with this reactive oxygen species. Moreover, because DOM can be a microheterogeneous environment in which $^1O_2$ potentially reaches higher steady-state concentrations[98,177] and QACs will associate with DOM, enhanced reactivity might occur if in fact they do react with $^1O_2$.

Experiments with RB showed no reaction between C_{12}-BAC (Figure B-3A) and $^1O_2$ (FFA was used to measure the bulk concentration of $^1O_2$ – $[^1O_2]_{ss} = (3.9 \pm 1.2) \times 10^{-12}$ M) (Figure B-3B, Table B-7) under air saturated conditions, and there was no statistically significant difference between the pseudo-first-order rate constant for C_{12}-BAC loss with RB and the histidine quenched and dark controls. No loss of C_{12}-BAC was observed in the deoxygenated control as well, indicating no reactivity with triplet excited states of RB.

BZT exhibited possible reactivity with the triplet excited state of RB based on decay in the histidine quenched control, and BZT loss in the dark control suggested that BZT was also potentially reacting with RB (Figure B-4). Additional control experiments (not shown) indicated that BZT interacts with RB under ambient, dark conditions and

therefore a different $^1O_2$ sensitizer, 2-AN, which is also a model $^3DOM^*$ sensitizer, was used.

The experiments with BZT and 2-AN illustrated minimal BZT loss due to $^1O_2$ (Figure B-5A), and there was no statistically significant difference between the 2-AN results and the dark control and the histidine control where $^1O_2$ is quenched. A deoxygenated control experiment was also conducted. Interestingly, in the deoxygenated solution containing 2-AN, BZT exhibited an approximately 84% decrease after 50 minutes of irradiation. Addition of sorbic acid, which quenches triplet-excited states (with energy > 200 kJ mol^{-1}) of organic compounds, to the deoxygenated 2-AN solution slowed the reaction by 95%. These results indicate that BZT is reacting with ^{3}2-AN*. FFA also reacted in the presence of 2-AN, but degassing the 2-AN solution resulted in a 23% decrease in the pseudo-first-order rate constant of FFA compared to FFA in air-saturated solution (Figure B-5B), indicating a role for both $^1O_2$ and ^{3}2-AN*. Furthermore, minimal loss of FFA was observed in the deoxygenated solution upon addition of sorbic acid, reiterating that FFA is susceptible to degradation by organic triplets.[186,187] Together, these results indicate that BZT does react with ^{3}2-AN*, but the reaction only occurs in the absence of oxygen, meaning quenching of the triplets by oxygen is faster than the reaction with BZT. Thus, BZT reaction with triplet excited state organic matter will likely be unimportant in environmental systems because dissolved oxygen in surface waters will efficiently scavenge triplets before they react with BZT.

3.4.3 Photochemical transformation of BACs in river water under simulated and natural sunlight

The transformation of BACs was then investigated in the presence of DOM in river water. Based on their chemical structures, no other processes besides reactivity with •OH would occur to transform ATMA and DADMA and further experiments were not conducted in river water. Figure 3-3A and B show the time course of C_{12}-BAC and C_{14}-BAC concentrations in phosphate buffer and Mississippi River water in the solar simulator. Tubes were irradiated for a total of 30 hours and this exposure was almost continuous with tubes being removed after 5 or 10-hour increments for sampling and then being returned to resume irradiation in the solar simulator. The loss in river water exhibits pseudo-first-order kinetics as attested to by logarithmic plots for QAC photolysis versus actinometer loss (Figure B-6). To evaluate the oxidation of BACs by •OH, the probe pCBA was added to each MRW tube with BAC, allowing for competition kinetics and quantification of $[^{\bullet}OH]_{ss}$.

For C_{12}-BAC, 9% loss of the compound was seen in the direct photolysis control and 4% in the IPA quenched control. No apparent loss was exhibited in the dark control; in fact, a slight increase was observed possibly due to evaporation or variation in analytical reproducibility. The slopes for the direct ($k_{direct} = (2 \pm 1) \times 10^{-3}$ h^{-1}) and IPA quenched ($k_{IPA} = (1.7 \pm 0.3) \times 10^{-3}$ h^{-1}) controls were within error. Estimating an indirect pseudo-first-order rate constant from the bimolecular reaction rate constant determined from H_2O_2 sensitizer experiments and the calculated $[^{\bullet}OH]_{ss}$ from pCBA loss in MRW (Table 3-1) gives $(2.7 \pm 0.3) \times 10^{-2}$ h^{-1}, which is nearly identical to the overall rate

constant for C_{12}-BAC degradation in MRW ($(2.9 \pm 0.4) \times 10^{-2}$ h^{-1} (Table B-8)), reaffirming the loss seen in the MRW is due to reaction with •OH.

For C_{14}-BAC, a slight increase was observed in the direct control possibly from evaporation in the solar simulator or instrumental error in the measurements. The data in the direct, dark, and IPA quenched controls had consistent trends from 5 to 30 hours. While C_{14}-BAC exhibited an average 14% and 18% decrease from the initial concentration in the dark and IPA quenched controls, respectively, the slopes ($k_{dark} = (3 \pm 3) \times 10^{-3}$ h^{-1} and $k_{IPA} = (5 \pm 3) \times 10^{-3}$ h^{-1}) demonstrate negligible depletion in these controls compared to loss in MRW. The overall rate constant for C_{14}-BAC degradation in MRW was $k_{MRW} = (2.8 \pm 0.6) \times 10^{-2}$ h^{-1}, which agrees with the estimated pseudo-first-order reaction rate constant for C_{14}-BAC loss due to reaction with •OH ($(2.9 \pm 0.4) \times 10^{-2}$ h^{-1}).

Photolysis proceeded faster in the presence of dissolved organic matter, indicating the importance of indirect photolysis (Table B-8). The addition of the radical inhibitor IPA reduced the photodegradation rates substantially in MRW for C_{12} ($k_{IPA}/k_{MRW} = (6 \pm 1) \times 10^{-2}$) and C_{14}-BAC ($k_{IPA}/k_{MRW} = (1.6 \pm 1.0) \times 10^{-2}$). The quencher results demonstrate that direct photochemical loss of BACs is likely to be relatively unimportant in natural systems and indicate that •OH produced is responsible for BAC loss.

Analogous outdoor experiments were conducted in river water to verify the transferability of indoor photolysis results for the BACs. Figure 3-3. C and D show the time course of C_{12}-BAC and C_{14}-BAC concentrations in phosphate buffer and Mississippi River water in natural sunlight. Logarithmic plots of BAC versus actinometer loss

(Figure B-7) indicate that outdoor photolysis also follows pseudo-first-order kinetics. pCBA was again added to MRW tubes.

The overall rate constant for C_{12}-BAC degradation in MRW in natural sunlight was $(2.2 \pm 0.1) \times 10^{-2}$ h^{-1}. Estimating an indirect pseudo-first-order rate constant from the bimolecular reaction rate constant determined from H_2O_2 sensitizer and solar simulator river water experiments and the calculated $[^{\bullet}OH]_{ss}$ from pCBA loss in MRW (Table 3-1) gives $(1.5 \pm 0.1) \times 10^{-2}$ h^{-1} and $(1.5 \pm 0.3) \times 10^{-2}$ h^{-1}, respectively. These estimates imply 67 to 71% of C_{12}-BAC loss in MRW in the outdoor experiment could be attributable to reaction with $^{\bullet}OH$. IPA suppressed the reaction in river water substantially ($k_{IPA}/k_{MRW} = (8 \pm 8) \times 10^{-2}$).

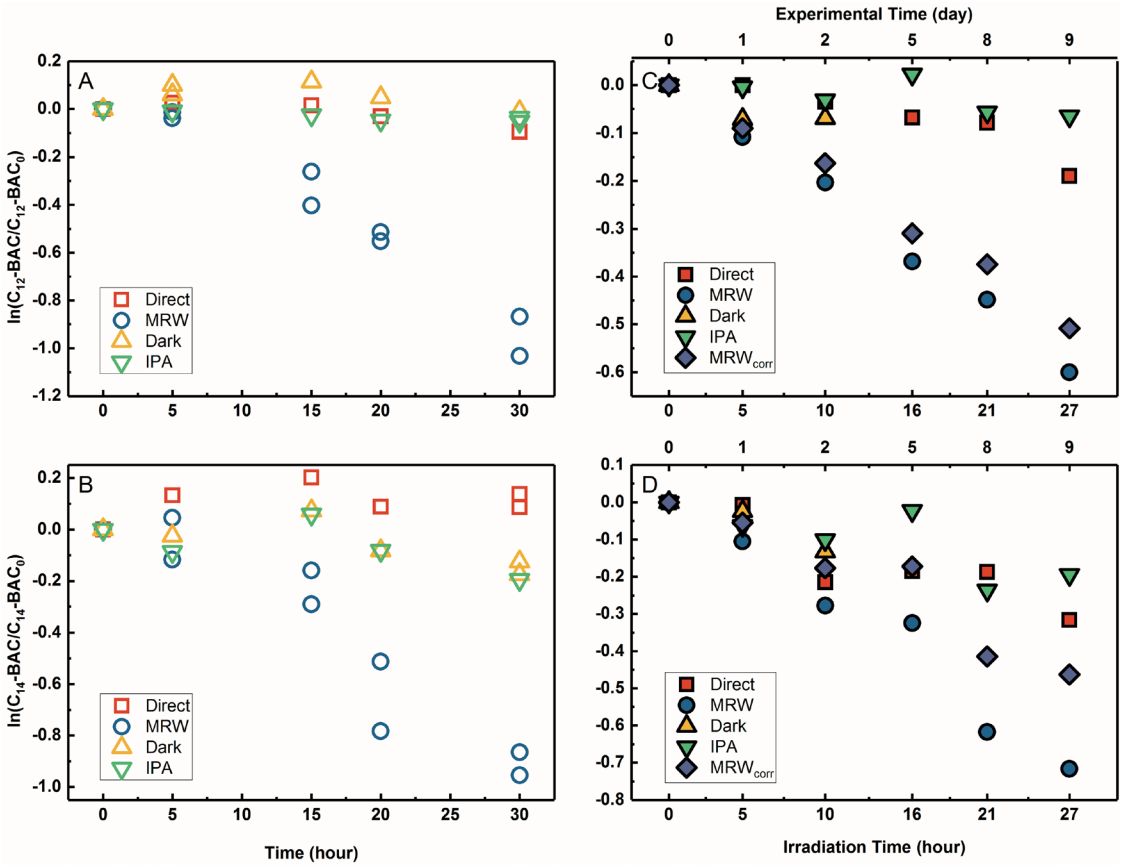

Figure 3-3. Photolysis of BACs with pCBA under simulated sunlight (C_{12}: A, C_{14}: B) or natural sunlight (C_{12}: C, C_{14}: D) in phosphate buffer (Direct, red squares), Mississippi River water (MRW, blue circles), MRW dark control (yellow triangle), MRW with 1% isopropanol (IPA, green upside down triangle). Indirect photochemical loss in river water is shown by purple diamonds (MRW_{corr}). Note the top x-axis for outdoor plots C and D showing the total duration of the experiment.

For C_{14}-BAC, the overall rate constant in MRW was $k_{MRW} = (2.6 \pm 0.4) \times 10^{-2}\ h^{-1}$. The indirect pseudo-first-order rate constant estimates ($(1.6 \pm 0.3) \times 10^{-2}$ h^{-1} from H_2O_2 sensitizer and $(1.6 \pm 0.4) \times 10^{-2}$ h^{-1} from solar simulator river water experiments) suggest 61 to 62% of C_{14}-BAC loss in MRW in the outdoor experiment could be attributable to reaction with •OH. IPA suppressed the reaction in river water, though not completely ($k_{IPA}/k_{MRW} = (3 \pm 2) \times 10^{-1}$). At the end of the experiment, about an 18% decrease in C_{14}-BAC concentration was seen in the quenched control and

27% in the direct control, though these losses are relatively minor compared to the losses in MRW over the same time period.

Because the overlap between the absorption spectra of the BACs and the solar spectrum is small, direct photochemical loss is slow and DOM might screen light affecting transformation rates. Additionally, BACs are hydrolytically stable. Though all C_{12}-BAC control slopes are relatively rather small and associated with proportionate error ($k_{direct}= (6 \pm 2) \times 10^{-3}$ h^{-1}, $k_{IPA}= (2 \pm 2) \times 10^{-3}$ h^{-1}, $k_{dark} = (8 \pm 9) \times 10^{-3}$ h^{-1}), slight loss seems to be occurring in the MRW outdoors due to other abiotic and/or biotic mechanisms. The losses in C_{14}-BAC are more pronounced. Slight thermal decay due to elevated temperatures outside, sorption to the walls of the test tube over the outdoor exposure period, and/or biodegradation could be occurring concomitantly with indirect photolysis to account for increased degradation in the controls.

Outdoor experiments took approximately 9 days while solar exposure time was a little over a day in total to account for weather and sunshine hours on the rooftop. While the river water was filter-sterilized prior to use in experiments and test tubes were capped, no special protocols were used to maintain sterile conditions for the entirety of the experiment. Therefore, it cannot be ruled out that the difference in predicted rate constants due to $^{\bullet}OH$ and the observed rate constant is due to biodegradation because BACs are known to be susceptible to aerobic biodegradation.[42,51,62,117,167]

The outdoor river water (MRW) rates were thusly corrected for concentration changes in the controls by equation 19.[188] The indirect losses were plotted separately (MRW_{corr} in Figure 3-3C & D), and the pseudo-first-order rate constants from MRW_{corr}

were used to calculate bimolecular reaction rate constants with •OH in the outdoor experiments (see below).

$$MRW_{Corr}(t) = MRW(t)e^{(-k_{obs,control} \times t)} \quad (19)$$

3.4.4 BZT direct photolysis in river water under simulated and natural light

The degradation of BZT in MRW appeared to be a combination of direct and indirect photolysis (Figure 3-4A) in the solar simulator. Correcting the BZT concentration measured in MRW to account for the loss due to direct photolysis using equation 19 allowed for calculation of the indirect photolysis pseudo-first-order rate constant and for competition kinetics calculations. The indirect photolysis of BZT in river water was shown in Figure 3-4 by the plotted MRW_{corr} data. The probe pCBA was used to evaluate the oxidation of BZT by •OH, by addition to each MRW tube with BAC, allowing for competition kinetics and quantification of $[•OH]_{ss}$.

The BZT direct photolysis quantum yield from solar simulator experiments was determined using equation 18 and the photon fluence of the solar simulator determined from actinometry and the photon irradiance provided by the manufacturer (spectral flux, I^0= 5.4 Es L^{-1} s^{-1}). Figure B-8 shows the logarithmic plot of BZT direct photolysis (from both the IPA quenched and direct controls) versus the PNAP actinometer. The slope of the line determined by linear regression (1.18 for IPA vs PNAP and 1.11 for Direct vs PNAP) was used to calculate quantum yields. $\Phi_{BZT,indoor,IPA}$ was determined to be 6.3 × 10^{-2} (mol Ei^{-1}) while $\Phi_{BZT,indoor,Direct}$ was 5.9 × 10^{-2} (mol Ei^{-1}). There is good agreement between the two estimates, demonstrating that the decrease of BZT seen in the IPA quenched control is due to direct photolysis and not any other process.

Outdoor experiments were carried out to compare data generated under simulated sunlight with natural sunlight and to verify the BZT quantum yield obtained in the laboratory because quantum yield calculations are sensitive to irradiance values. For BZT sunlight experiments (Figure 3-4B), BZT loss exhibited pseudo-first-order kinetics in river

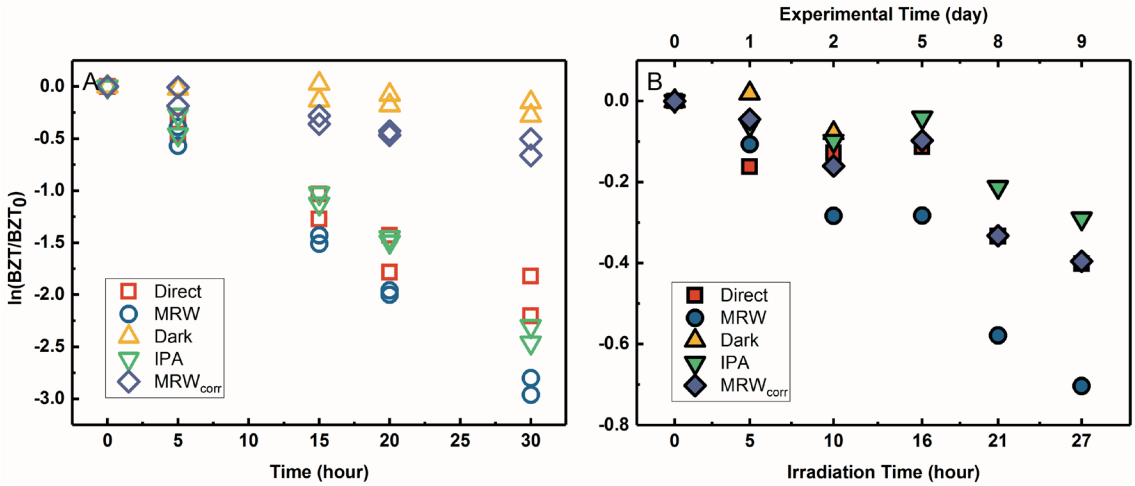

Figure 3-4. Photolysis of BZT with pCBA under simulated sunlight (A) or natural sunlight (B) in phosphate buffer (Direct, red squares), Mississippi River water (MRW, blue circles), MRW dark control (yellow triangle), MRW with 1% isopropanol (IPA, green upside down triangle). Indirect photochemical loss in river water is shown by purple diamonds (MRW_{corr}). Note the top x-axis for outdoor plot B showing the total duration of the experiment.

water as seen in logarithmic plots for QAC photolysis versus actinometer loss (Figure B-7). As with the solar simulator experiment, pCBA was simultaneously irradiated in the MRW tubes.

The slopes of linear regressions for the BZT quenched and direct photolysis controls were identical within error due to overlapping confidence intervals. The data points were subsequently combined and fitted using a linear fit of concatenated data in Figure B-8, which shows the logarithmic plot of BZT direct photolysis versus

actinometer loss. The direct photolysis quantum yield, $\Phi_{BZT,outdoor}$, was determined to be 1.7×10^{-2} (mol Ei^{-1}) using equation 18, the slope of 0.21 from Figure B-8, and the average global tilted irradiance over the timecourse of the rooftop exposures from SMARTS. The discrepancy in calculated quantum yields and half-lives can be explained by the fact that, as has been reported previously,[100] though the Xe lamp has a filter that prevents the transmission of wavelengths below 290 nm, there is bleed of wavelengths <290 nm, which introduces systematic error. This error is important for QACs like BZT which absorb weakly above 290 nm and thus direct photolysis rates are over-emphasized.[76] In the terrestrial aquatic environment, direct photolysis occurs for chemicals that absorb photons at wavelengths ≥ 290 nm because the upper atmosphere screens out solar irradiance at shorter wavelengths. Despite errors introduced by the solar simulator and differences in quantum yields due to spectral overlap, direct photolysis of BZT would still occur in the environment, but the quantum yield determined in sunlight should be used in calculation of predicted half-life.

3.4.5 Second-order rate constants with •OH in river water

Because pCBA was included in the river water experiments, competition kinetics can be used to determine the second order rate constant with •OH to test for any effect of the matrix or light source by comparing the results to those measured with H_2O_2. Figure 3-5 shows the competitive oxidation of the QACs by •OH in MRW under simulated and natural sunlight corrected for losses not due to indirect photolysis. As with the •OH sensitizer experiments, BZT, C_{12}-BAC, and C_{14}-BAC react with •OH in the river water at or near diffusion controlled rates (Table 3-1). Association with dissolved organic matter did not significantly influence the photochemical transformation rates of QACs with •OH

based on the similarity of the values (within 10%) to those determined using H_2O_2 as a sensitizer.

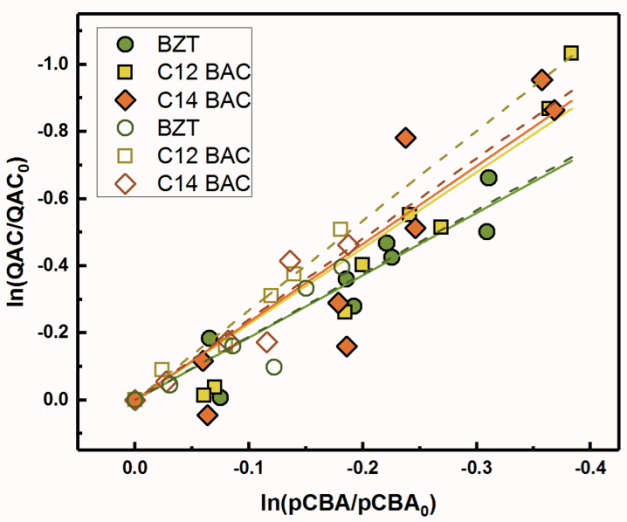

Figure 3-5. Log-concentrations of QACs versus para-chlorobenzoic acid from solar simulator (solid symbols) and natural sunlight (open symbols) irradiation experiments in MRW. QAC concentrations are corrected to only reflect indirect photochemical loss due to •OH. Solid and dashed lines represent linear regressions for solar simulator and natural sunlight experiments, respectively.

The outdoor experimental data overlays the indoor results in river water demonstrating that simulated sunlight experiments serve as good proxies for understanding the photochemical behavior of QACs in surface waters with respect to reaction with •OH. All calculated bimolecular reaction rate constants (Table 3-1) are within the 95% confidence intervals for the 3 sets of experiments serving as robust validation of the values. Due to the overlap of the indoor and outdoor results, we can be reasonably assured in our assumptions about the outdoor experimental data and that the indirect photolysis estimates are correct. Figure 3-5 reaffirms that the photochemical fate of QACs in the environment will be highly dependent on •OH generation in natural waters.

3.4.6 Calculated half-lives in surface waters

The relative contributions of indirect and direct photolysis were evaluated by comparison of pseudo-first-order rate constants from experiments with river and ultrapure water under simulated and natural sunlight. For most of the QACs studied, direct photolysis under environmental conditions is either slow or nonexistent. Only BZT exhibited appreciable direct photochemical degradation. Direct photolysis half-lives for BZT were estimated to be 5.4 - 5.7 days under simulated sunlight and 20.6 days in natural sunlight using a direct photolysis rate constant calculated using the solar spectra modeled by SMARTS (Figure B-1). While the reaction between QACs and •OH is diffusion controlled, QAC degradation via this process will be relatively slow in the environment. Bimolecular reaction rate constants with •OH were used to estimate half-lives of the tested QACs in sunlit surface waters using equation 20 and assuming an $[^{\bullet}OH]_{ss}$ of 1×10^{-16} M on average over 7 hours of daily sunshine.[82] Maximum near-surface steady-state •OH concentrations range from 10^{-17} to 10^{-15} M in sunlit surface waters depending on concentrations of photoproducing and scavenging species, latitude, and time of year.[73,77,97] The half-lives of QACs in the photic zone presented in Table 3-2 reflect a lower bound (minimum persistence) because they are estimated based on conditions in which average maximum rates of ·OH photoproduction occur in the photic zone of a water body at midday during the summertime.

$$t_{1/2} = \frac{ln(2)}{k_{\cdot OH,QAC} \times [\cdot OH]_{ss}} \quad (20)$$

Because BZT is susceptible to both indirect and direct photolysis under relevant environmental conditions, the half-life of BZT in river water is estimated by extrapolating the experimental results for BZT and using the overall pseudo-first-order

rate constant for photolytic loss (equation 21), where k_c (Appendix B equation 26) is the direct photolysis pseudo-first-order rate constant of BZT in river water under natural sunlight.

$$k_{obs,BZT} = k_{\cdot OH,BZT} \times [\cdot OH]_{ss} + k_c \quad (21)$$

While QACs demonstrate shorter lifetimes compared to ionic liquid cations,[82] they still have half-lives on the order of weeks to months, highlighting their slow photochemical transformation in rivers and lakes, and their persistence in the aquatic environment. Results and half-life estimates were consistent for outdoor and indoor river water photolysis experiments as well as for H_2O_2 sensitizer experiments, reiterating the importance of ·OH over other PPRIs in the fate of QACs in surface waters.

Table 3-2. Estimated QAC half-lives in surface water in H_2O_2 sensitizer, simulated sunlight (indoor) river water, and natural sunlight (outdoor) river water experiments.[a, b]

QAC	$t_{1/2}$ (days) H_2O_2	$t_{1/2}$ (days)[c] river water indoor	$t_{1/2}$ (days)[c] river water outdoor
C_{12}-BAC	26 ± 2	24 ± 4	24 ± 2
C_{14}-BAC	23 ± 3	24 ± 5	23 ± 6
BZT	26 ± 1	12 ± 1	12 ± 2
ATMA	27 ± 4		
DADMA	94 ± 32		

[a]Errors represent 95% confidence intervals

[b]Calculated assuming 7 hours of sunshine per day

[c]BZT $t_{1/2}$ including direct photolysis + •OH

3.5 Conclusions

The current study elucidates the photochemical fate of QACs in surface waters. For most of the QACs evaluated, indirect photolysis is more important than direct photolysis under simulated and natural sunlight. Through model sensitizer and quencher experiments, it is clear that all QACs studied will react predominantly with •OH produced in natural waters despite variations in structure, such as side-chain length and presence of

aromatic rings. In waters with low steady-state •OH concentrations and deeper in the water column, rates of reaction between QACs and •OH will be substantially slower and thus QAC lifetimes will be longer. The results of this study contribute to a more holistic and systematic evaluation of the fate of QACs in near-surface waters as well as the potential for their attenuation in the environment. Reported half-lives and rate constants can be used in future models to predict the fate of QACs in the environment, which could inform risk assessments and regulatory decisions on biocide usage given growing public health concern over the proliferation of antibiotic resistant bacteria in the environment. Additionally, the hydroxyl radical reaction data could be applied to assessing the removal of QACs during advanced oxidation treatment.

Conflicts of Interest

The authors declare no conflicts of interest.

Acknowledgements

We would like to acknowledge Dr. Sarah Pati for help with LC-MS/MS measurements as well as Makenzie Pillsbury. Mass spectrometry was carried out in the Analytical Biochemistry Shared Resources of the Masonic Cancer Center, University of Minnesota, funded in part by Cancer Center Support Grant CA-77598. The authors thank Annika Heaps and Bryanna Lopez-Moran for assistance with laboratory work. This work was funded by the Minnesota Environmental and Natural Resources Trust fund (M.L. 2017, Chp. 96, Sec. 2, Subd. 04a) as recommended by the Legislative and Citizen Commission on Minnesota Resources.

Chapter 4. Biotransformation of Quaternary Ammonium Compounds in River Water

4.1 Preface

The biotransformation of a sub-inhibitory mixture of quaternary ammonium compounds (QACs) was investigated, along with the impact that these compounds had on a subset of a native river water microbial population. The ability of short term, low-level exposures of QACs to increase the number of antibiotic resistance genes present or cause substantial microbial community compositional changes was specifically investigated. Environmentally relevant concentrations of QACs (e.g., 1 - 40 μg/L) were transformed over the course of multiple exposures, possibly via metabolic processes despite low concentrations and methanol addition. There was neither a statistically significant nor lasting impact of QAC exposure on the presence of antibiotic resistance genes when comparing river water microcosms amended with a QAC mixture and microcosms to which no QACs were added. Exposure to the QAC mixture did cause compositional changes in the community, though it was unclear whether this was the result of exposure to the QACs themselves or if methanol amended with the QACs caused these changes.

4.2 Introduction

Quaternary ammonium compounds (QACs) are one of the most extensively used classes of biocides, disinfectants, sanitizers, antimicrobials, and cleaners.[22–24,189] Because of their broad-spectrum antimicrobial properties against bacteria, fungi, and viruses, QACs are applied in household, food-processing, agriculture, and clinical settings to control the spread of environmentally transmitted pathogens.[189,190] QACs like BACs, ATMACs, and DADMACs are designated by the U.S. Environmental Protection Agency

and the Organization for Economic Cooperation and Development as high production volume chemicals (≥1 million pounds per year imported or manufactured).

QACs are organic chemicals that contain a positively charged quaternary nitrogen atom covalently bonded to four carbon-containing substituents, which can include at least one hydrophobic hydrocarbon chain and other alkyl groups that tend to be mostly short-chain substituents such as methyl or benzyl functional groups.[22,30] The three major classes of QACs are: benzylalkyl dimethyl ammonium compounds (BACs), alkyltrimethyl ammonium compounds (ATMACs), and dialkyldimethyl ammonium compounds (DADMACs). BACs, ATMACs, and DADMACs are typically formulated as homologue mixtures with alkyl chain lengths ranging from 10 to 20 carbon atoms. C_8 to C_{18} DADMACs, C_{12} to C_{18} ATMACs, and C_{12} to C_{18} BACs are most frequently detected in the environment.[27,48,160,161] QACs are classified based on the carbon-containing substituents. The carbon chain influences the antimicrobial activity of QACs against certain microorganisms.[189] Generally, alkyl chain lengths of C_{12} to C_{16} exhibit greater antimicrobial activity, and twin-chained compounds such as DADMACs demonstrate better bioactivity towards some Gram-positive bacteria compared to BACs.[54,189] Due to their amphiphilic nature, QACs act as detergents or surface-active agents against microorganisms, targeting and breaking apart the bacterial cell membrane.[54] These compounds are algistatic and bacteriostatic at concentrations ranging from 0.5 to 5 mg L^{-1} and microbiocidal at concentrations of 10 to 50 mg L^{-1}.[189]

QAC degradation has been explored more thoroughly in the context of wastewater treatment using inoculums from activated sludge, digester solids, and wastewater effluent.[25,29,40,50,67,166,191] Studies on degradation mechanisms in enrichment

cultures from sediment and soil have also been performed.[51,53,55,62] Some of these previous studies have relied on enrichment (QAC as sole carbon and energy source) by feeding QAC concentrations higher than what might be regularly detected in the aquatic environment. [53,62,117] From these studies, QAC-resistant bacteria capable of degrading the compounds have been isolated. Bacterial species have been identified that degrade QACs, using them as an energy source, eventually mineralizing them to carbon dioxide.[24,54] Biotransformation pathways have also been identified for several QACs by bacterial isolates. These include strains of *Pseudomonas*, *Xanthomonas*, *Aeromonas*, *Stenetrophomonas*, and *Achromobacter*.[52,53,167,168,192] A few studies have reported the microbial degradation of BAC by several pure cultures (*Pseudomonas* strains such as *P. nitroreducens* and *Aeromonas hydrophila* and *Bacillus niabensis*) through dealkylation to benzyldimethylamine by amine oxidase and related enzymes.[54] Other identified enzymes include tetradecyl trimethyl ammonium bromide monooxygenase, a Rieske-type oxygenase oxyBAC, as well as three genes encoding oxygenases that metabolize naturally occurring QACs.[167] Nevertheless, rates can vary from hours to months and depend on factors such as QAC structure, concentration, and microbial acclimation.[51,62,167,168] Results from some of these studies suggest that biodegradation rates decrease with increasing hydrophobic alkyl chain length. Aerobic biodegradation of QACs in surface waters has been demonstrated in comparatively fewer bench-scale studies.[193] The data indicate that QACs with a benzyl group do not biodegrade as well and degradation of ATMACs and BACs occurred over 5 - 10 days in seawater.

Published research suggests exposure to biocides like QACs exerts selective pressure on microbes, increasing resistance to QACs and antibiotics.[53,171,173,174,194] This

previous research has linked QAC exposure to the enrichment of QAC-resistance genes, antibiotic resistance genes, and class 1 integrons in the environment as well as during treatment. Clinically relevant microorganisms have been found to develop either tolerance or resistance to QACs and widespread use of biocides could co-select for antibiotic resistance genes and promote spread of multi-drug-resistant plasmids.[189] Antibiotic resistance is a major public health concern.[58]

This study examines the microbial degradation of a low concentration mixture of QACs at environmentally relevant concentrations[49,165] in surface water as well as potential impacts of the QACs on the microbial community and genes due to exposure to these minute QAC concentrations through high-throughput sequencing and real-time quantitative polymerase chain reaction (qPCR). Though aerobic degradation of QACs has been explored previously, research tended to focus on the fate and impact of QACs in wastewater treatment processes rather than in natural environments.[29,40,50,115,168,170,195–197] When studied in the environment, research on QAC degradation has centered on the enrichment and identification of specific QAC-degrading microorganisms that utilize QACs as their carbon and energy sources[42,51,53,62,117] with the QAC concentrations investigated in many of the aforementioned studies higher (mg/L range) than what has typically been observed in surface waters (not directly downstream of industrial effluent discharge). The research presented herein investigated a mixture of commonly used QAC classes at environmentally relevant concentrations and the impact of these chemicals on a subset of a native river water microbial population. Because some of the previous work on microbial community impact and antibiotic resistance proliferation involved enrichment in soil, sediment, or sewage (focused primarily on BACs) and used sub-

inhibitory concentrations that were higher than those in surface waters, this study also considered whether short term, lower-level exposures resulted in an increase in antibiotic resistance genes or in substantial microbial community compositional changes to compare with studies evaluating the effects of a range of concentrations, differing microbial community origins, and/or single QAC classes.[53,56,198] To probe the potential for antibiotic resistance development due to repeated amendments of very low QAC concentrations, several antibiotic resistance genes that encode for resistance to specific antibiotics were measured, specifically widely used sulfonamide, tetracycline, and beta-lactam antibiotics.

4.2 Materials and methods

4.2.1 Chemicals and reagents

The QACs used in this study were: benzyldimethyl-n-dodecylammonium chloride (C_{12}-BAC, 98%, Alfa Aesar), didodecyldimethylammonium bromide (C_{12}-DADMA, 99.9%, Santa Cruz Biotechnology), didodecyltrimethyl ammonium bromide (C_{12}-ATMA, 99%, Acros Organics). Sodium azide (2.5 g/L) was used to deactivate microbial metabolism in abiotic controls.[199] Experimental aqueous stocks, solutions, and buffers were prepared using ultrapure water (resistivity 18.2 MΩ-cm, EMD Millipore Corp.). QAC stock and standard solutions for high-pressure liquid chromatography tandem mass spectrometry analysis were prepared in methanol or acetonitrile and unbuffered ultrapure water.

4.2.2 Water collection and processing

Mississippi River water was collected in clean (soaked in Alconox overnight and rinsed 3× with tap water, deionized water, and ultrapure water), combusted (550 °C for 5

hours) flint glass gallon jugs at Saint Anthony Falls Laboratory around 10:00 AM on November 8, 2018 (average Mississippi River water temperature recorded as 41 °F at Lock and Dam 02 by US Army Corps of Engineers). The river water was immediately vacuum filtered in the lab through 0.7 μm combusted glass fiber filters to remove larger solids.

Dissolved organic carbon (DOC), as non-purgeable organic carbon, was measured with a Shimadzu TOC-L total organic carbon analyzer. Calibration curves were generated using potassium hydrogen phthalate. River water pH was measured using a calibrated Thermo Orion pH probe and Thermo Orion DUAL STAR pH/ISE meter (pH 4, 7, and 10 standard solutions from BDH VWR Analytical). Anions were measured by ion chromatography using a Metrohm Compact ion chromatograph. Combined standards made with sodium salts were also run to generate calibration curves.

4.2.3 Microcosm set-up

All microcosms were prepared in quadruplicate. Erlenmeyer flasks were autoclaved to sterilize prior to use. An autoclaved graduated cylinder was used to aseptically apportion 495 mL of river water into the sterile control reactors. Sodium azide, which is a strong respiratory inhibitor, was dosed into abiotic sterile controls (SQ) to inactivate the microorganisms in the reactor. Sterile controls were used to measure abiotic degradation. For the amended biotic (AQ) and ambient bottle control (BC) reactors, 500 mL of river water was dispensed into the flasks. The ambient bottle controls, with no QAC addition, were used as baseline blanks and to account for the effect of laboratory conditions on the microbial community. QACs were added to amended and sterile reactors from a concentrated methanol (first and second amendments) and then aqueous stock solution

(third amendment) to achieve a concentration of 50 nM each in the reactors. Concentrations were based on QAC concentrations measured in surface waters and treated wastewater effluent and reported bacterial minimum inhibitory concentrations (MICs) and critical micelle concentrations (CMCs).[24] Flasks were capped with autoclaved foam plugs and stirred continuously on a magnetic stir plate. The microcosms were incubated aerobically at room temperature (22.7 ± 0.4 °C). Amended biotic and sterile or abiotic microcosms were periodically sampled by uncapping the flasks and collecting 900 µL of the well-mixed contents using autoclaved 1 mL pipette tips and dispensing into amber HPLC vials with 100 µL of internal standard in acetonitrile. The internal standard mixture was prepared in acetonitrile to act as a preservative for storage of refrigerated microcosm samples before liquid chromatography tandem mass spectrometry (LC-MS/MS) analysis.

The reactors were sampled for LC-MS/MS analysis prior to the first QAC amendment to determine a baseline QAC concentration, if any, in the river water and directly after dosing (Day 0). The amended biotic reactors were sampled at least once a day for the 7 days following QAC amendment.

Samples (25 mL) were collected for microbial analysis using autoclaved pipette tips on Days 0, 8, 27, 62, and 63 from amended biotic and bottle control reactors. The biotic microcosms were amended two additional times with an aqueous QAC stock solution, after affording ample time for complete degradation, on Days 18 (~53.4 nM each) and 38 (~57.1 nM each or 15.1 µg/L C-12 ATMA, 19.4 µg/L C-12 BAC, 26.4 µg/L C-12 DADMA). Only one 1 mL aliquot of 25 µM concentrated QAC stock was added to the sterile control microcosms on Day 0.

4.2.4 Analytical method

C_{12}-ATMA, C_{12}-BAC, and C_{12}-DADMA were quantified on a Thermo Dionex UltiMate 3000 RSLCnano system equipped with a Thermo TSQ Vantage triple quadrupole tandem mass spectrometer in positive electrospray ionization mode at the University of Minnesota Masonic Cancer Center under the following parameters: heated electrospray ionization, spray voltage of 2.6 kV, vaporizer temperature 250 °C, sheath gas pressure of 25 psi, aux gas pressure of 20 psi, capillary temperature of 300 °C, SRM scan width (m/z) of 0.1 and scan time (s) of 0.25. Separation was performed on a Waters XSelect CSH C18 (3.5 μm, 130 Å, 50×2.1mm) column. Flow rate was maintained at 250 μL/min, sample temperature was 10 °C, the column was kept at room temperature, and 4 μL was injected on the column. Isocratic methods 10 min in duration of mobile phases A: 2 mM ammonium acetate with 0.1% formic acid in water, B: 0.1% formic acid in acetonitrile, and C: isopropanol were used (65% A, 20% B, and 15% C for C_{12}-ATMA; 60% A, 20% B, and 20% C for C_{12}-BAC; and 37% A, 33% B, and 30% C for C_{12}-DADMA). Flow was diverted to waste from 0 to 4.5 minutes. For C_{12}-ATMA the m/z values monitored were 228.26 and 60.15 and the retention time was 6.62 – 7.54 min, for C_{12}-BAC they were 256.28, 60.14, 6.02 – 7.15 min, and for C_{12}-DADMA they were 382.44, 214.28, and 6.14 – 7.22 min. Tetraoctylammonium bromide (C_8-TAA, 98%, Sigma Aldrich), tetrapentylammonium bromide (C_5-TAA, 99%, Sigma Aldrich), and tetradecyltrimethylammonium bromide (C_{14}-ATMA, 99%, Acros Organics) in acetonitrile were used as internal standards for LC-MS/MS.

4.2.5 Microbial community analysis

DNA extraction. The 25 mL samples collected from the QAC-amended and bottle control microcosms with sterile pipettes were immediately vacuum filtered using autoclaved cellulose nitrate filters (diameter = 47 mm, pore size = 0.2 μm; GE Whatman) to concentrate biomass. Autoclaved ultrapure water was used to wet the filters prior to sample addition. Filters were cut or folded with sterile scissors and tweezers and directly immersed in microcentrifuge tubes containing 0.5 mL of Cell Lysis Solution for Tissues and Cells (CLS-TC lysis buffer; MP Biomedicals). Filters were stored at -20 °C to preserve samples until genomic DNA extraction and purification. Three consecutive freeze-thaw cycles were performed followed by a 90-min incubation at 70 °C for cell lysis. DNA was extracted from the filters and purified using a FastDNA SPIN Kit (MP Biomedicals) and stored at -20 °C until DNA was used for qPCR and sequencing.

qPCR. Real-time quantitative qPCR was used to detect and quantify genes of interest: the 16S rRNA gene for *Bacteria* as a measure of total bacterial biomass abundance, the *qacF* gene for QAC resistance, and a suite of antibiotic resistance (ARG) or integron genes. The bla_{OXA}, *mexB*, *sul1*, and *tetA* genes encode for β-lactam resistance, a multidrug efflux pump, sulfonamide, and tetracycline resistance, respectively. The *intI1*, *intI2*, *intI3* genes encode class 1, 2, and 3 integron integrases, respectively. Integrons are mobile genetic elements associated with the spread of antibiotic resistance.[172] Sample qPCR primers and methodology were as described by Sandberg et al. (2018).[200] The number of gene copies in each sample was determined with serially diluted standards of concentration range 10^8 to 10^1 gene copies μL^{-1} for *qacF*, ARGs, or integrons ($R^2 \geq 0.999$). The number of gene copies in each sample was determined with a

serially diluted standard curve of concentration ranges 10^9 to 10^2 gene copies L^{-1} for the 16S rRNA gene ($R^2 = 0.997$). Standards for qPCR were purchased as gBlocks from Integrated DNA Technologies. The qPCR mixture for all primer sets contained 2 μL undiluted template DNA, 1 μL bovine serum albumin (BSA), 10 μL SsoFast EvaGreen Supermix with Low ROX, 0.08 μL of 100 μM forward primer and 0.04 μL of 100 μM reverse primer, and 6.9 μL PCR H_2O per reaction. Amplification curves were visually inspected for PCR inhibition and compared between standards and samples to ensure amplification with similar efficiency (96.6 ± 4.3%). Melt curves were analyzed to ensure the absence of primer-dimer and non-specific amplification. The censoring limit was defined as the lowest standard for a given qPCR assay that amplified (100 copies per μL for 16S rRNA gene, 10 copies per μL for *qacF* , ARGs, and integrons) normalized by filtrate volume (0.25 L) of the microcosm water sample used for DNA extraction.

High-throughput 16S rRNA gene sequencing. Illumina MiSeq paired end sequencing (2 × 300 bp) was completed on the V5-V6 region of the 16S rRNA gene for bacterial community analysis. The University of Minnesota Genomics Center (UMGC) performed amplification and sequencing using UMGC 16S primers targeting the V5V6 region on an Illumina MiSeq platform.[201] Sequence reads were demultiplexed, trimmed, and filtered using QIIME2 version 2018.2. Amplicon sequence variants (ASVs) were determined using DADA2[202,203] and then assigned consensus taxonomy using the SILVA 132 rRNA database.[204]

Both alpha (Shannon, Simpson, Chao1, and Observed ASVs) and beta diversity (Bray-Curtis and Weighted UniFrac distance matrices) were computed using QIIME2 (pipeline: core-metrics-phylpenetic) after sequence libraries were randomly trimmed

down to 35,000 sequences per profile. Principal coordinate analysis (PCoA) plots were created to visualize the community dissimilarity using the *cmdscale* command in R (version 3.6.2).

Statistical analyses. For qPCR data, statistical tests were performed on log-transformed 16S rRNA gene, ARG, and integron quantities using R.[205] Two-sided t-tests (95% confidence level) were conducted to assess differences between amended and bottle control microcosms on specific days. Histograms and QQ plots were generated to assess the reasonableness of assumptions that the data represented a random sampling from a Normal distribution prior to proceeding with two independent samples t-test analysis. T-tests were used due to the unbalanced nature of the data because replicates ranged from 3 to 4. One-way analysis of variance (ANOVA), however, was also performed using the *aov* function in R and these results agreed with the t-tests. For many ARGs and integrons, measurements were consistently left-censored (below the censoring limit or limit of quantification of 4 log copies/L). When censored data was present, hypothesis testing was performed using a generalized Wilcoxon rank sum test (nonparametric Peto-Prentice score test) using the *cendiff* function in the "NADA" package in R on $\log_{10}$-transformed gene quantities to determine statistically significant differences between groups.

For microbial community data, Mantel tests were used to test statistically significant effects of experimental conditions and variables on microbial community structure through matrix correlation between two dissimilarity matrices (beta diversity matrices and Euclidean matrices of experimental factors). The tests were conducted using the *mantel* function in the "vegan" R package and Mantel statistics based on Spearman's rank correlation rho (999 permutations). Permutational multivariate analysis of variance

(PERMANOVA) tests (999 permutations) were performed using the *adonis* function in "vegan" to determine if there was a statistically significant difference in sample groups.

4.3 Results and Discussion

4.3.1 QAC Degradation Over Time

Figure 4-1 shows the relative QAC concentration over time and sequential spikes in amended biotic and abiotic (or sterile) microcosms. Concentrations measured in the river water prior to amendment were below the limit of detection (2 nM for ATMA, 1 nM for BAC, and 7 – 9 nM for DADMA). After the first amendment with the methanol stock, a lag phase of one to two days was observed before QAC loss commenced. Abiotic losses appeared to be negligible while clear biotic degradation was observed. For DADMA and BAC, scatter was observed in the sterile control results due to analytical variability. Despite this, there is no clear trend of QAC loss on the time scale that degradation is seen in the biotic microcosms. At day 7, average biotic removal was 84% for BAC, 73% for ATMA, and 56% for DADMA. For the sequential amendments, a similar trend of biodegradation rates of BAC > ATMA > DADMA was observed, and degradation occurred more quickly in the second and third amendments compared to the first amendment. The methanol in the QAC spike perhaps had a stimulating effect on the community after an initial lag phase.

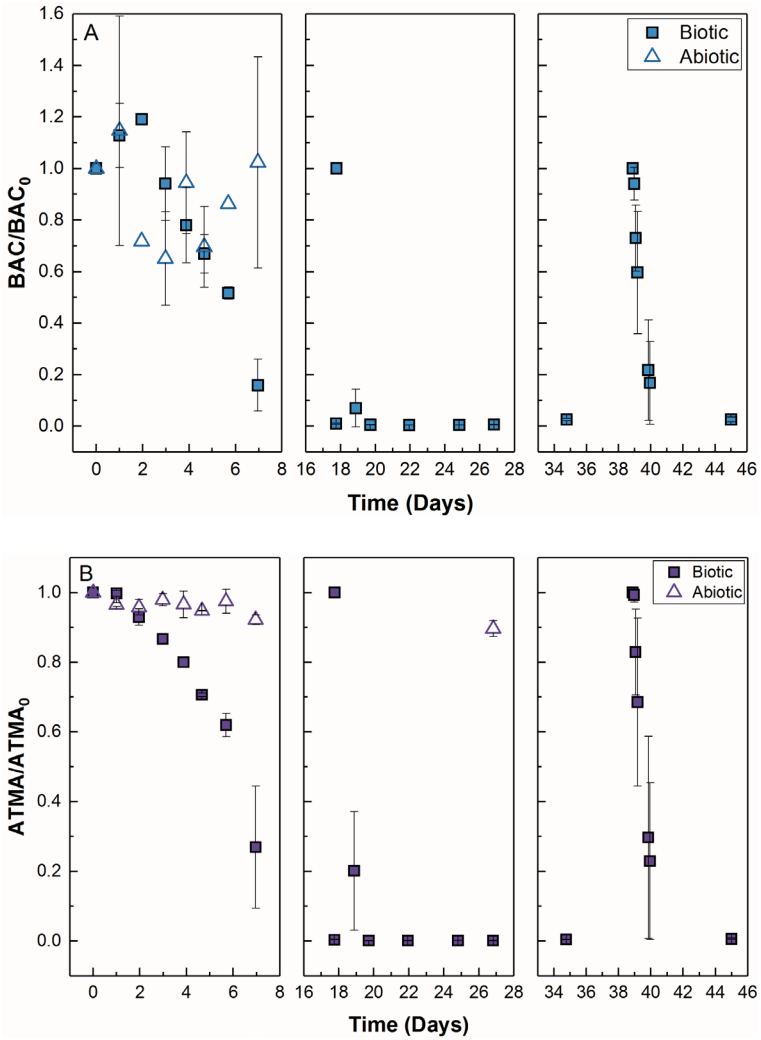

Figure 4-1. Relative QAC concentration over time after sequential amendments for A) C_{12}-BAC, B) C_{12}-ATMA, and C) C_{12}-DADMA in amended biotic and sterile (abiotic) microcosms. Error bars represent one standard deviation of replicates (n = 3 - 4).

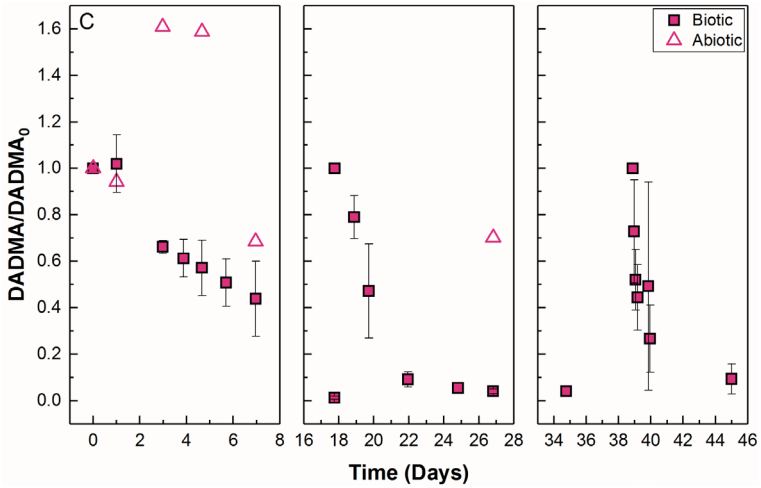

Figure 4-1 continued. Relative QAC concentration over time after sequential amendments for A) C_{12}-BAC, B) C_{12}-ATMA, and C) C_{12}-DADMA in amended biotic and sterile (abiotic) microcosms. Error bars represent one standard deviation of replicates (n = 3 - 4).

4.3.2 qPCR

Results from qPCR analysis for 16S rRNA genes are shown in Figure 4-2. The abundance of 16S rRNA genes was determined in river water prior to QAC amendment (Day 0) to range from 2.3×10^6 to 1.8×10^7 gene copies/L. Eight days after the first QAC amendment, a significant increase in bacterial biomass was observed in the amended biotic microcosms (AQ) compared to the river water at day 0 (p-value = 0.02), but not in the ambient bottle control (BC; p-value = 0.17). Based on a two-sided t-test, the results for AQ and BC were statistically different (p-value = 1.8×10^{-3}) from each other at Day 8. This is likely to be a result of the addition of methanol into the amended microcosms with the first spike from the QAC stock. It was determined that 1.8 mg/L of C was added to the microcosms from the methanol, compared to 0.4 mg/L of C added from the QACs. The differential between the ambient river water temperature when it was collected and the microcosm operational temperature, however, might have also influenced the increase in bacterial biomass. At 27 days (after the second QAC amendment at 18 days), there was

no statistically significant difference between 16S rRNA $\log_{10}$ gene copies/L in the amended and control microcosms (p-value = 0.24) despite another methanol addition with the second QAC spike. A third QAC amendment (from aqueous stock) occurred at 39 days and final biological sampling occurred at 62 and 63 days for BC and AQ, respectively, at which time there was a statistically significant difference in the number of 16S rRNA $\log_{10}$ gene copies/L between the two treatments (p-value = 0.03). The amended microcosms saw a lasting increase in biomass quantity compared to the initial value (p-value = 0.04); this was not the case for the BC treatments where the number of 16S rRNA genes were statistically similar on Day 62 versus Day 0 (p-value = 0.17). Overall, there was a significant difference at Day 8 and 62 between AQ and BC. It is possible the addition of methanol as opposed to the presence of QACs altered the bacterial biomass in the microcosms, in particular at Day 8 after the initial spike. The fact there was not a statistical difference between the microcosms on Day 27 suggests that the microbial community rebounded or did not experience lasting changes from the methanol and QAC addition and that laboratory conditions also promoted concurrent changes in the community.

The antibiotic resistance genes analyzed were: *sul1*, a specific antibiotic resistance gene that encodes for resistance to sulfonamide antibiotics; *tet*(A), one specific gene of the generic *tet* class of antibiotic resistance genes that encode for resistance to tetracycline; bla_{OXA}, which encodes for β-lactamase and metallo-β-lactamase associated with penicillin resistance. Additionally, a gene encoding a multi drug efflux pump, *mexB*, and *qacF*, a homologue of QAC resistance genes which belongs to the multidrug resistance family found on class 1 integrons, were analyzed. Integrons are genetic

elements that facilitate the integration, expression, and exchange of DNA. Integrons like transposons and plasmids are considered mobile genetic elements, which encode enzymes or other proteins to facilitate spread of genetic material between bacteria. Integrons are not antibiotic resistance genes, but class 1 integron, for example, is commonly found in polluted environments and shows a positive correlation with ARGs. Figure 4-2, panels B-I, show the quantity of gene copies per volume for *qacF*, the ARGs, and the integron-integrase genes. Two ARGs (*bla*$_{OXA}$ and *tetA*) and two integrons (*intI1* and *intI3)* were detected in the microcosms in most sampling events; the other genes were either detected at quantities below censoring limits or not detectable. There was a statistically significant difference between the AQ versus BC treatments for *bla*$_{OXA}$ gene copies at Day 27 (p-value = 0.01), *tetA* gene copies at Day 8 (p-value = 0.03), and *intI1* gene copies at Day 8 (p-value = 0.03) using the Wilcoxon test.

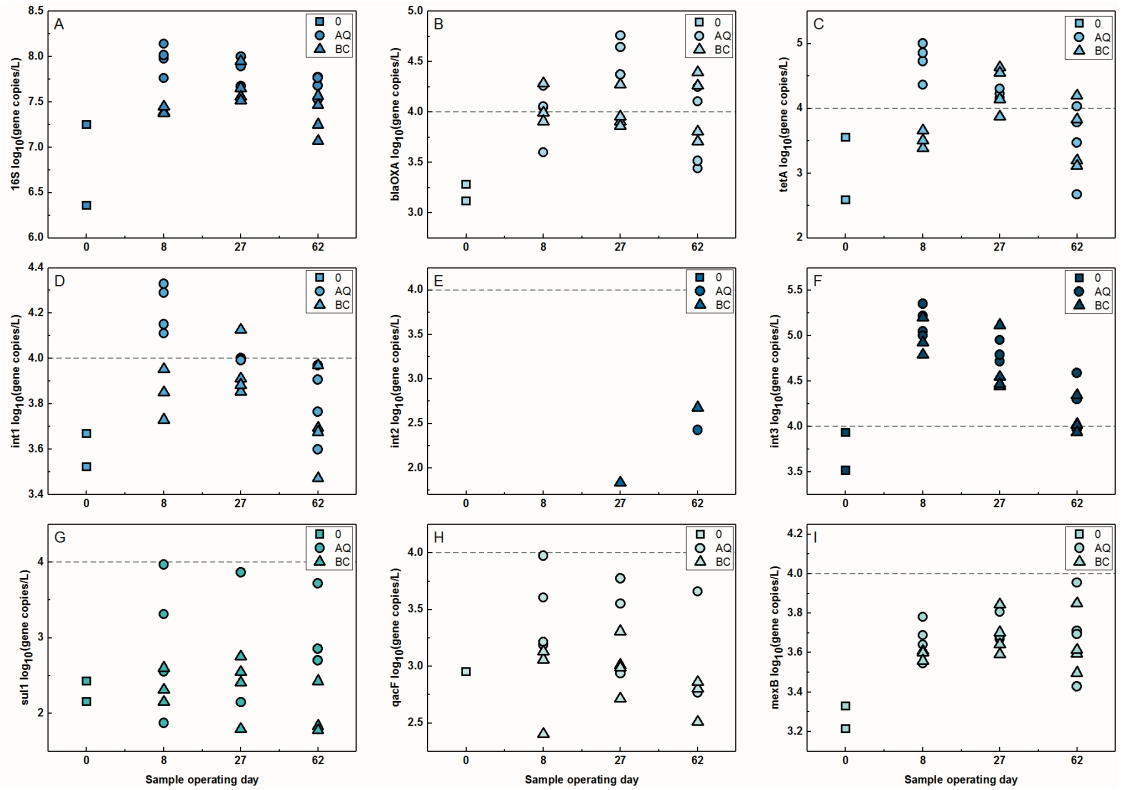

Figure 4-2. Abundance of 16S rRNA gene copies (A) and antibiotic and qac resistance gene copies (B – I) over time in initial river water samples (□, 0), QAC amended microcosms (○, AQ), and bottle controls (△, BC). The dashed line in plots B – I indicates the censoring limit. Non-detects are not displayed.

Relative abundance results (i.e., the normalized quantity of genes to 16S rRNA gene copy numbers) are shown in Figure 4-3 and reveal little differentiation between the relative numbers of these genes in AQ versus BC microcosms over time. This indicates that the community does not seem to be acquiring resistance. The presence of QACs is not enriching or conferring negative function on the community or the response is limited and transitory. Rather, the increases seen in abundance of these genes trend with growth of the community as a whole possibly due to the methanol addition. The growth seen in the microcosms could be because of the methanol addition, which might have a protective effect on at least some organisms with respect to conferring and transferring

antibiotic resistance. Microorganisms in high growth mode would be under less stress and thus less likely to pick up antibiotic resistance genes. The impact of QACs under nutrient limited or stressed conditions might lead to different results.

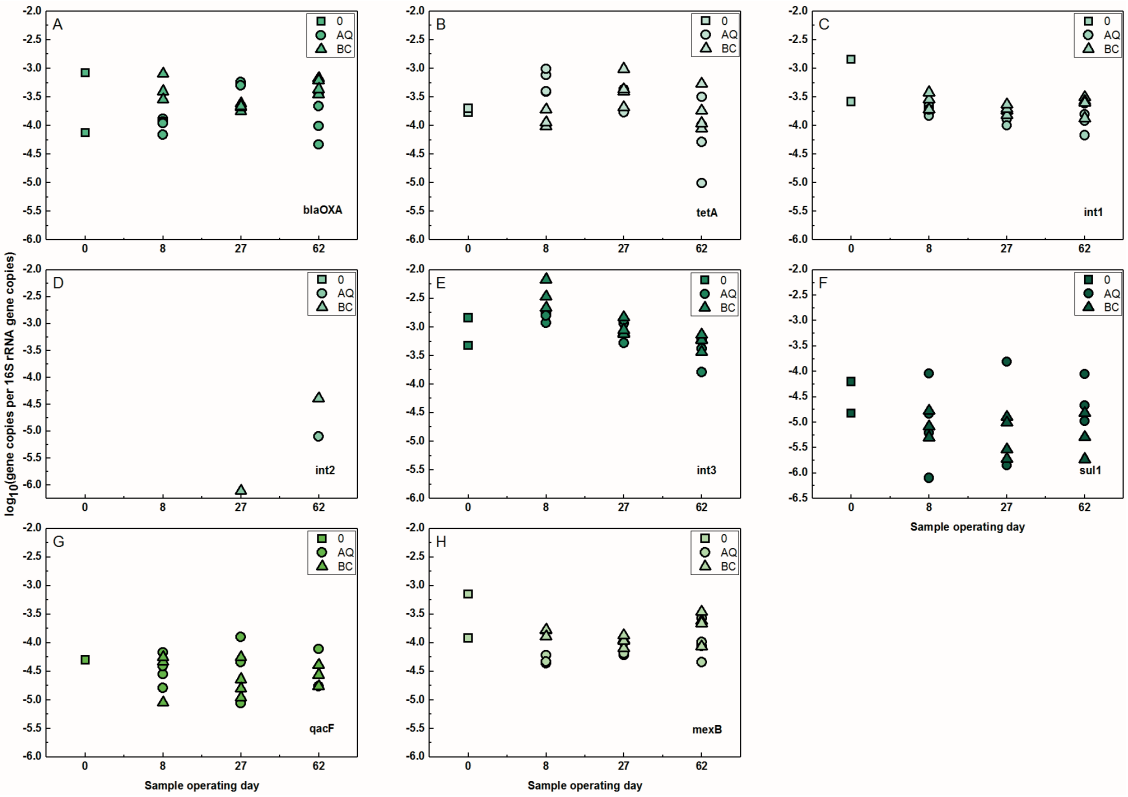

Figure 4-3. Relative abundance of antibiotic and QAC resistance gene copies over time in initial river water samples (□, 0), QAC amended microcosms (○, AQ), and bottle controls (△, BC). Non-detects are not displayed.

4.3.3 Microbial Community Changes

The taxonomy of the river water population in the AQ and BC microcosms is shown in Appendix C. Different richness and evenness alpha diversity metrics were used to compare the AQ and BC microcosms over time (Figure 4-4). Richness – measured by Shannon, Observed ASVs, and Chao1 – noticeably decreased after QAC amendment, though the difference is less apparent for Simpson. The decrease in alpha diversity for AQ and increase for BC at Day 8 were statistically significant from Day 0 only for

Shannon (p-value = 0.05 and p-value = 0.01, respectively) based on a two-sided t-test. Richness and evenness in the amended microcosms was consistently lower than the control over the course of sequential amendments (in particular Shannon Day 8, p-value = 0.001; Chao1 Day 8, p-value = 0.02; Chao1 Day 27, p-value = 0.004; Observed ASV Day 8, p-value = 0.02; Observed ASV Day 27, p-value = 0.004) and the experimental duration, though both saw an increase over time. At the end of the experiment, however, the diversity differences are largely erased, which suggests acclimation. The control microcosms maintained higher richness when looking at the Observed ASV metric, which focuses on unique ASVs, and Chao1, which focuses on rare ASVs. The differences seen in alpha diversity between the microcosms are consistent with the methanol addition from QAC amendment – the methanol most likely enriched certain microorganisms within the sub-population, accounting for the decrease in alpha diversity in AQ compared to BC after the first and second spikes. The temporal shift in richness, as indicated by Shannon, for both AQ and BC at the end is also suggestive of the influence of lab conditions on both microcosms and eventual depletion and limitation of nutrients. Evenness as indicated by Simpson was more consistent for AQ and BC at each time point.

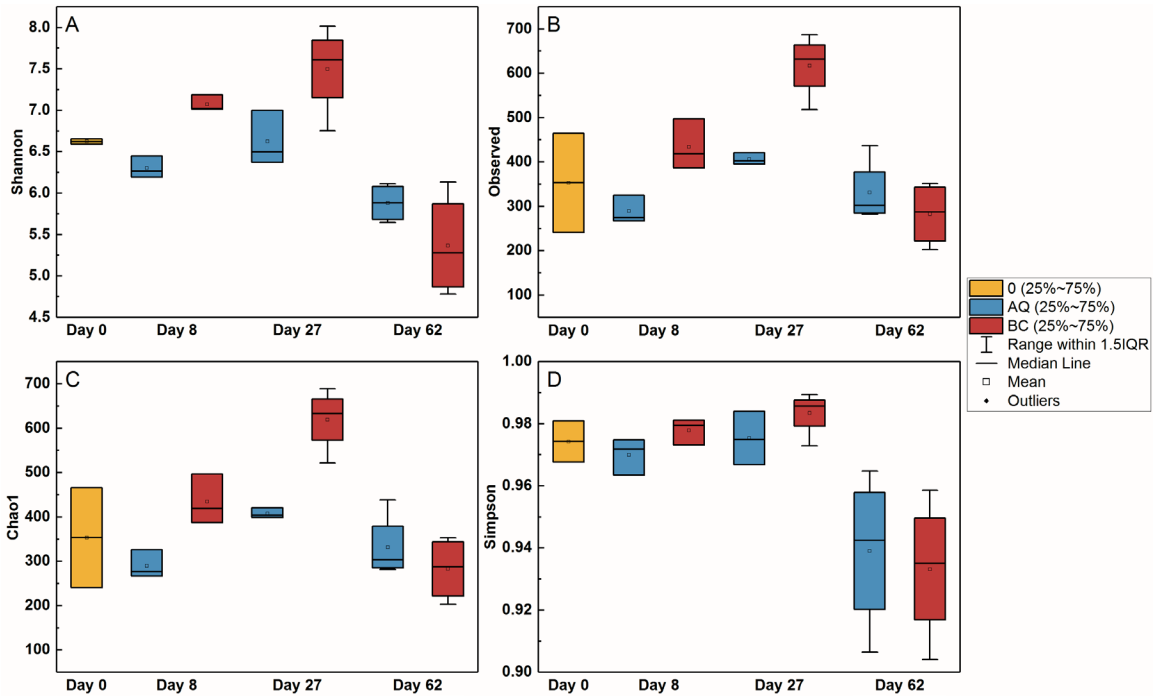

Figure 4-4. Alpha diversity measurements over sampling time. Richness and evenness alpha diversity metrics comparing QAC amended (AQ) and bottle control (BC) microcosms over time: A) Shannon index, B) Observed ASV, C) Chao1, D) Simpson's index.

Beta diversity was calculated using weighted Bray-Curtis and Weighted UniFrac distance matrices. Data was ordinated using a Principal Coordinate Analysis (PCoA) (Figure 4-5 and Figure 4-6). Clustering by PCo 1 explains 51.7% variation in the microbial community for Weighted UniFrac and 22.5% for Bray-Curtis. Clustering by PCo 2 explains 17.2 % (Weighted UniFrac) and 18.2% (Bray-Curtis) while clustering by PCo 3 explains 10.7% (Weighted UniFrac) and 12.2% (Bray-Curtis) variation. There was visible clustering by microcosm (or "Reactor") type and day. Based on a Mantel tests for amended (AQ) microcosms, temperature, QAC amendment concentration, and time were statistically significant drivers with concentration and day having higher Spearman's rank correlation coefficients (Table 4-1), suggesting these factors account for much of the

microbial community variance. The PCoA plots show a clear temporal variation in community composition. The effect of QAC amendment was also significant. Weighted UniFrac and Bray-Curtis, however, point to different conclusions. The separation between AQ and BC was clear in the Bray-Curtis PCoA but not evident in the Weighted UniFrac PCoA.

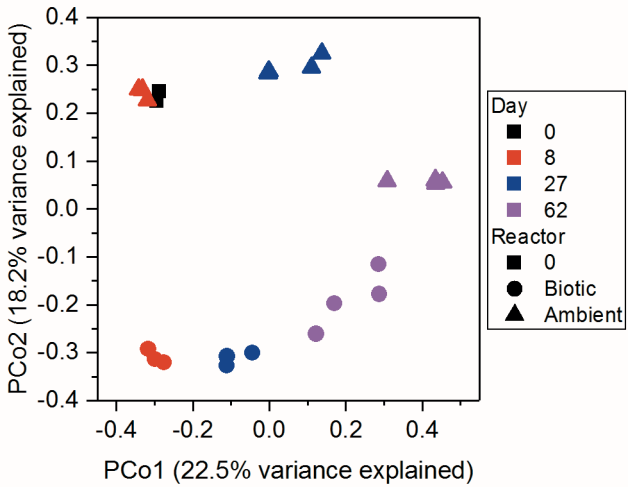

Figure 4-5. Principal coordinate analysis (PCoA) plot of microbial community changes over time in QAC-amended biotic and ambient bottle control microcosms. Bray-Curtis beta diversity measurements where PCo1 explains 22.5% of the variance and PCo2 explains 18.2%.

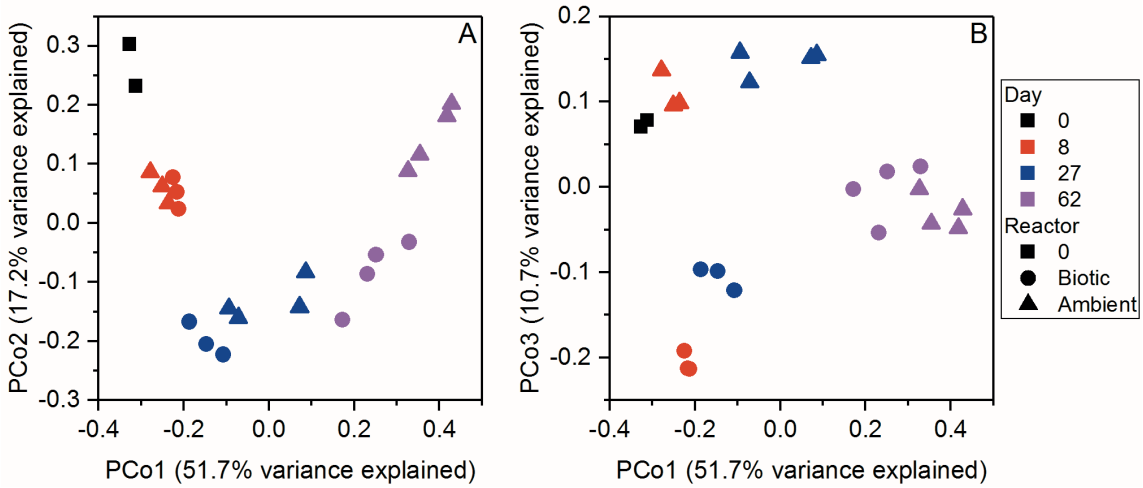

Figure 4-6. Principal coordinate analysis (PCoA) plot of microbial community changes over time in QAC-amended biotic and ambient bottle control microcosms. Weighted UniFrac beta diversity measurements where PCo1 explains 51.7% of the variance, PCo2 explains 17.2%, and PCo3 explains 10.7%.

Comparing Weighted UniFrac (Figure 4-6A) results with Unweighted UniFrac (Figure 4-7A) provides insight on whether rare organisms are driving the shift seen between AQ and BC. Weighted UniFrac accounts for the abundance of observed organisms, weighting phylogenetic tree branch lengths by the abundances and thus emphasizing dominant microorganisms. Unweighted is based on presence or absence of organisms and generally emphasizes minor microogranisms. With Weighted UniFrac there is a visible monotonic clustering correlated with time along PCo1. This temporal trend is also seen along PCo1 for Unweighted UniFrac. While there is clustering between the two reactor types along PCo2 for Weighted UniFrac, a separation is seen, however, for Unweighted UniFrac. The results show a divergence between AQ and BC due to rarer ASVs after the QAC amendment with methanol.

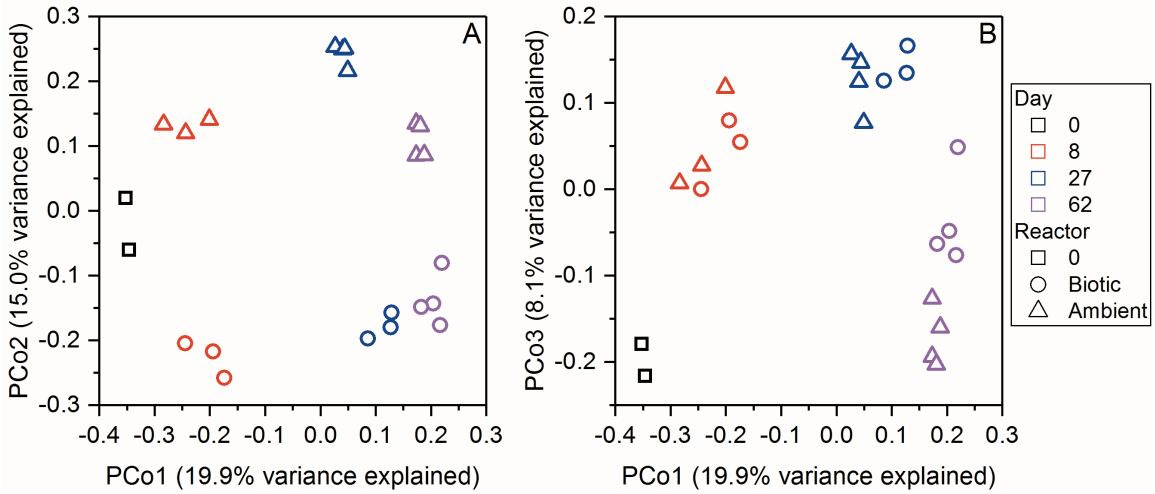

Figure 4-7. Principal coordinate analysis (PCoA) plot of microbial community changes over time in QAC-amended biotic and ambient bottle control microcosms. Unweighted UniFrac beta diversity measurements where PCo1 explains 19.9% of the variance, PCo2 explains 15.0%, and PCo3 explains 8.1%.

Table 4-1. Spearman's rank correlation coefficient (rho) of Mantel tests between beta diversity distance matrices for AQ and the dissimilarity matrix of experimental parameters

Beta Diversity	"Temperature"	*P*-value[1]	"QAC concentration"	*P*-value[1]	"Sample operating day"	*P*-value[1]
Bray-Curtis	0.3962	**0.042**	0.86	**0.002**	0.86	**0.001**
Weighted UniFrac	0.4452	**0.029**	0.947	**0.003**	0.947	**0.002**

[1]Levels of statistical significance based on 999 free permutations.

4.4 Conclusion

A portion of the microbial community in Mississippi River water has the capability to aerobically degrade QACs at low concentrations, which supports the general conclusions of previous research that QACs are aerobically biodegradable in the environment.[42,52,117] As far as we are aware, the work presented here is the first to evaluate this phenomenon in river water considering a subset of the native microbial population and at QAC concentrations of tens of μg/L. There was relatively rapid depletion of the mixture of 3 different QAC classes after sequential spikes in spite of methanol addition with the first two QAC amendments. While several antibiotic resistance genes were detected in microcosms, there was no clear connection between exposure to low QAC concentrations and increase in gene abundance. Based on community analysis, the bacterial communities cluster and separate based on microcosm, and both AQ and BC undergo temporal shifts throughout the experiment. The difference between Bray-Curtis and Weighted UniFrac results suggests that even though the community compositional difference is large between the amended biotic and bottle control microcosms, there is not a large phylogenetic difference. The QAC amendment caused a compositional difference but not significant ecological drift considering phylogeny. It seems that bacteria that were phylogenetically similar to the predominant bacteria in the control microcosms were eventually enriched based on these beta-diversity measurements. Comparing Weighted UniFrac with Unweighted UniFrac demonstrates that rarer (i.e. less dominant) ASVs account for the separation seen between the QAC amended and ambient bottle control microcosms, which could be due to the methanol.

Conflicts of Interest

The authors declare no conflicts of interest.

Acknowledgements

The authors thank Dr. Sarah Pati for assistance with LC-MS/MS measurements and informative discussions, Dr. Ben Ma for guidance on sequencing, Emma O'Leary for performing qPCR measurements, and Annika Heaps for assistance with laboratory work. We would also like to acknowledge Makenzie Pillsbury for help with LC-MS/MS measurements. Mass spectrometry was carried out in the Analytical Biochemistry Shared Resources of the Masonic Cancer Center, University of Minnesota, funded in part by Cancer Center Support Grant CA-77598. The authors acknowledge the Minnesota Supercomputing Institute (MSI) at the University of Minnesota for providing resources that contributed to the sequencing results. This work was funded by the Minnesota Environmental and Natural Resources Trust fund (M.L. 2017, Chp. 96, Sec. 2, Subd. 04a) as recommended by the Legislative and Citizen Commission on Minnesota Resources.

Chapter 5. Conclusions

5.1 Summary

Because organic chemicals found in frequently used consumer, personal care, industrial, and health products continue to be detected in surface waters, alarm has been raised within the scientific community as well as by the general public about the impacts of these contaminants of emerging concern on ecosystem and human health. This dissertation expands understanding of attenuation pathways within engineered and natural systems for contaminants of emerging concern like pharmaceuticals and surfactants/biocides. The work presented in this dissertation provides concrete metrics on the photochemical and microbiological fate of a variety of CECs and the data produced can be used to better understand their fate as well as guide any future regulatory decisions.

The second chapter of this work explored direct and indirect photolysis of frequently detected pharmaceuticals within the context of wastewater disinfection. In particular, it evaluated the potential to use NO_2^- generated from partial nitritation/anaerobic ammonium oxidation, an anaerobic nitrogen removal process that has gained interest due to the prospect of energy-savings, to generate radicals such as hydroxyl radical upon absorption of UV or sunlight. The incomplete removal of many pharmaceuticals during conventional and anaerobic wastewater treatment has been documented. Hydroxyl radical is a potent oxidant and could be harnessed to breakdown pharmaceuticals. This work demonstrated a de-facto advanced oxidation process could be devised through theoretical unit process modifications. Nitrite generated sufficient hydroxyl radical to break down the pharmaceuticals. About one half-life was achieved

within 2 hours for wavelengths greater than 280 nm with indirect photolysis dominating while about 2 half-lives were achieved within an hour for wavelengths greater than 220 nm with direct and indirect photolysis factoring in pharmaceutical losses. Nitrosamines were generated in the process, however, with modeling suggesting there is a risk for high nitrosamine accumulation.

The third chapter looked at the direct and indirect photolysis of widely used quaternary ammonium compounds (QACs) in surface water, a topic that had previously not been extensively explored. The roles of various photochemically produced reactive intermediates were evaluated through a series of model sensitizer and quencher experiments under simulated sunlight. Hydroxyl radical was determined to play an important role in the photochemical fate of the QACs studied though one QAC, benzethonium, also underwent direct photochemical degradation. Bimolecular reaction rate constants were calculated for the QACs and hydroxyl radical under simulated sunlight for the sensitized experiments as well as for experiments conducted in actual river water. To verify the transferability of laboratory results, outdoor photolysis was carried out in river water. The results demonstrated and validated that reaction with hydroxyl radical is a major controlling factor in the photochemical fate of QACs. Though bimolecular reaction rate constants calculated from laboratory and outdoor experiments showed that QACs readily and rapidly react with hydroxyl radical at or near diffusion controlled rates, estimated photochemical half-lives are on the order of weeks to months. The half-lives, which could be considered lower bound estimates based on assumptions of hydroxyl radical steady-state concentration and sunlight exposure, point to the relative persistence of QACs in the aquatic environment if only abiotic degradation is considered.

The fourth chapter investigated the biotransformation of a sub-inhibitory mixture of three QACs. While aerobic biodegradation has been explored over the years, there was a need to reevaluate the topic because previous work on degradation in an environmental context has involved enrichment of QAC-resistant degraders from sediment and soil and focused mostly on BACs. The concentrations used in these studies were also higher than what has been detected in surface waters. The study presented in Chapter 4 looked at a mixture of QACs, in particular at low environmentally relevant concentrations, and the impact on a subset of a native river water microbial population not enriched from contaminated soil or sediment and maintained on QACs. Furthermore, it was of interest to consider whether short term, low-level exposures resulted in an increase in antibiotic resistance genes or in substantial microbial community compositional changes as a means of delving into the ecotoxicological risks QACs allegedly pose. Results demonstrated that low concentrations of QACs are transformed over multiple exposures. There was no statistically significant and lasting impact on presence of antibiotic resistance genes between river microcosms amended with QAC mix and those that were not. Exposure to the QAC mix did induce community compositional changes (based on beta diversity as measured by Bray-Curtis dissimilarity) though it is as of yet unclear whether this is the result of the QACs themselves or if methanol present in the initial dosing of the QAC mix was a confounding factor due to a stimulating affect.

5.2 Recommendations and future work

The results presented in this dissertation can be used to inform treatment and regulatory decisions with regard to curtailing the release of CECs in the environment as well as evaluating the overall risk to ecosystem health and impact on public water

supplies. Additionally, this work points towards the possibility of construction and use of shallow treatment wetlands as a polishing step to enhance the removal of the studied compounds from wastewater effluents prior to discharge into surface or groundwater. Future work involving field and pilot studies could be useful, especially for compounds that are photolabile and biodegradable.

Future work on the role of reactive nitrogen species generated from nitrite photolysis might be worth investigating. While hydroxyl radical – based on bimolecular reaction rate constants and steady-state concentrations – might be of relative greater importance in degradation of certain CECs depending on presence of scavengers and sinks, reactive nitrogen species like $NO_2^{\bullet}$ could play a part, in particular for compounds with electron-rich moieties. Additionally, nitrite photolysis potentially generates nitrated or nitrosated transformation products (as demonstrated with formation of nitrosamines in chapter 2) that could be more toxic compared to the parent compound.[206] Identification of pharmaceutical transformation products in this setting would be useful from a public health perspective to ensure products are not more toxic, mutagenic, and carcinogenic. Assessing the biodegradability of these transformation products to confirm whether they are more or less biodegradable than the parent compounds would also be informative. Moreover, there is a paucity of research on nitrosamine formation from nitrite photolysis. A better understanding is needed of precursors and rates and mechanism of formation in order to mitigate nitrosamine formation.

Anaerobic degradation of QACs has largely been considered to be very limited to nonexistent. With recent work tracking and quantifying QAC concentrations in sediment cores over a decade apart in sampling time, *in situ* degradation was observed for ATMAC

and BAC while DADMAC was concluded to be recalcitrant.[162] The time scale of anaerobic degradation for shorter alkyl chain homologues of ATMAC was on the order of several hundred days in sludge.[25] Longer term research tracking the anaerobic degradation of QACs like ATMAC and BAC, determining mechanisms, and studying the microbial communities and benthic organisms in sediments where QACs accumulate would fill gaps in knowledge on their chronic environmental impact.

While biodegradation/biotransformation and photolysis of QACs have been investigated separately, a combined study on the co-occurrence of microbiological and photochemical transformation could give a better picture of the overall fate of QACs, teasing out parallel and consecutive processes. It is conceivable that for certain QACs phototransformation could affect their biodegradation potential. The interplay between photolysis and biodegradation could especially be of interest when evaluating the suitability of an engineered wetland to remove these compounds from wastewater effluent.

Bibliography

(1) Eggen, R. I. L.; Hollender, J.; Joss, A.; Schärer, M.; Stamm, C. Reducing the Discharge of Micropollutants in the Aquatic Environment: The Benefits of Upgrading Wastewater Treatment Plants. *Environ. Sci. Technol.* **2014**, *48* (14), 7683–7689. https://doi.org/10.1021/es500907n.

(2) Petrie, B.; Barden, R.; Kasprzyk-Hordern, B. A Review on Emerging Contaminants in Wastewaters and the Environment: Current Knowledge, Understudied Areas and Recommendations for Future Monitoring. *Water Res.* **2014**, *72*, 3–27. https://doi.org/10.1016/j.watres.2014.08.053.

(3) Keen, O. S.; Baik, S.; Linden, K. G.; Aga, D. S.; Love, N. G. Enhanced Biodegradation of Carbamazepine after UV/H2O2 Advanced Oxidation. *Environ. Sci. Technol.* **2012**, *46* (11), 6222–6227. https://doi.org/10.1021/es300897u.

(4) Lam, M. W.; Young, C. J.; Brain, R. A.; Johnson, D. J.; Hanson, M. A.; Wilson, C. J.; Richards, S. M.; Solomon, K. R.; Mabury, S. A. Aquatic Persistence of Eight Pharmaceuticals in a Microcosm Study. *Environ. Toxicol. Chem.* **2004**, *23* (6), 1431–1440. https://doi.org/10.1897/03-421.

(5) Monsalvo, V. M.; McDonald, J. A.; Khan, S. J.; Le-Clech, P. Removal of Trace Organics by Anaerobic Membrane Bioreactors. *Water Res.* **2014**, *49*, 103–112. https://doi.org/10.1016/j.watres.2013.11.026.

(6) Alvarino, T.; Suarez, S.; Katsou, E.; Vazquez-Padin, J.; Lema, J. M.; Omil, F. Removal of PPCPs from the Sludge Supernatant in a One Stage Nitritation/Anammox Process. *Water Res.* **2015**, *68*, 701–709. https://doi.org/10.1016/j.watres.2014.10.055.

(7) Wijekoon, K. C.; McDonald, J. A.; Khan, S. J.; Hai, F. I.; Price, W. E.; Nghiem, L. D. Development of a Predictive Framework to Assess the Removal of Trace Organic Chemicals by Anaerobic Membrane Bioreactor. *Bioresour. Technol.* **2015**, *189*, 391–398. https://doi.org/10.1016/j.biortech.2015.04.034.

(8) Sathyamoorthy, S.; Chandran, K.; Ramsburg, C. A. Biodegradation and Cometabolic Modeling of Selected Beta Blockers during Ammonia Oxidation. *Environ. Sci. Technol.* **2013**, *47* (22), 12835–12843. https://doi.org/10.1021/es402878e.

(9) Hird, C. M.; Urbina, M. A.; Lewis, C. N.; Snape, J. R.; Galloway, T. S. Fluoxetine Exhibits Pharmacological Effects and Trait-Based Sensitivity in a Marine Worm. *Environ. Sci. Technol.* **2016**, *50* (15), 8344–8352. https://doi.org/10.1021/acs.est.6b03233.

(10) Arnnok, P.; Singh, R. R.; Burakham, R.; Pérez-Fuentetaja, A.; Aga, D. S. Selective Uptake and Bioaccumulation of Antidepressants in Fish from Effluent-Impacted Niagara River. *Environ. Sci. Technol.* **2017**, *51* (18), 10652–10662. https://doi.org/10.1021/acs.est.7b02912.

(11) Yan, S.; Wang, M.; Zha, J.; Zhu, L.; Li, W.; Luo, Q.; Sun, J.; Wang, Z. Environmentally Relevant Concentrations of Carbamazepine Caused Endocrine-Disrupting Effects on Nontarget Organisms, Chinese Rare Minnows (Gobiocypris Rarus). *Environ. Sci. Technol.* **2018**, *52* (2), 886–894. https://doi.org/10.1021/acs.est.7b06476.

(12) Keen, O. S.; Linden, K. G. Degradation of Antibiotic Activity during UV/H2O2

Advanced Oxidation and Photolysis in Wastewater Effluent. *Environ. Sci. Technol.* **2013**, *47* (22), 13020–13030. https://doi.org/10.1021/es402472x.
(13) Snyder, S. A.; Westerhoff, P.; Yoon, Y.; Sedlak, D. L. Pharmaceuticals, Personal Care Products, and Endocrine Disruptors in Water: Implications for the Water Industry. *Environ. Eng. Sci.* **2003**, *20* (5), 449–469. https://doi.org/10.1089/109287503768335931.
(14) Clarke, B. O.; Smith, S. R. Review of "emerging" Organic Contaminants in Biosolids and Assessment of International Research Priorities for the Agricultural Use of Biosolids. *Environ. Int.* **2011**, *37* (1), 226–247. https://doi.org/10.1016/j.envint.2010.06.004.
(15) Michael, I.; Rizzo, L.; McArdell, C. S.; Manaia, C. M.; Merlin, C.; Schwartz, T.; Dagot, C.; Fatta-Kassinos, D. Urban Wastewater Treatment Plants as Hotspots for the Release of Antibiotics in the Environment: A Review. *Water Res.* **2013**, *47* (3), 957–995. https://doi.org/10.1016/j.watres.2012.11.027.
(16) Furlong, E. T.; Batt, A. L.; Glassmeyer, S. T.; Noriega, M. C.; Kolpin, D. W.; Mash, H.; Schenck, K. M. Nationwide Reconnaissance of Contaminants of Emerging Concern in Source and Treated Drinking Waters of the United States: Pharmaceuticals. *Sci. Total Environ.* **2017**, *579*, 1629–1642. https://doi.org/10.1016/j.scitotenv.2016.03.128.
(17) Oulton, R. L.; Kohn, T.; Cwiertny, D. M. Pharmaceuticals and Personal Care Products in Effluent Matrices: A Survey of Transformation and Removal during Wastewater Treatment and Implications for Wastewater Management. *J. Environ. Monit.* **2010**, *12* (11), 1956. https://doi.org/10.1039/c0em00068j.
(18) Benotti, M. J.; Trenholm, R. A.; Vanderford, B. J.; Holady, J. C.; Stanford, B. D.; Snyder, S. A. Pharmaceuticals and Endocrine Disrupting Compounds in U.S. Drinking Water. *Environ. Sci. Technol.* **2009**, *43* (3), 597–603. https://doi.org/10.1021/es801845a.
(19) Kostich, M. S.; Batt, A. L.; Lazorchak, J. M. Concentrations of Prioritized Pharmaceuticals in Effluents from 50 Large Wastewater Treatment Plants in the US and Implications for Risk Estimation. *Environ. Pollut.* **2014**, *184*, 354–359. https://doi.org/10.1016/j.envpol.2013.09.013.
(20) Westerhoff, P.; Yoon, Y.; Snyder, S.; Wert, E. Fate of Endocrine-Disruptor, Pharmaceutical, and Personal Care Product Chemicals during Simulated Drinking Water Treatment Processes. *Environ. Sci. Technol.* **2005**, *39* (17), 6649–6663. https://doi.org/10.1021/es0484799.
(21) Verlicchi, P.; Al Aukidy, M.; Zambello, E. Occurrence of Pharmaceutical Compounds in Urban Wastewater: Removal, Mass Load and Environmental Risk after a Secondary Treatment—A Review. *Sci. Total Environ.* **2012**, *429*, 123–155. https://doi.org/10.1016/j.scitotenv.2012.04.028.
(22) Zhang, C.; Cui, F.; Zeng, G.; Jiang, M.; Yang, Z.; Yu, Z.; Zhu, M.; Shen, L. Quaternary Ammonium Compounds (QACs): A Review on Occurrence, Fate and Toxicity in the Environment. *Sci. Total Environ.* **2015**, *518–519*, 352–362. https://doi.org/10.1016/j.scitotenv.2015.03.007.
(23) Ying, G.-G. G. Fate, Behavior and Effects of Surfactants and Their Degradation Products in the Environment. *Environ. Int.* **2006**, *32* (3), 417–431. https://doi.org/10.1016/j.envint.2005.07.004.

(24) Tezel, U.; Pavlostathis, S. G. Role of Quaternary Ammonium Compounds on Antimicrobial Resistance in the Environment. In *Antimicrobial Resistance in the Environment*; John Wiley & Sons, Inc.: Hoboken, NJ, USA, 2011; pp 349–387. https://doi.org/10.1002/9781118156247.ch20.
(25) García, M. T.; Campos, E.; Sanchez-Leal, J.; Ribosa, I. Effect of the Alkyl Chain Length on the Anaerobic Biodegradability and Toxicity of Quaternary Ammonium Based Surfactants. *Chemosphere* **1999**, *38* (15), 3473–3483. https://doi.org/10.1016/S0045-6535(98)00576-1.
(26) Hong, J.; Tezel, U.; Okutman Tas, D.; Pavlostathis, S. G. Influence of Quaternary Ammonium Compounds on the Microbial Reductive Dechlorination of Pentachloroaniline. *Water Res.* **2013**, *47* (17), 6780–6789. https://doi.org/10.1016/j.watres.2013.09.014.
(27) Kahrilas, G. A.; Blotevogel, J.; Stewart, P. S.; Borch, T. Biocides in Hydraulic Fracturing Fluids: A Critical Review of Their Usage, Mobility, Degradation, and Toxicity. *Environ. Sci. Technol.* **2015**, *49* (1), 16–32. https://doi.org/10.1021/es503724k.
(28) Li, X.; Brownawell, B. J. Quaternary Ammonium Compounds in Urban Estuarine Sediment Environments - A Class of Contaminants in Need of Increased Attention? *Environ. Sci. Technol.* **2010**, *44* (19), 7561–7568. https://doi.org/10.1021/es1011669.
(29) Boethling, R. S. Environmental Fate and Toxicity in Wastewater Treatment of Quaternary Ammonium Surfactants. *Water Res.* **1984**, *18* (9), 1061–1076. https://doi.org/10.1016/0043-1354(84)90220-3.
(30) Yang, J.; Tezel, U.; Li, K.; Pavlostathis, S. G. Prolonged Exposure of Mixed Aerobic Cultures to Low Temperature and Benzalkonium Chloride Affect the Rate and Extent of Nitrification. *Bioresour. Technol.* **2015**, *179*, 193–201. https://doi.org/10.1016/j.biortech.2014.12.030.
(31) Olkowska, E.; Ruman, M.; Polkowska, Ż. Occurrence of Surface Active Agents in the Environment. *J. Anal. Methods Chem.* **2014**, *2014*, 1–15. https://doi.org/10.1155/2014/769708.
(32) Olkowska, E.; Polkowska, Z.; Namieśnik, J. Analytics of Surfactants in the Environment: Problems and Challenges. *Chem. Rev.* **2011**, *111* (9), 5667–5700. https://doi.org/10.1021/cr100107g.
(33) Chiaia-Hernandez, A. C.; Krauss, M.; Hollender, J. Screening of Lake Sediments for Emerging Contaminants by Liquid Chromatography Atmospheric Pressure Photoionization and Electrospray Ionization Coupled to High Resolution Mass Spectrometry. *Environ. Sci. Technol.* **2013**, *47* (2), 976–986. https://doi.org/10.1021/es303888v.
(34) Lara-Martín, P. A.; Li, X.; Bopp, R. F.; Brownawell, B. J.; Lara-Martín, P. A.; Li, X.; Bopp, R. F.; Brownawell, B. J. Occurrence of Alkyltrimethylammonium Compounds in Urban Estuarine Sediments: Behentrimonium as a New Emerging Contaminant. *Environ. Sci. Technol.* **2010**, *44* (19), 7569–7575. https://doi.org/10.1021/es101169a.
(35) Li, X.; Brownawell, B. J. Analysis of Quaternary Ammonium Compounds in Estuarine Sediments by LC-ToF-MS: Very High Positive Mass Defects of Alkylamine Ions as Powerful Diagnostic Tools for Identification and Structural

Elucidation. *Anal. Chem.* **2009**, *81* (19), 7926–7935. https://doi.org/10.1021/ac900900y.
(36) Ferrer, I.; Furlong, E. T. Accelerated Solvent Extraction Followed by On-Line Solid-Phase Extraction Coupled to Ion Trap LC/MS/MS for Analysis of Benzalkonium Chlorides in Sediment Samples. *Anal. Chem.* **2002**, *74* (6), 1275–1280. https://doi.org/10.1021/ac010969l.
(37) Pateiro-Moure, M.; Pérez-Novo, C.; Arias-Estévez, M.; Rial-Otero, R.; Simal-Gándara, J. Effect of Organic Matter and Iron Oxides on Quaternary Herbicide Sorption-Desorption in Vineyard-Devoted Soils. *J. Colloid Interface Sci.* **2009**, *333* (2), 431–438. https://doi.org/10.1016/j.jcis.2009.02.019.
(38) Droge, S. T. J.; Goss, K. U. Development and Evaluation of a New Sorption Model for Organic Cations in Soil: Contributions from Organic Matter and Clay Minerals. *Environ. Sci. Technol.* **2013**, *47* (24), 14233–14241. https://doi.org/10.1021/es4031886.
(39) Droge, S. T. J.; Goss, K. U. Ion-Exchange Affinity of Organic Cations to Natural Organic Matter: Influence of Amine Type and Nonionic Interactions at Two Different PHs. *Environ. Sci. Technol.* **2013**, *47* (2), 798–806. https://doi.org/10.1021/es3033499.
(40) Sütterlin, H.; Alexy, R.; Coker, A.; Kümmerer, K. Mixtures of Quaternary Ammonium Compounds and Anionic Organic Compounds in the Aquatic Environment: Elimination and Biodegradability in the Closed Bottle Test Monitored by LC-MS/MS. *Chemosphere* **2008**, *72* (3), 479–484. https://doi.org/10.1016/j.chemosphere.2008.03.008.
(41) van Wijk, D.; Gyimesi-van den Bos, M.; Garttener-Arends, I.; Geurts, M.; Kamstra, J.; Thomas, P. Bioavailability and Detoxification of Cationics: I. Algal Toxicity of Alkyltrimethyl Ammonium Salts in the Presence of Suspended Sediment and Humic Acid. *Chemosphere* **2009**, *75* (3), 303–309. https://doi.org/10.1016/j.chemosphere.2008.12.047.
(42) García, M. T.; Ribosa, I.; Guindulain, T.; Sánchez-Leal, J.; Vives-Rego, J. Fate and Effect of Monoalkyl Quaternary Ammonium Surfactants in the Aquatic Environment. *Environ. Pollut.* **2001**, *111* (1), 169–175. https://doi.org/10.1016/S0269-7491(99)00322-X.
(43) Clara, M.; Scharf, S.; Scheffknecht, C.; Gans, O. Occurrence of Selected Surfactants in Untreated and Treated Sewage. *Water Res.* **2007**, *41* (19), 4339–4348. https://doi.org/10.1016/j.watres.2007.06.027.
(44) Doherty, A. C. The Distribution, Fate and Application as Tracers of Quaternary Ammonium Compounds (QACs) in Sewage Impacted Estuaries., The Graduate School, Stony Brook University: Stony Brook, NY., 2013.
(45) Ruan, T.; Song, S.; Wang, T.; Liu, R.; Lin, Y.; Jiang, G. Identification and Composition of Emerging Quaternary Ammonium Compounds in Municipal Sewage Sludge in China. *Environ. Sci. Technol.* **2014**, *48* (8), 4289–4297. https://doi.org/10.1021/es4050314.
(46) Martínez-Carballo, E.; González-Barreiro, C.; Sitka, A.; Kreuzinger, N.; Scharf, S.; Gans, O. Determination of Selected Quaternary Ammonium Compounds by Liquid Chromatography with Mass Spectrometry. Part II. Application to Sediment and Sludge Samples in Austria. *Environ. Pollut.* **2007**, *146* (2), 543–547.

https://doi.org/10.1016/j.envpol.2006.07.016.
(47) Pateiro-Moure, M.; Arias-Estévez, M.; Simal-Gándara, J. Critical Review on the Environmental Fate of Quaternary Ammonium Herbicides in Soils Devoted to Vineyards. *Environ. Sci. Technol.* **2013**, *47* (10), 4984–4998. https://doi.org/10.1021/es400755h.
(48) Stringfellow, W. T.; Domen, J. K.; Camarillo, M. K.; Sandelin, W. L.; Borglin, S. Physical, Chemical, and Biological Characteristics of Compounds Used in Hydraulic Fracturing. *J. Hazard. Mater.* **2014**, *275*, 37–54. https://doi.org/10.1016/j.jhazmat.2014.04.040.
(49) Martínez-Carballo, E.; Sitka, A.; González-Barreiro, C.; Kreuzinger, N.; Fürhacker, M.; Scharf, S.; Gans, O. Determination of Selected Quaternary Ammonium Compounds by Liquid Chromatography with Mass Spectrometry. Part I. Application to Surface, Waste and Indirect Discharge Water Samples in Austria. *Environ. Pollut.* **2007**, *145* (2), 489–496. https://doi.org/10.1016/j.envpol.2006.04.033.
(50) Zhang, C.; Tezel, U.; Li, K.; Liu, D.; Ren, R.; Du, J.; Pavlostathis, S. G. Evaluation and Modeling of Benzalkonium Chloride Inhibition and Biodegradation in Activated Sludge. *Water Res.* **2011**, *45* (3), 1238–1246. https://doi.org/10.1016/j.watres.2010.09.037.
(51) Ertekin, E.; Hatt, J. K.; Konstantinidis, K. T.; Tezel, U. Similar Microbial Consortia and Genes Are Involved in the Biodegradation of Benzalkonium Chlorides in Different Environments. *Environ. Sci. Technol.* **2016**, *50* (8), 4304–4313. https://doi.org/10.1021/acs.est.5b05959.
(52) Tezel, U.; Pavlostathis, S. G. Quaternary Ammonium Disinfectants: Microbial Adaptation, Degradation and Ecology. *Curr. Opin. Biotechnol.* **2015**, *33* (Mic), 296–304. https://doi.org/10.1016/j.copbio.2015.03.018.
(53) Tandukar, M.; Oh, S.; Tezel, U.; Konstantinidis, K. T.; Pavlostathis, S. G. Long-Term Exposure to Benzalkonium Chloride Disinfectants Results in Change of Microbial Community Structure and Increased Antimicrobial Resistance. *Environ. Sci. Technol.* **2013**, *47* (17), 9730–9738. https://doi.org/10.1021/es401507k.
(54) Jennings, M. C.; Minbiole, K. P. C.; Wuest, W. M. Quaternary Ammonium Compounds: An Antimicrobial Mainstay and Platform for Innovation to Address Bacterial Resistance. *ACS Infect. Dis.* **2015**, *1* (7), 288–303. https://doi.org/10.1021/acsinfecdis.5b00047.
(55) Oh, S.; Kurt, Z.; Tsementzi, D.; Weigand, M. R.; Kim, M.; Hatt, J. K.; Tandukar, M.; Pavlostathis, S. G.; Spain, J. C.; Konstantinidis, K. T. Microbial Community Degradation of Widely Used Quaternary Ammonium Disinfectants. *Appl. Environ. Microbiol.* **2014**, *80* (19), 5892–5900. https://doi.org/10.1128/AEM.01255-14.
(56) Kim, M.; Weigand, M. R.; Oh, S.; Hatt, J. K.; Krishnan, R.; Tezel, U.; Pavlostathis, S. G.; Konstantinidis, K. T. Widely Used Benzalkonium Chloride Disinfectants Can Promote Antibiotic Resistance. *Appl. Environ. Microbiol.* **2018**, *84* (17), e01201-18. https://doi.org/10.1128/AEM.01201-18.
(57) Graham, D. W.; Collignon, P.; Davies, J.; Larsson, D. G. J.; Snape, J. Underappreciated Role of Regionally Poor Water Quality on Globally Increasing Antibiotic Resistance. *Environ. Sci. Technol.* **2014**, *48* (20), 11746–11747. https://doi.org/10.1021/es504206x.

(58) Vikesland, P. J.; Pruden, A.; Alvarez, P. J. J.; Aga, D.; Bürgmann, H.; Li, X. D.; Manaia, C. M.; Nambi, I.; Wigginton, K.; Zhang, T.; Zhu, Y. G. Toward a Comprehensive Strategy to Mitigate Dissemination of Environmental Sources of Antibiotic Resistance. *Environ. Sci. Technol.* **2017**, *51* (22), 13061–13069. https://doi.org/10.1021/acs.est.7b03623.

(59) Kemper, J. M.; Walse, S. S.; Mitch, W. A. Quaternary Amines as Nitrosamine Precursors: A Role for Consumer Products? *Environ. Sci. Technol.* **2010**, *44* (4), 1224–1231. https://doi.org/10.1021/es902840h.

(60) Padhye, L.; Luzinova, Y.; Cho, M.; Mizaikoff, B.; Kim, J.-H.; Huang, C.-H. PolyDADMAC and Dimethylamine as Precursors of N -Nitrosodimethylamine during Ozonation: Reaction Kinetics and Mechanisms. *Environ. Sci. Technol.* **2011**, *45* (10), 4353–4359. https://doi.org/10.1021/es104255e.

(61) Park, S.; Wei, S.; Mizaikoff, B.; Taylor, A. E.; Favero, C.; Huang, C. Degradation of Amine-Based Water Treatment Polymers during Chloramination as N-Nitrosodimethylamine (NDMA) Precursors. *Environ. Sci. Technol.* **2009**, *43* (5), 1360–1366. https://doi.org/10.1021/es802732z.

(62) Tezel, U.; Tandukar, M.; Martinez, R. J.; Sobecky, P. A.; Pavlostathis, S. G. Aerobic Biotransformation of n -Tetradecylbenzyldimethylammonium Chloride by an Enriched Pseudomonas Spp. Community. *Environ. Sci. Technol.* **2012**, *46* (16), 8714–8722. https://doi.org/10.1021/es300518c.

(63) Wang, T.; Zhang, H.; Gao, D.; Yang, F.; Yang, S.; Jiang, T.; Zhang, G. Enrichment of Anammox Bacteria in Seed Sludges from Different Wastewater Treating Processes and Start-up of Anammox Process. *Desalination* **2011**, *271* (1–3), 193–198. https://doi.org/10.1016/j.desal.2010.12.034.

(64) Bergero, M. F.; Lucchesi, G. I. Degradation of Cationic Surfactants Using Pseudomonas Putida A ATCC 12633 Immobilized in Calcium Alginate Beads. *Biodegradation* **2013**, *24* (3), 353–364. https://doi.org/10.1007/s10532-012-9592-3.

(65) Dean-Raymond, D.; Alexander, M. Bacterial Metabolism of Quaternary Ammonium Compounds. *Appl. Envir. Microbiol.* **1977**, *33* (5), 1037–1041.

(66) Tezel, U. Fate and Effect of Quaternary Ammonium Compounds in Biological Systems, Georgia Institute of Technology, 2009.

(67) Tezel, U.; Pavlostathis, S. G. Transformation of Benzalkonium Chloride under Nitrate Reducing Conditions. *Environ. Sci. Technol.* **2009**, *43* (5), 1342–1348. https://doi.org/10.1021/es802177f.

(68) Watson, M. K.; Tezel, U.; Pavlostathis, S. G. Biotransformation of Alkanoylcholines under Methanogenic Conditions. *Water Res.* **2012**, *46* (9), 2947–2956. https://doi.org/10.1016/j.watres.2012.03.021.

(69) Mack, J.; Bolton, J. R. Photochemistry of Nitrite and Nitrate in Aqueous Solution: A Review. *J. Photochem. Photobiol. A Chem.* **1999**, *128* (1–3), 1–13. https://doi.org/10.1016/S1010-6030(99)00155-0.

(70) Jankowski, J. J.; Kieber, D. J.; Mopper, K. Nitrate and Nitrite Ultraviolet Actinometers. *Photochem. Photobiol.* **1999**, *70* (3), 319–328. https://doi.org/10.1111/j.1751-1097.1999.tb08143.x.

(71) Chu, L.; Anastasio, C. Temperature and Wavelength Dependence of Nitrite Photolysis in Frozen and Aqueous Solutions. *Environ. Sci. Technol.* **2007**, *41* (10),

3626–3632. https://doi.org/10.1021/es062731q.
(72) Kim, D.; Lee, J.; Ryu, J.; Kim, K.; Choi, W. Arsenite Oxidation Initiated by the UV Photolysis of Nitrite and Nitrate. *Environ. Sci. Technol.* **2014**, *48* (7), 4030–4037. https://doi.org/10.1021/es500001q.
(73) Brezonik, P. L.; Fulkerson-Brekken, J. Nitrate-Induced Photolysis in Natural Waters: Controls on Concentrations of Hydroxyl Radical Photo-Intermediates by Natural Scavenging Agents. *Environ. Sci. Technol.* **1998**, *32* (19), 3004–3010. https://doi.org/10.1021/es9802908.
(74) Vaughan, P. P.; Blough, N. V. Photochemical Formation of Hydroxyl Radical by Constituents of Natural Waters. *Environ. Sci. Technol.* **1998**, *32* (19), 2947–2953. https://doi.org/10.1021/es9710417.
(75) Zafiriou, O. C.; True, M. B. Nitrite Photolysis in Seawater by Sunlight. *Mar. Chem.* **1979**, *8* (1), 9–32. https://doi.org/10.1016/0304-4203(79)90029-X.
(76) Lam, M. W.; Mabury, S. A. Photodegradation of the Pharmaceuticals Atorvastatin, Carbamazepine, Levofloxacin, and Sulfamethoxazole in Natural Waters. *Aquat. Sci.* **2005**, *67* (2), 177–188. https://doi.org/10.1007/s00027-004-0768-8.
(77) Zepp, R. G.; Hoigne, J.; Bader, H. Nitrate-Induced Photooxidation of Trace Organic Chemicals in Water. *Environ. Sci. Technol.* **1987**, *21* (5), 443–450. https://doi.org/10.1021/es00159a004.
(78) Zafiriou, O. C.; True, M. B. Nitrite Photolysis as a Source of Free Radicals in Productive Surface Waters. *Geophys. Res. Lett.* **1979**, *6* (2), 81–84. https://doi.org/10.1029/GL006i002p00081.
(79) Andreozzi, R.; Raffaele, M.; Nicklas, P. Pharmaceuticals in STP Effluents and Their Solar Photodegradation in Aquatic Environment. *Chemosphere* **2003**, *50* (10), 1319–1330. https://doi.org/10.1016/S0045-6535(02)00769-5.
(80) Jasper, J. T. Treatment of Trace Organic Contaminants and Nutrients in Open-Water Unit Process Wetlands, University of California, Berkeley, 2014.
(81) Wang, L.; Xu, H.; Cooper, W. J.; Song, W. Photochemical Fate of Beta-Blockers in NOM Enriched Waters. *Sci. Total Environ.* **2012**, *426*, 289–295. https://doi.org/10.1016/J.SCITOTENV.2012.03.031.
(82) Pati, S. G.; Arnold, W. A. Photochemical Transformation of Four Ionic Liquid Cation Structures in Aqueous Solution. *Environ. Sci. Technol.* **2017**, *51* (20), 11780–11787. https://doi.org/10.1021/acs.est.7b04016.
(83) Jasper, J. T.; Sedlak, D. L. Phototransformation of Wastewater-Derived Trace Organic Contaminants in Open-Water Unit Process Treatment Wetlands. *Environ. Sci. Technol.* **2013**, *47* (19), 10781–10790. https://doi.org/10.1021/es304334w.
(84) Karpuzcu, M. E.; McCabe, A. J.; Arnold, W. A. Phototransformation of Pesticides in Prairie Potholes: Effect of Dissolved Organic Matter in Triplet-Induced Oxidation. *Environ. Sci. Process. Impacts* **2016**, *18* (2), 237–245. https://doi.org/10.1039/C5EM00374A.
(85) Keen, O. S.; Love, N. G.; Linden, K. G. The Role of Effluent Nitrate in Trace Organic Chemical Oxidation during UV Disinfection. *Water Res.* **2012**, *46* (16), 5224–5234. https://doi.org/10.1016/j.watres.2012.06.052.
(86) Rosario-Ortiz, F. L.; Wert, E. C.; Snyder, S. A. Evaluation of UV/H2O2 Treatment for the Oxidation of Pharmaceuticals in Wastewater. *Water Res.* **2010**, *44* (5), 1440–1448. https://doi.org/10.1016/j.watres.2009.10.031.

(87) Bahnmüller, S.; von Gunten, U.; Canonica, S. Sunlight-Induced Transformation of Sulfadiazine and Sulfamethoxazole in Surface Waters and Wastewater Effluents. *Water Res.* **2014**, *57*, 183–192. https://doi.org/10.1016/j.watres.2014.03.019.
(88) Buxton, G. V.; Greenstock, C. L.; Helman, W. P.; Ross, A. B. Critical Review of Rate Constants for Reactions of Hydrated Electrons, Hydrogen Atoms and Hydroxyl Radicals (·OH/·O − in Aqueous Solution. *J. Phys. Chem. Ref. Data* **1988**, *17* (2), 513–886. https://doi.org/10.1063/1.555805.
(89) Neta, P.; Maruthamuthu, P.; Carton, P. M.; Fessenden, R. W. Formation and Reactivity of the Amino Radical. *J. Phys. Chem.* **1978**, *82* (17), 1875–1878. https://doi.org/10.1021/j100506a004.
(90) Lee, C.; Yoon, J. UV-A Induced Photochemical Formation of N-Nitrosodimethylamine (NDMA) in the Presence of Nitrite and Dimethylamine. *J. Photochem. Photobiol. A Chem.* **2007**, *189* (1), 128–134. https://doi.org/10.1016/j.jphotochem.2007.01.022.
(91) Kuenen, J. G. Anammox Bacteria: From Discovery to Application. *Nat. Rev. Microbiol.* **2008**, *6* (4), 320–326. https://doi.org/10.1038/nrmicro1857.
(92) Delgado Vela, J.; Stadler, L. B.; Martin, K. J.; Raskin, L.; Bott, C. B.; Love, N. G. Prospects for Biological Nitrogen Removal from Anaerobic Effluents during Mainstream Wastewater Treatment. *Environ. Sci. Technol. Lett.* **2015**, *2* (9), 234–244. https://doi.org/10.1021/acs.estlett.5b00191.
(93) Cao, Y.; van Loosdrecht, M. C. M.; Daigger, G. T. Mainstream Partial Nitritation–Anammox in Municipal Wastewater Treatment: Status, Bottlenecks, and Further Studies. *Appl. Microbiol. Biotechnol.* **2017**, *101* (4), 1365–1383. https://doi.org/10.1007/s00253-016-8058-7.
(94) Kouba, V.; Vejmelkova, D.; Proksova, E.; Wiesinger, H.; Concha, M.; Dolejs, P.; Hejnic, J.; Jenicek, P.; Bartacek, J. High-Rate Partial Nitritation of Municipal Wastewater after Psychrophilic Anaerobic Pretreatment. *Environ. Sci. Technol.* **2017**, acs.est.7b02078. https://doi.org/10.1021/acs.est.7b02078.
(95) Gurr, C. J.; Reinhard, M. Harnessing Natural Attenuation of Pharmaceuticals and Hormones in Rivers. *Environ. Sci. Technol.* **2006**, *40* (9), 2872–2876. https://doi.org/10.1021/es062677d.
(96) Arnold, W. A.; McNeill, K. Chapter 3.2 Transformation of Pharmaceuticals in the Environment: Photolysis and Other Abiotic Processes. In *Comprehensive Analytical Chemistry*; Elsevier, 2007; Vol. 50, pp 361–385. https://doi.org/10.1016/S0166-526X(07)50011-5.
(97) Schwarzenbach, R. P.; Gschwend, P. M.; Imboden, D. M. *Environmental Organic Chemistry*; John Wiley & Sons, Inc.: Hoboken, NJ, USA, 2002. https://doi.org/10.1002/0471649643.
(98) Rosario-Ortiz, F. L.; Canonica, S. Probe Compounds to Assess the Photochemical Activity of Dissolved Organic Matter. *Environ. Sci. Technol.* **2016**, *50* (23), 12532–12547. https://doi.org/10.1021/acs.est.6b02776.
(99) Zeng, T.; Arnold, W. A. Pesticide Photolysis in Prairie Potholes: Probing Photosensitized Processes. *Environ. Sci. Technol.* **2013**, *47* (13), 6735–6745. https://doi.org/10.1021/es3030808.
(100) McCabe, A. J.; Arnold, W. A. Reactivity of Triplet Excited States of Dissolved Natural Organic Matter in Stormflow from Mixed-Use Watersheds. *Environ. Sci.*

Technol. **2017**, *51* (17), 9718–9728. https://doi.org/10.1021/acs.est.7b01914.
(101) Page, S. E.; Arnold, W. A.; McNeill, K. Assessing the Contribution of Free Hydroxyl Radical in Organic Matter-Sensitized Photohydroxylation Reactions. *Environ. Sci. Technol.* **2011**, *45* (7), 2818–2825. https://doi.org/10.1021/es2000694.
(102) Mill, T. Predicting Photoreaction Rates in Surface Waters. *Chemosphere* **1999**, *38* (6), 1379–1390. https://doi.org/10.1016/S0045-6535(98)00540-2.
(103) Hoigné, J.; Faust, B. C.; Haag, W. R.; Scully, F. E.; Zepp, R. G. Aquatic Humic Substances as Sources and Sinks of Photochemically Produced Transient Reactants. In *Aquatic Humic Substances: Influence on Fate and Treatment of Pollutants*; Suffet, I. H., MacCarthy, P., Eds.; American Chemical Society, 1988; Vol. 219, pp 363–381. https://doi.org/10.1021/ba-1988-0219.ch023.
(104) Sharpless, C. M.; Linden, K. G. UV Photolysis of Nitrate: Effects of Natural Organic Matter and Dissolved Inorganic Carbon and Implications for UV Water Disinfection. *Environ. Sci. Technol.* **2001**, *35* (14), 2949–2955. https://doi.org/10.1021/es0020431.
(105) Sharpless, C. M.; Seibold, D. A.; Linden, K. G. Nitrate Photosensitized Degradation of Atrazine during UV Water Treatment. *Aquat. Sci.* **2003**, *65* (4), 359–366. https://doi.org/10.1007/s00027-003-0674-5.
(106) Calza, P.; Vione, D.; Novelli, A.; Pelizzetti, E.; Minero, C. The Role of Nitrite and Nitrate Ions as Photosensitizers in the Phototransformation of Phenolic Compounds in Seawater. *Sci. Total Environ.* **2012**, *439*, 67–75. https://doi.org/10.1016/j.scitotenv.2012.09.009.
(107) Vione, D.; Scozzaro, A. Photochemistry of Surface Fresh Waters in the Framework of Climate Change. *Environ. Sci. Technol.* **2019**, *53* (14), 7945–7963. https://doi.org/10.1021/acs.est.9b00968.
(108) Zepp, R. G.; Faust, B. C.; Hoigne, J. Hydroxyl Radical Formation in Aqueous Reactions (PH 3-8) of Iron(II) with Hydrogen Peroxide: The Photo-Fenton Reaction. *Environ. Sci. Technol.* **1992**, *26* (2), 313–319. https://doi.org/10.1021/es00026a011.
(109) Murphy, S. A.; Solomon, B. M.; Meng, S.; Copeland, J. M.; Shaw, T. J.; Ferry, J. L. Geochemical Production of Reactive Oxygen Species From Biogeochemically Reduced Fe. *Environ. Sci. Technol.* **2014**, *48* (7), 3815–3821. https://doi.org/10.1021/es4051764.
(110) Latch, D. E. The Role of Singlet Oxygen in Surface Water Photochemistry. In *Surface Water Photochemistry*; Calza, P., Vione, D., Eds.; The Royal Society of Chemistry, 2015; pp 139–165. https://doi.org/10.1039/9781782622154-00139.
(111) Appiani, E.; Ossola, R.; Latch, D. E.; Erickson, P. R.; McNeill, K. Aqueous Singlet Oxygen Reaction Kinetics of Furfuryl Alcohol: Effect of Temperature, PH, and Salt Content. *Environ. Sci. Process. Impacts* **2017**, *19* (4), 507–516. https://doi.org/10.1039/C6EM00646A.
(112) McNeill, K.; Canonica, S. Triplet State Dissolved Organic Matter in Aquatic Photochemistry: Reaction Mechanisms, Substrate Scope, and Photophysical Properties. *Environ. Sci. Process. Impacts* **2016**, *18* (11), 1381–1399. https://doi.org/10.1039/C6EM00408C.
(113) Barra Caracciolo, A.; Topp, E.; Grenni, P. Pharmaceuticals in the Environment:

Biodegradation and Effects on Natural Microbial Communities. A Review. *J. Pharm. Biomed. Anal.* **2015**, *106*, 25–36. https://doi.org/10.1016/j.jpba.2014.11.040.
(114) Durán-Álvarez, J. C.; Prado, B.; González, D.; Sánchez, Y.; Jiménez-Cisneros, B. Environmental Fate of Naproxen, Carbamazepine and Triclosan in Wastewater, Surface Water and Wastewater Irrigated Soil — Results of Laboratory Scale Experiments. *Sci. Total Environ.* **2015**, *538*, 350–362. https://doi.org/10.1016/j.scitotenv.2015.08.028.
(115) Hajaya, M. G.; Pavlostathis, S. G. Modeling the Fate and Effect of Benzalkonium Chlorides in a Continuous-Flow Biological Nitrogen Removal System Treating Poultry Processing Wastewater. *Bioresour. Technol.* **2013**, *130*, 278–287. https://doi.org/10.1016/j.biortech.2012.11.103.
(116) Jardak, K.; Drogui, P.; Daghrir, R. Surfactants in Aquatic and Terrestrial Environment: Occurrence, Behavior, and Treatment Processes. *Environ. Sci. Pollut. Res.* **2016**, *23* (4), 3195–3216. https://doi.org/10.1007/s11356-015-5803-x.
(117) Oh, S.; Kurt, Z.; Tsementzi, D.; Weigand, M. R.; Kim, M.; Hatt, J. K.; Tandukar, M.; Pavlostathis, S. G.; Spain, J. C.; Konstantinidis, K. T. Microbial Community Degradation of Widely Used Quaternary Ammonium Disinfectants. *Appl. Environ. Microbiol.* **2014**, *80* (19), 5892–5900. https://doi.org/10.1128/AEM.01255-14.
(118) Hajaya, M. G. Fate and Effect of Quaternary Ammonium Antimicrobial Compounds on Biological Nitrogen Removal Within High-Strength Wastewater Treatment Systems, Georgia Institute of Technology, 2011.
(119) Bergero, M. F.; Lucchesi, G. I. Immobilization of Pseudomonas Putida A (ATCC 12633) Cells: A Promising Tool for Effective Degradation of Quaternary Ammonium Compounds in Industrial Effluents. *Int. Biodeterior. Biodegradation* **2015**, *100*, 38–43. https://doi.org/10.1016/j.ibiod.2015.02.004.
(120) Clara, M.; Strenn, B.; Kreuzinger, N. Carbamazepine as a Possible Anthropogenic Marker in the Aquatic Environment: Investigations on the Behaviour of Carbamazepine in Wastewater Treatment and during Groundwater Infiltration. *Water Res.* **2004**, *38* (4), 947–954. https://doi.org/10.1016/J.WATRES.2003.10.058.
(121) Lam, M. W.; Young, C. J.; Mabury, S. A. Aqueous Photochemical Reaction Kinetics and Transformations of Fluoxetine. *Environ. Sci. Technol.* **2005**, *39* (2), 513–522. https://doi.org/10.1021/es0494757.
(122) Chiron, S.; Minero, C.; Vione, D. Photodegradation Processes of the Antiepileptic Drug Carbamazepine, Relevant to Estuarine Waters. *Environ. Sci. Technol.* **2006**, *40* (19), 5977–5983. https://doi.org/10.1021/es060502y.
(123) Zeng, C.; Ji, Y.; Zhou, L.; Zhang, Y.; Yang, X. The Role of Dissolved Organic Matters in the Aquatic Photodegradation of Atenolol. *J. Hazard. Mater.* **2012**, *239–240*, 340–347. https://doi.org/10.1016/j.jhazmat.2012.09.005.
(124) Pereira, V. J.; Weinberg, H. S.; Linden, K. G.; Singer, P. C. UV Degradation Kinetics and Modeling of Pharmaceutical Compounds in Laboratory Grade and Surface Water via Direct and Indirect Photolysis at 254 Nm. *Environ. Sci. Technol.* **2007**, *41* (5), 1682–1688. https://doi.org/10.1021/es061491b.
(125) Pereira, V. J.; Linden, K. G.; Weinberg, H. S. Evaluation of UV Irradiation for Photolytic and Oxidative Degradation of Pharmaceutical Compounds in Water.

Water Res. **2007**, *41* (19), 4413–4423. https://doi.org/10.1016/j.watres.2007.05.056.
(126) Ryan, C. C.; Tan, D. T.; Arnold, W. A. Direct and Indirect Photolysis of Sulfamethoxazole and Trimethoprim in Wastewater Treatment Plant Effluent. *Water Res.* **2011**, *45* (3), 1280–1286. https://doi.org/10.1016/j.watres.2010.10.005.
(127) Wols, B. A.; Hofman-Caris, C. H. M.; Harmsen, D. J. H.; Beerendonk, E. F. Degradation of 40 Selected Pharmaceuticals by UV/H2O2. *Water Res.* **2013**, *47* (15), 5876–5888. https://doi.org/10.1016/j.watres.2013.07.008.
(128) Gao, H.; Scherson, Y. D.; Wells, G. F. Towards Energy Neutral Wastewater Treatment: Methodology and State of the Art. *Environ. Sci. Process. Impacts* **2014**, *16* (6), 1223–1246. https://doi.org/10.1039/C4EM00069B.
(129) Jetten, M.; Schmid, M.; Van De Pas-Schoonen, K.; Damsté, J. S.; Strous, M. Anammox Organisms: Enrichment, Cultivation, and Environmental Analysis. *Methods Enzymol.* **2005**, *397*, 34–57. https://doi.org/10.1016/S0076-6879(05)97003-1.
(130) Lackner, S.; Gilbert, E. M.; Vlaeminck, S. E.; Joss, A.; Horn, H.; van Loosdrecht, M. C. M. Full-Scale Partial Nitritation/Anammox Experiences – An Application Survey. *Water Res.* **2014**, *55*, 292–303. https://doi.org/10.1016/j.watres.2014.02.032.
(131) Peterson, K. N.; Tan, D. T.; Bezares-Cruz, J. C.; Novak, P. J. Estrone Biodegradation in Laboratory-Scale Systems Designed for Total Nitrogen Removal from Wastewater. *Environ. Sci. Water Res. Technol.* **2017**, *3* (6), 1051–1060. https://doi.org/10.1039/c7ew00164a.
(132) Huber, M. M.; Canonica, S.; Park, G. Y.; Von Gunten, U. Oxidation of Pharmaceuticals during Ozonation and Advanced Oxidation Processes. *Environ. Sci. Technol.* **2003**, *37* (5), 1016–1024. https://doi.org/10.1021/es025896h.
(133) Klavarioti, M.; Mantzavinos, D.; Kassinos, D. Removal of Residual Pharmaceuticals from Aqueous Systems by Advanced Oxidation Processes. *Environ. Int.* **2009**, *35* (2), 402–417. https://doi.org/10.1016/j.envint.2008.07.009.
(134) Lado Ribeiro, A. R.; Moreira, N. F. F.; Li Puma, G.; Silva, A. M. T. Impact of Water Matrix on the Removal of Micropollutants by Advanced Oxidation Technologies. *Chem. Eng. J.* **2019**, *363*, 155–173. https://doi.org/10.1016/j.cej.2019.01.080.
(135) Sgroi, M.; Vagliasindi, F. G. A.; Snyder, S. A.; Roccaro, P. N-Nitrosodimethylamine (NDMA) and Its Precursors in Water and Wastewater: A Review on Formation and Removal. *Chemosphere* **2018**, *191*, 685–703. https://doi.org/10.1016/J.CHEMOSPHERE.2017.10.089.
(136) Zeng, T.; Mitch, W. A. Impact of Nitrification on the Formation of *N* -Nitrosamines and Halogenated Disinfection Byproducts within Distribution System Storage Facilities. *Environ. Sci. Technol.* **2016**, *50* (6), 2964–2973. https://doi.org/10.1021/acs.est.5b05668.
(137) Zeng, T.; Mitch, W. A. Contribution of *N* -Nitrosamines and Their Precursors to Domestic Sewage by Greywaters and Blackwaters. *Environ. Sci. Technol.* **2015**, *49* (22), 13158–13167. https://doi.org/10.1021/acs.est.5b04254.
(138) Zeng, T.; Glover, C. M.; Marti, E. J.; Woods-Chabane, G. C.; Karanfil, T.; Mitch, W. A.; Dickenson, E. R. V. Relative Importance of Different Water Categories as

Sources of N -Nitrosamine Precursors. *Environ. Sci. Technol.* **2016**, *50* (24), 13239–13248. https://doi.org/10.1021/acs.est.6b04650.
(139) Thorn, K. A.; Cox, L. G. Ultraviolet Irradiation Effects Incorporation of Nitrate and Nitrite Nitrogen into Aquatic Natural Organic Matter. *J. Environ. Qual.* **2012**, *41* (3), 865. https://doi.org/10.2134/jeq2011.0335.
(140) Krasner, S. W.; Mitch, W. A.; McCurry, D. L.; Hanigan, D.; Westerhoff, P. Formation, Precursors, Control, and Occurrence of Nitrosamines in Drinking Water: A Review. *Water Research*. September 2013, pp 4433–4450. https://doi.org/10.1016/j.watres.2013.04.050.
(141) Ohta, T.; Suzuki, J.; Iwano, Y.; Suzuki, S. Photochemical Nitrosation of Dimethylamine in Aqueous Solution Containing Nitrite. *Chemosphere* **1982**, *11* (8), 797–801. https://doi.org/10.1016/0045-6535(82)90108-4.
(142) Sharpless, C. M.; Linden, K. G. Experimental and Model Comparisons of Low- and Medium-Pressure Hg Lamps for the Direct and H2O2 Assisted UV Photodegradation of N -Nitrosodimethylamine in Simulated Drinking Water. *Environ. Sci. Technol.* **2003**, *37* (9), 1933–1940. https://doi.org/10.1021/es025814p.
(143) Burns, J. M.; Cooper, W. J.; Ferry, J. L.; King, D. W.; DiMento, B. P.; McNeill, K.; Miller, C. J.; Miller, W. L.; Peake, B. M.; Rusak, S. A.; Rose, A. L.; Waite, T. D. Methods for Reactive Oxygen Species (ROS) Detection in Aqueous Environments. *Aquat. Sci.* **2012**, *74* (4), 683–734. https://doi.org/10.1007/s00027-012-0251-x.
(144) Canonica, S.; Meunier, L.; von Gunten, U. Phototransformation of Selected Pharmaceuticals during UV Treatment of Drinking Water. *Water Res.* **2008**, *42* (1–2), 121–128. https://doi.org/10.1016/j.watres.2007.07.026.
(145) Lotti, T.; Kleerebezem, R.; Hu, Z.; Kartal, B.; Jetten, M. S. M.; van Loosdrecht, M. C. M. Simultaneous Partial Nitritation and Anammox at Low Temperature with Granular Sludge. *Water Res.* **2014**, *66*, 111–121. https://doi.org/10.1016/j.watres.2014.07.047.
(146) Packer, J. L.; Werner, J. J.; Latch, D. E.; McNeill, K.; Arnold, W. A. Photochemical Fate of Pharmaceuticals in the Environment: Naproxen, Diclofenac, Clofibric Acid, and Ibuprofen. *Aquat. Sci.* **2003**, *65* (4), 342–351. https://doi.org/10.1007/s00027-003-0671-8.
(147) Bolton, J. R.; Mayor-Smith, I.; Linden, K. G. Rethinking the Concepts of Fluence (UV Dose) and Fluence Rate: The Importance of Photon-Based Units - A Systemic Review. *Photochem. Photobiol.* **2015**, *91* (6), 1252–1262. https://doi.org/10.1111/php.12512.
(148) Barazesh, J. M.; Hennebel, T.; Jasper, J. T.; Sedlak, D. L. Modular Advanced Oxidation Process Enabled by Cathodic Hydrogen Peroxide Production. *Environ. Sci. Technol.* **2015**, *49* (12), 7391–7399. https://doi.org/10.1021/acs.est.5b01254.
(149) Neta, P.; Huie, R. E.; Ross, A. B. Rate Constants for Reactions of Inorganic Radicals in Aqueous Solution. *J. Phys. Chem. Ref. Data* **1988**, *17* (3), 1027–1284. https://doi.org/10.1063/1.555808.
(150) Kulshrestha, P.; McKinstry, K. C.; Fernandez, B. O.; Feelisch, M.; Mitch, W. A. Application of an Optimized Total N -Nitrosamine (TONO) Assay to Pools: Placing N -Nitrosodimethylamine (NDMA) Determinations into Perspective.

Environ. Sci. Technol. **2010**, *44* (9), 3369–3375. https://doi.org/10.1021/es100361f.
(151) Dai, N.; Zeng, T.; Mitch, W. A. Predicting N-Nitrosamines: N-Nitrosodiethanolamine as a Significant Component of Total N-Nitrosamines in Recycled Wastewater. *Environ. Sci. Technol. Lett.* **2015**, *2* (3), 54–58. https://doi.org/10.1021/acs.estlett.5b00005.
(152) Dong, M. M.; Trenholm, R.; Rosario-Ortiz, F. L. Photochemical Degradation of Atenolol, Carbamazepine, Meprobamate, Phenytoin and Primidone in Wastewater Effluents. *J. Hazard. Mater.* **2015**, *282*, 216–223. https://doi.org/10.1016/J.JHAZMAT.2014.04.028.
(153) Shu, Z.; Bolton, J. R.; Belosevic, M.; Gamal El Din, M. Photodegradation of Emerging Micropollutants Using the Medium-Pressure UV/H2O2 Advanced Oxidation Process. *Water Res.* **2013**, *47* (8), 2881–2889. https://doi.org/10.1016/j.watres.2013.02.045.
(154) Song, W.; Cooper, W. J.; Mezyk, S. P.; Greaves, J.; Peake, B. M. Free Radical Destruction of β-Blockers in Aqueous Solution. *Environ. Sci. Technol.* **2008**, *42* (4), 1256–1261. https://doi.org/10.1021/es702245n.
(155) Dai, N.; Mitch, W. A. Relative Importance of N -Nitrosodimethylamine Compared to Total N -Nitrosamines in Drinking Waters. *Environ. Sci. Technol.* **2013**, *47* (8), 3648–3656. https://doi.org/10.1021/es305225b.
(156) Miklos, D. B.; Remy, C.; Jekel, M.; Linden, K. G.; Drewes, J. E.; Hübner, U. Evaluation of Advanced Oxidation Processes for Water and Wastewater Treatment – A Critical Review. *Water Res.* **2018**, *139*, 118–131. https://doi.org/10.1016/j.watres.2018.03.042.
(157) Keen, O. S.; Love, N. G.; Aga, D. S.; Linden, K. G. Biodegradability of Iopromide Products after UV/H2O2 Advanced Oxidation. *Chemosphere* **2016**, *144*, 989–994. https://doi.org/10.1016/j.chemosphere.2015.09.072.
(158) Batt, A. L.; Kim, S.; Aga, D. S. Enhanced Biodegradation of Lopromide and Trimethoprim in Nitrifying Activated Sludge. *Environ. Sci. Technol.* **2006**, *40* (23), 7367–7373. https://doi.org/10.1021/es060835v.
(159) Ghattas, A.-K.; Fischer, F.; Wick, A.; Ternes, T. A. Anaerobic Biodegradation of (Emerging) Organic Contaminants in the Aquatic Environment. *Water Res.* **2017**, *116*, 268–295. https://doi.org/10.1016/J.WATRES.2017.02.001.
(160) Butkovskyi, A.; Bruning, H.; Kools, S. A. E.; Rijnaarts, H. H. M.; Van Wezel, A. P. Organic Pollutants in Shale Gas Flowback and Produced Waters: Identification, Potential Ecological Impact, and Implications for Treatment Strategies. *Environ. Sci. Technol.* **2017**, *51* (9), 4740–4754. https://doi.org/10.1021/acs.est.6b05640.
(161) Elsner, M.; Hoelzer, K. Quantitative Survey and Structural Classification of Hydraulic Fracturing Chemicals Reported in Unconventional Gas Production. *Environ. Sci. Technol.* **2016**, *50* (7), 3290–3314. https://doi.org/10.1021/acs.est.5b02818.
(162) Li, X.; Doherty, A. C.; Brownawell, B.; Lara-Martin, P. A. Distribution and Diagenetic Fate of Synthetic Surfactants and Their Metabolites in Sewage-Impacted Estuarine Sediments. *Environ. Pollut.* **2018**, *242*, 209–218. https://doi.org/10.1016/j.envpol.2018.06.064.
(163) Pati, S. G.; Arnold, W. A. Comprehensive Screening of Quaternary Ammonium

Surfactants and Ionic Liquids in Wastewater Effluents and Lake Sediments. *Environ. Sci. Process. Impacts* **2020**, *22* (2), 430–441. https://doi.org/10.1039/C9EM00554D.
(164) Ferrer, I.; Thurman, E. M. Analysis of Hydraulic Fracturing Additives by LC/Q-TOF-MS. *Anal. Bioanal. Chem.* **2015**, *407* (21), 6417–6428. https://doi.org/10.1007/s00216-015-8780-5.
(165) Ferrer, I.; Furlong, E. T. Identification of Alkyl Dimethylbenzylammonium Surfactants in Water Samples by Solid-Phase Extraction Followed by Ion Trap LC / MS and LC / MS / MS. *Environ. Sci. Technol.* **2001**, *35* (12), 2583–2588.
(166) García, M. T.; Campos, E.; Sánchez-Leal, J.; Ribosa, I. Anaerobic Degradation and Toxicity of Commercial Cationic Surfactants in Anaerobic Screening Tests. *Chemosphere* **2000**, *41* (5), 705–710. https://doi.org/10.1016/S0045-6535(99)00455-5.
(167) Ertekin, E.; Konstantinidis, K. T.; Tezel, U. A Rieske-Type Oxygenase of *Pseudomonas* Sp. BIOMIG1 Converts Benzalkonium Chlorides to Benzyldimethyl Amine. *Environ. Sci. Technol.* **2017**, *51* (1), 175–181. https://doi.org/10.1021/acs.est.6b03705.
(168) Lai, Y. J. S.; Ontiveros-Valencia, A.; Ilhan, Z. E.; Zhou, Y.; Miranda, E.; Maldonado, J.; Krajmalnik-Brown, R.; Rittmann, B. E. Enhancing Biodegradation of C16-Alkyl Quaternary Ammonium Compounds Using an Oxygen-Based Membrane Biofilm Reactor. *Water Res.* **2017**, *123*, 825–833. https://doi.org/10.1016/j.watres.2017.07.003.
(169) Brownawell, B. J.; Chen, H.; Collier, J. M.; Westall, J. C. Adsorption of Organic Cations to Natural Materials. *Environ. Sci. Technol.* **1990**, *24* (8), 1234–1241. https://doi.org/10.1021/es00078a011.
(170) Kreuzinger, N.; Fuerhacker, M.; Scharf, S.; Uhl, M.; Gans, O.; Grillitsch, B. Methodological Approach towards the Environmental Significance of Uncharacterized Substances - Quaternary Ammonium Compounds as an Example. *Desalination* **2007**, *215* (1–3), 209–222. https://doi.org/10.1016/j.desal.2006.10.036.
(171) Gaze, W. H.; Abdouslam, N.; Hawkey, P. M.; Wellington, E. M. H. Incidence of Class 1 Integrons in a Quaternary Ammonium Compound-Polluted Environment. *Antimicrob. Agents Chemother.* **2005**, *49* (5), 1802–1807. https://doi.org/10.1128/AAC.49.5.1802-1807.2005.
(172) Gillings, M. R. Integrons: Past, Present, and Future. *Microbiol. Mol. Biol. Rev.* **2014**, *78* (2), 257–277. https://doi.org/10.1128/MMBR.00056-13.
(173) Gillings, M. R.; Holley, M. P.; Stokes, H. W. Evidence for Dynamic Exchange of Qac Gene Cassettes between Class 1 Integrons and Other Integrons in Freshwater Biofilms. *FEMS Microbiol. Lett.* **2009**, *296* (2), 282–288. https://doi.org/10.1111/j.1574-6968.2009.01646.x.
(174) Gillings, M. R.; Xuejun, D.; Hardwick, S. A.; Holley, M. P.; Stokes, H. W. Gene Cassettes Encoding Resistance to Quaternary Ammonium Compounds: A Role in the Origin of Clinical Class 1 Integrons? *ISME J.* **2009**, *3* (2), 209–215. https://doi.org/10.1038/ismej.2008.98.
(175) Mulder, I.; Siemens, J.; Sentek, V.; Amelung, W.; Smalla, K.; Jechalke, S. Quaternary Ammonium Compounds in Soil: Implications for Antibiotic Resistance

Development. *Rev. Environ. Sci. Bio/Technology* **2018**, *17* (1), 159–185. https://doi.org/10.1007/s11157-017-9457-7.
(176) USEPA. *Reregistration Eligibility Decision for Alkyl Dimethyl Benzyl Ammonium Chloride (ADBAC)*; Washington, DC, 2006.
(177) Grandbois, M.; Latch, D. E.; McNeill, K. Microheterogeneous Concentrations of Singlet Oxygen in Natural Organic Matter Isolate Solutions. *Environ. Sci. Technol.* **2008**, *42* (24), 9184–9190. https://doi.org/10.1021/es8017094.
(178) Leifer, A. *The Kinetics of Environmental Aquatic Photochemistry: Theory and Practice*; American Chemical Society: Washington, DC, 1988.
(179) Dulin, D.; Mill, T. Development and Evaluation of Sunlight Actinometers. *Environ. Sci. Technol.* **1982**, *16* (11), 815–820. https://doi.org/10.1021/es00105a017.
(180) Grebel, J. E.; Pignatello, J. J.; Mitch, W. A. Effect of Halide Ions and Carbonates on Organic Contaminant Degradation by Hydroxyl Radical-Based Advanced Oxidation Processes in Saline Waters. *Environ. Sci. Technol.* **2010**, *44* (17), 6822–6828. https://doi.org/10.1021/es1010225.
(181) Grebel, J. E.; Pignatello, J. J.; Mitch, W. A. Sorbic Acid as a Quantitative Probe for the Formation, Scavenging and Steady-State Concentrations of the Triplet-Excited State of Organic Compounds. *Water Res.* **2011**, *45* (19), 6535–6544. https://doi.org/10.1016/J.WATRES.2011.09.048.
(182) NREL. SMARTS: Simple Model of the Atmospheric Radiative Transfer of Sunshine https://www.nrel.gov/grid/solar-resource/smarts.html (accessed Sep 6, 2019).
(183) Gueymard, C. A. Parameterized Transmittance Model for Direct Beam and Circumsolar Spectral Irradiance. *Sol. Energy* **2001**, *71* (5), 325–346. https://doi.org/10.1016/S0038-092X(01)00054-8.
(184) Gueymard, C. *SMARTS2, A Simple Model of the Atmospheric Radiative Transfer of Sunshine: Algorithms and Performance Assessment*; 1995.
(185) Laszakovits, J. R.; Berg, S. M.; Anderson, B. G.; O'Brien, J. E.; Wammer, K. H.; Sharpless, C. M. P-Nitroanisole/Pyridine and p-Nitroacetophenone/Pyridine Actinometers Revisited: Quantum Yield in Comparison to Ferrioxalate. *Environ. Sci. Technol. Lett.* **2017**, *4* (1), 11–14. https://doi.org/10.1021/acs.estlett.6b00422.
(186) Minella, M.; Rapa, L.; Carena, L.; Pazzi, M.; Maurino, V.; Minero, C.; Brigante, M.; Vione, D. An Experimental Methodology to Measure the Reaction Rate Constants of Processes Sensitised by the Triplet State of 4-Carboxybenzophenone as a Proxy of the Triplet States of Chromophoric Dissolved Organic Matter, under Steady-State Irradiation Conditions. *Environ. Sci. Process. Impacts* **2018**, *20* (7), 1007–1019. https://doi.org/10.1039/C8EM00155C.
(187) al Housari, F.; Vione, D.; Chiron, S.; Barbati, S. Reactive Photoinduced Species in Estuarine Waters. Characterization of Hydroxyl Radical, Singlet Oxygen and Dissolved Organic Matter Triplet State in Natural Oxidation Processes. *Photochem. Photobiol. Sci.* **2010**, *9* (1), 78–86. https://doi.org/10.1039/B9PP00030E.
(188) Wenk, J.; von Gunten, U.; Canonica, S. Effect of Dissolved Organic Matter on the Transformation of Contaminants Induced by Excited Triplet States and the Hydroxyl Radical. *Environ. Sci. Technol.* **2011**, *45* (4), 1334–1340.

https://doi.org/10.1021/es102212t.
(189) Gerba, C. P. Quaternary Ammonium Biocides: Efficacy in Application. *Appl. Environ. Microbiol.* **2015**, *81* (2), 464–469. https://doi.org/10.1128/AEM.02633-14.
(190) Merchel Piovesan Pereira, B.; Tagkopoulos, I. Benzalkonium Chlorides: Uses, Regulatory Status, and Microbial Resistance. *Appl. Environ. Microbiol.* **2019**, *85* (13), 1–13. https://doi.org/10.1128/AEM.00377-19.
(191) Nishiyama, N.; Toshima, Y.; Ikeda, Y. Biodegradation of Alkyltrimethylammonium Salts in Activated Sludge. *Chemosphere* **1995**, *30* (3), 593–603. https://doi.org/10.1016/0045-6535(94)00406-K.
(192) Oh, S.; Tandukar, M.; Pavlostathis, S. G.; Chain, P. S. G.; Konstantinidis, K. T. Microbial Community Adaptation to Quaternary Ammonium Biocides as Revealed by Metagenomics. *Environ. Microbiol.* **2013**, *15*, 2850–2864. https://doi.org/10.1111/1462-2920.12154.
(193) García, M. T.; Ribosa, I.; Guindulain, T.; Sánchez-Leal, J.; Vives-Rego, J. Fate and Effect of Monoalkyl Quaternary Ammonium Surfactants in the Aquatic Environment. *Environ. Pollut.* **2001**, *111* (1), 169–175. https://doi.org/10.1016/S0269-7491(99)00322-X.
(194) Gaze, W. H.; Zhang, L.; Abdouslam, N. A.; Hawkey, P. M.; Calvo-Bado, L.; Royle, J.; Brown, H.; Davis, S.; Kay, P.; Boxall, A. B. A.; Wellington, E. M. H. Impacts of Anthropogenic Activity on the Ecology of Class 1 Integrons and Integron-Associated Genes in the Environment. *ISME J.* **2011**, *5* (8), 1253–1261. https://doi.org/10.1038/ismej.2011.15.
(195) Ismail, Z. Z.; Tezel, U.; Pavlostathis, S. G. Sorption of Quaternary Ammonium Compounds to Municipal Sludge. *Water Res.* **2010**, *44* (7), 2303–2313. https://doi.org/10.1016/j.watres.2009.12.029.
(196) Hajaya, M. G.; Tezel, U.; Pavlostathis, S. G. Effect of Temperature and Benzalkonium Chloride on Nitrate Reduction. *Bioresour. Technol.* **2011**, *102* (8), 5039–5047. https://doi.org/10.1016/j.biortech.2011.01.080.
(197) Sutterlin, H.; Trittler, R.; Bojanowski, S.; Stadlbauer, E. A.; Kummerer, K. Fate of Benzalkonium Chloride in a Sewage Sludge Low Temperature Conversion Process Investigated by LC-LC/ESI-MS/MS. *Clean Soil, Air, Water* **2007**, *35* (1), 81–87.
(198) Harrison, K. R.; Kappell, A. D.; McNamara, P. J. Benzalkonium Chloride Alters Phenotypic and Genotypic Antibiotic Resistance Profiles in a Source Water Used for Drinking Water Treatment. *Environ. Pollut.* **2020**, *257*, 113472. https://doi.org/10.1016/j.envpol.2019.113472.
(199) Wolf, D. C.; Dao, T. H.; Scott, H. D.; Lavy, T. L. Influence of Sterilization Methods on Selected Soil Microbiological, Physical, and Chemical Properties. *J. Environ. Qual.* **1989**, *18* (1), 39–44. https://doi.org/10.2134/jeq1989.00472425001800010007x.
(200) Sandberg, K. D.; Ishii, S.; LaPara, T. M. A Microfluidic Quantitative Polymerase Chain Reaction Method for the Simultaneous Analysis of Dozens of Antibiotic Resistance and Heavy Metal Resistance Genes. *Environ. Sci. Technol. Lett.* **2018**, *5* (1), 20–25. https://doi.org/10.1021/acs.estlett.7b00552.
(201) Gohl, D. M.; Vangay, P.; Garbe, J.; MacLean, A.; Hauge, A.; Becker, A.; Gould, T. J.; Clayton, J. B.; Johnson, T. J.; Hunter, R.; Knights, D.; Beckman, K. B.

Systematic Improvement of Amplicon Marker Gene Methods for Increased Accuracy in Microbiome Studies. *Nat. Biotechnol.* **2016**, *34* (9), 942–949. https://doi.org/10.1038/nbt.3601.
(202) Callahan, B. J.; McMurdie, P. J.; Rosen, M. J.; Han, A. W.; Johnson, A. J. A.; Holmes, S. P. DADA2: High-Resolution Sample Inference from Illumina Amplicon Data. *Nat. Methods* **2016**, *13* (7), 581–583. https://doi.org/10.1038/nmeth.3869.
(203) Callahan, B. J.; McMurdie, P. J.; Holmes, S. P. Exact Sequence Variants Should Replace Operational Taxonomic Units in Marker-Gene Data Analysis. *ISME J.* **2017**, *11* (12), 2639–2643. https://doi.org/10.1038/ismej.2017.119.
(204) Quast, C.; Pruesse, E.; Yilmaz, P.; Gerken, J.; Schweer, T.; Yarza, P.; Peplies, J.; Glöckner, F. O. The SILVA Ribosomal RNA Gene Database Project: Improved Data Processing and Web-Based Tools. *Nucleic Acids Res.* **2012**, *41* (D1), D590–D596. https://doi.org/10.1093/nar/gks1219.
(205) R Core Team. R: A Language and Environment for Statistical Computing. R Foundation for Statistical Computing: Vienna, Austria 2019.
(206) Scholes, R. C.; Prasse, C.; Sedlak, D. L. The Role of Reactive Nitrogen Species in Sensitized Photolysis of Wastewater-Derived Trace Organic Contaminants. *Environ. Sci. Technol.* **2019**, *53* (11), 6483–6491. https://doi.org/10.1021/acs.est.9b01386.
(207) Apell, J. N.; McNeill, K. Updated and Validated Solar Irradiance Reference Spectra for Estimating Environmental Photodegradation Rates. *Environ. Sci. Process. Impacts* **2019**, *21* (3), 427–437. https://doi.org/10.1039/C8EM00478A.
(208) Staley, J. T. Prosthecomicrobium and Ancalomicrobium: New Prosthecate Freshwater Bacteria. *J. Bacteriol.* **1968**, *95* (5), 1921 LP – 1942.
(209) Staley, J. T.; de Bont, J. A. M.; de Jonge, K. Prosthecobacter Fusiformis Nov. Gen. et Sp., the Fusiform Caulobacter. *Antonie Van Leeuwenhoek* **1976**, *42* (3), 333–342. https://doi.org/10.1007/BF00394132.

Appendix A. Supplementary Information for Chapter 2

Table A-1. Target Pharmaceuticals Used in the Study

Compound	Therapeutic Class	Molecular Structure
Carbamazepine	Anticonvulsant	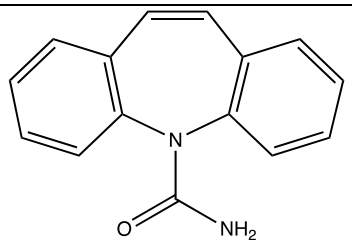
Trimethoprim	Antibiotic	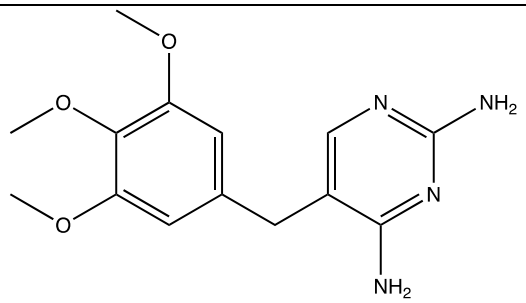
Fluoxetine Hydrochloride	Antidepressant	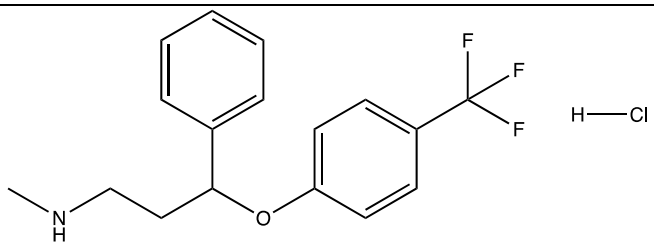
Atenolol	beta-blocker	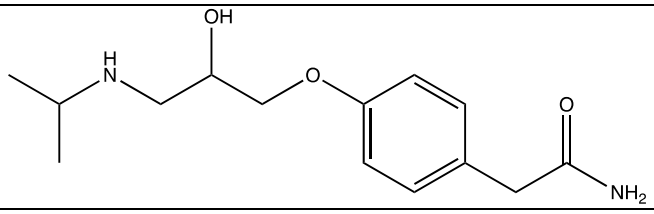

Table A-2. Water quality parameters of the effluent used in photochemical study

Water Quality Parameter	Method	Effluent[a]
Nitrite (NO_2^- mg-N/L)	Metrohm ion chromatograph	0.0146
Nitrate (NO_3^- mg-N/L)	Metrohm ion chromatograph	9.311
Ammonia (NH_3 mg-N/L)	Hach colorimetric test kit	7
Dissolved organic carbon (DOC mg-C/L)	Shimadzu TOC-L analyzer	4.151
Dissolved inorganic carbon (DIC mg-C/L)	Shimadzu TOC-L analyzer	46.27
pH	Thermo Orion pH meter	7.5

[a]Before experiments, amended with $NaNO_2$ and $(NH_4)_2SO_4$ to achieve ~20 mg-N/L each of NO_2^- and NH_4^+.

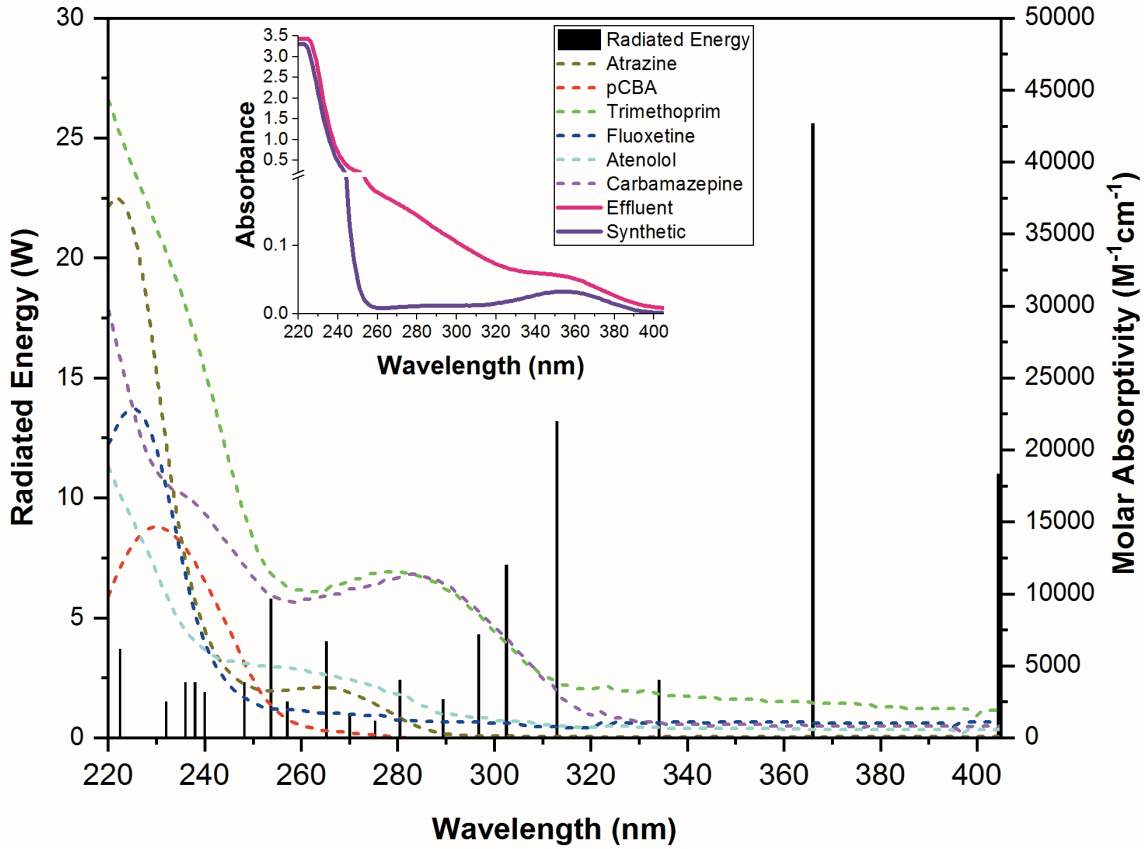

Figure A-1. Molar absorptivity of pharmaceuticals, probe, and actinometer on a per wavelength basis (right y-axis); radiated energy in watts of mercury vapor lamp per lamp centerlines (left y-axis); absorption spectra of matrices (inset).

A.1 Analytical Methods

Table A-3. RP-HPLC Methods for Pharmaceuticals, Probe, and Actinometer

Compound	Column[a]	Mobile Phase (v:v)	Injection V (µL)	Flow Rate (mL/min)	Detector λ (nm)
para-Cholorobenzoic acid	Eclipse XDB-C18 (4.6x150 mm, 3.5 µm)	45% Acetonitrile 55% Phosphate Buffer (10mM; pH3; 10% ACN)	40	1.0	238
Atenolol	Eclipse XDB-C18 (4.6x150 mm, 5.0 µm)	5% Acetonitrile 95% 0.1% (v/v) phosphoric acid	90	1.0	224
Carbamazepine	Eclipse XDB-C18 (4.6x150 mm, 3.5 µm)	65% Acetonitrile 35% Phosphate Buffer (10mM; pH3; 10% ACN)	50	1.0	290
Trimethoprim	Eclipse XDB-C18 (4.6x150 mm, 3.5 µm)	90% Acetonitrile 10% Phosphate Buffer (10mM; pH3; 10% ACN)	100	1.0	274
Fluoxetine	Eclipse XDB-C18 (4.6x150 mm, 3.5 µm)	65% Acetonitrile 35% Phosphate Buffer (10mM; pH3; 10% ACN)	40	1.0	230
Atrazine	Supelco Discovery RP-Amide C16 (15 cmx4.6 mm, 5 µm)	50% Acetonitrile 50% 0.1% (v/v) phosphoric acid	35	1.0	220

[a]Columns were at room temperature (~20 °C) except for atenolol (maintained at 30 °C)

A.1.2 Total N-Nitrosamine (TONO) Analysis

TONO analysis followed the method of Kulshrestha et al.[150] All samples were diluted to 200 mL (4-fold dilution) and quenched with 2 g/L of sulfamic acid overnight (to prevent nitrite interference) prior to solid phase extraction (SPE). Tandem SPE (activated carbon and Oasis HLB) was performed and the extracts combined and concentrated on a rotary evaporator and via N_2 blow down to concentrate the final samples to 1 mL in methanol. The limit of quantification (LOQ) for the original samples was 10 ng/L as nitrosodimethylamine (NDMA). A lab blank control and positive control were also performed for quality assurance. The final concentration is an average of two measurements and the standard deviations were calculated.

Table A-4. Pseudo-first-order reaction rate constants for direct photolysis controls (k_{dir}) and experiments with synthetic matrix (k_{sw}) and amended effluent (k_{eff}) for $\lambda \geq$ 280 nm [a]

Compound	k_{dir} (min^{-1})	k_{sw} (min^{-1})	k_{eff} (min^{-1})
Carbamazepine	$5.31\pm0.39\times10^{-4}$	$5.28\pm0.26\times10^{-3}$	$5.34\pm0.50\times10^{-3}$
Trimethoprim	$8.38\pm2.34\times10^{-4}$	$5.62\pm0.13\times10^{-3}$	$5.17\pm0.26\times10^{-3}$
Fluoxetine	$1.43\pm0.10\times10^{-3}$	$5.84\pm0.47\times10^{-3}$	$7.07\pm0.29\times10^{-3}$
Atenolol	$6.84\pm0.66\times10^{-4}$	$5.23\pm0.68\times10^{-3}$	$7.50\pm0.31\times10^{-3}$
pCBA	$2.01\pm0.18\times10^{-4}$	$2.75\pm0.08\times10^{-3}$	$2.81\pm0.09\times10^{-3}$

[a]Errors are 95% confidence intervals.

Table A-5. Pseudo-first-order reaction rate constants for direct photolysis controls (k_{dir}) and experiments with synthetic matrix (k_{sw}) and amended effluent (k_{eff}) $\lambda \geq 220$ nm [a]

Compound	k_{dir} (min^{-1})	k_{sw} (min^{-1})	k_{eff} (min^{-1})
Carbamazepine	$1.08\pm0.02\times10^{-2}$	$1.40\pm0.04\times10^{-2}$	$1.37\pm0.01\times10^{-2}$
Trimethoprim	$3.78\pm0.22\times10^{-2}$	$1.23\pm0.08\times10^{-2}$	$1.20\pm0.10\times10^{-2}$
Fluoxetine	N/A	N/A	N/A
Atenolol	$1.39\pm0.21\times10^{-2}$	$1.10\pm0.23\times10^{-2}$	$1.93\pm0.03\times10^{-2}$
pCBA	$4.72\pm0.14\times10^{-2}$	$1.64\pm0.05\times10^{-2}$	$1.48\pm0.03\times10^{-2}$

[a]Errors are 95% confidence intervals.

A.3 Screening Factors:

Screening factors (S_{i_j}) were calculated following McCabe and Arnold and Karpuzcu, et al.[84,100] as the ratio of light absorption rates (R_a) in pharmaceutical or probe (species *i*) solutions with and without screening species (*j*) present (i.e., comparing the rate of light absorption of compound in buffer versus effluent) over a range of wavelengths λ. The screening factors help to attribute differences in observed photolysis rates to: 1)

physical screening due to absorption of light otherwise available for direct photolysis by the matrix; or, 2) other reduction or enhancement reactions.

$$R_{a,i} = \sum_{\lambda} \frac{W_{\lambda}(1-10^{-a_{i\lambda}z})}{z} \quad (22)$$

$$R_{a,i\_j} = \sum_{\lambda} \frac{W_{\lambda}(1-10^{-(a_{i_\lambda}+a_{j_\lambda})z})}{z} \frac{a_{i_\lambda}}{a_{i_\lambda}+a_{j_\lambda}} \quad (23)$$

$$S_{i\_j} = \frac{R_{a,i\_j}}{R_{a,i}} \quad (24)$$

Where W_{λ} $(mEi\ cm^{-2}s^{-1})$ is the spectral photon fluence rate derived from actinometry, $z = 1.12\ cm$ [178] is the effective light path length in the 13×100 mm quartz test tubes accounting for reflection and refraction, $a_{\lambda}(cm^{-1})$ is the light attenuation coefficient (measured absorbance in a quartz cuvette with path length 1 cm)). Values for S_{i_j} are between 0 and 1, with 0 indicating no light is absorbed by species *i* (i.e., all light absorbed by screening species *j*), and 1 indicating no light is screened by species *j*. Tabulated screening factors are presented below in Table A-6.

Pseudo-first-order rate constants for direct photolysis in buffer in the λ≥220 nm experiments were corrected by multiplying by the respective S_{i_j} as illustrated in equation 25.

$$k'_{direct,corrected} = k'_{direct} \times S_{i\_j} \quad (25)$$

Table A-6. Light Screening Correction Factors

Compound	$S_{i,j,nit}$	$S_{i,j,eff}$
Carbamazepine	0.735	0.625
Trimethoprim	0.665	0.563
Fluoxetine	0.480	0.405
Atenolol	0.628	0.525
pCBA	0.464	0.376

A.4 Additional Figures:

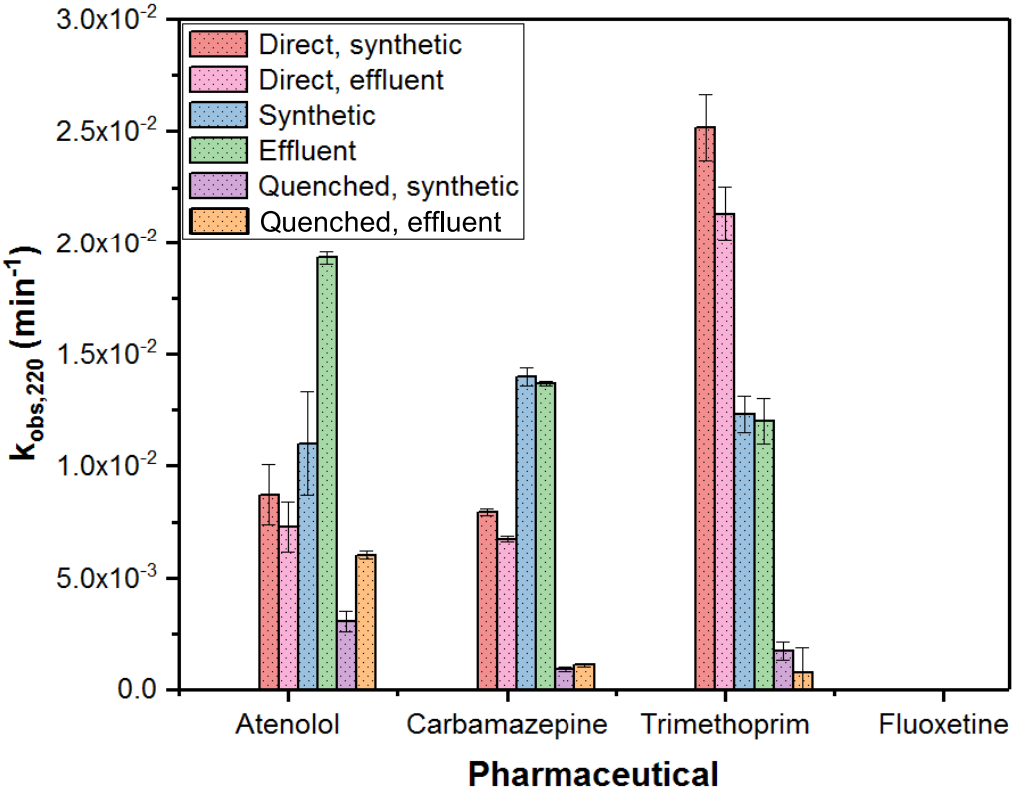

Figure A-2. Pseudo-first order rate constants with the 220-nm cutoff.

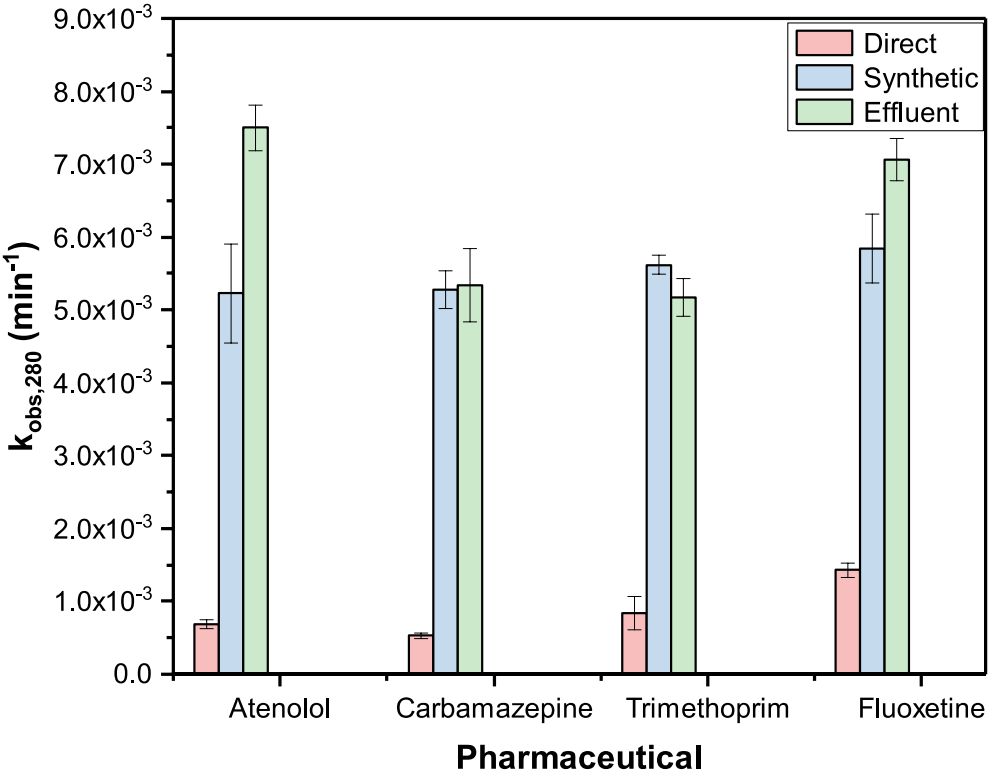

Figure A-3. Pseudo-first order rate constants with the 280-nm cutoff.

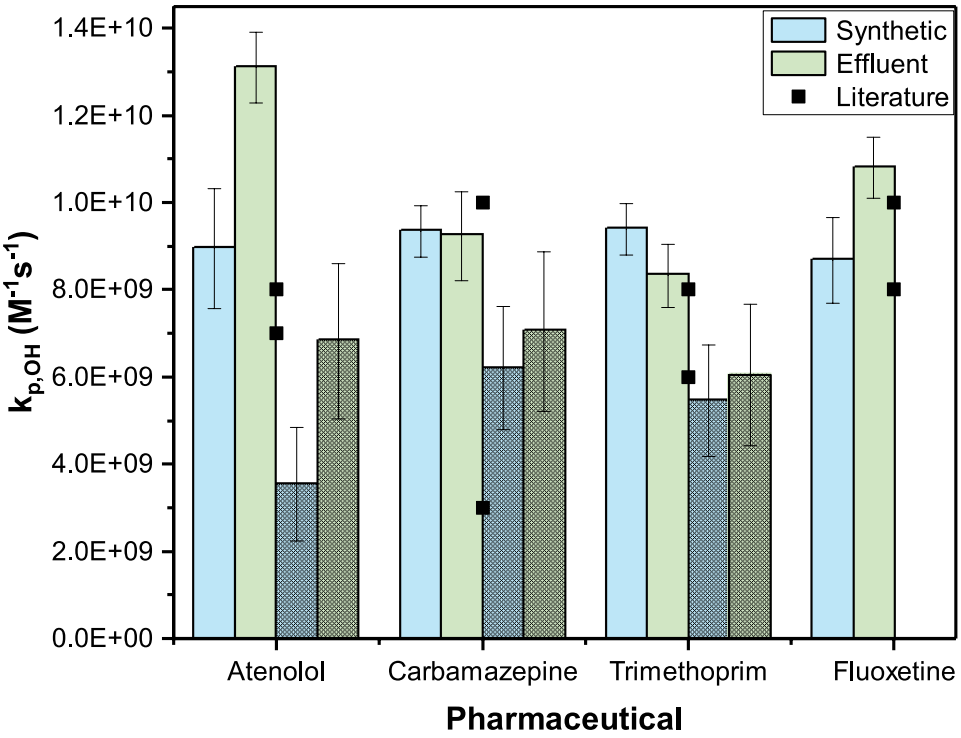

Figure A-4. Second-order reaction rate constants with hydroxyl radical.

Appendix B. Supplementary Information for Chapter 3

B.1 Experimental Section

B.1.1 Materials and Methods

B.1.1.1 Absorption spectra

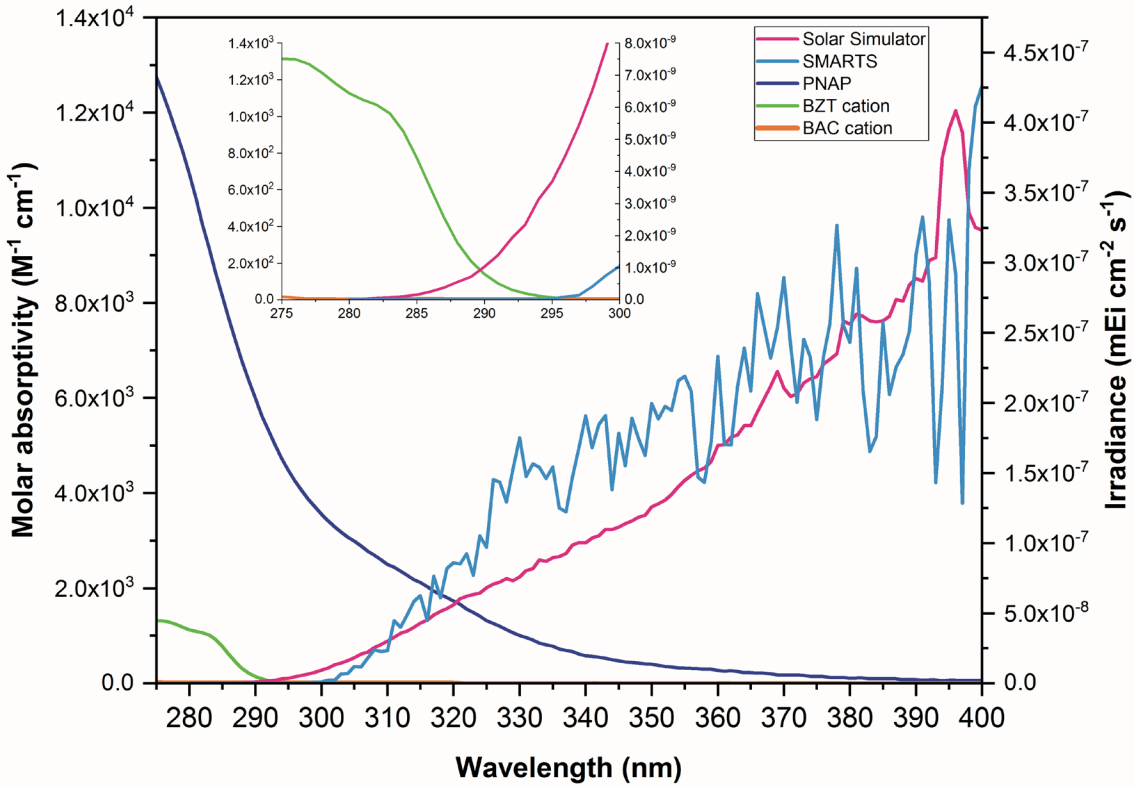

Figure B-1. Solar simulator and sunlight spectral irradiances and molar absorption coefficients.

B.1.1.2 Chemicals and reagents.

Table B-1. QAC Structures

Benzethonium Chloride (BZT)	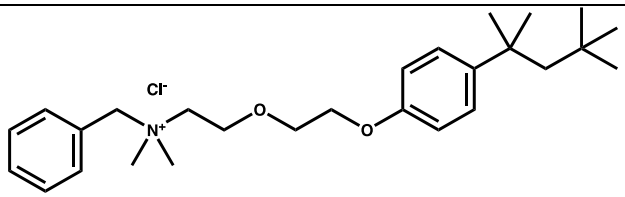
C_{12}-Benzalkonium Chloride (BAC)	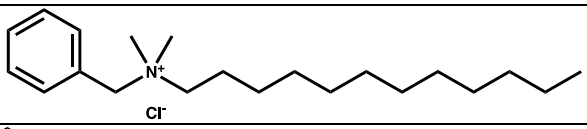
C_{14}-BAC	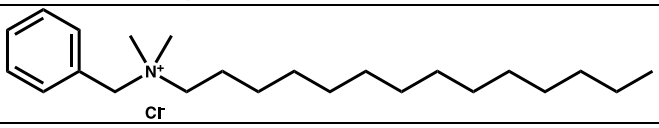
C_{12}-Alkyltrimethylammonium (ATMA) Bromide	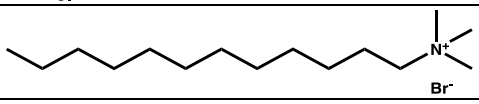
C_{12}-Dialkyldimethylammonium (DADMA) Bromide	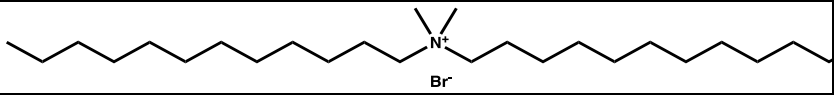

B.1.1.3 River water sample collection and analysis

Table B-2. Water quality parameters of the Mississippi river water used in photochemical study

Water Quality Parameter	Method	6/5/18	2/27/19
Nitrite (NO_2^- mg of N/L)	Metrohm ion chromatograph	<0.1	<0.1
Nitrate (NO_3^- mg of N/L)	Metrohm ion chromatograph	0.7	0.8 ± 0.1
Dissolved organic carbon (NPOC mg-C/L)	Shimadzu TOC-L analyzer	9.8	9.2
Dissolved inorganic carbon (DIC mg-C/L)	Shimadzu TOC-L analyzer	32	39
pH	Thermo Orion pH meter	8.5 ± 0.1	8.2

B.1.1.4 Analytical methods

Concentrations of BACs and BZT were measured by high-pressure liquid chromatography (HPLC) on an Agilent 1100 LC with a variable wavelength detector set at 210 nm with 50 µL injection volume. An Eclipse XDB column (4.6 × 150 mm, 3.5 or 5

μm, Agilent) was used with isocratic mixtures of methanol and 10 mM ammonium acetate with 0.1% glacial acetic acid or formic acid and 10% methanol at a flow rate of 1 mL min^{-1}.

Table B-3. RP-HPLC Methods

Compound	Column[a]	Mobile Phase (v:v)[b]	Injection V (μL)	Flow Rate ($mLmin^{-1}$)	Detector λ (nm)
C_{12}-BAC	Eclipse XDB-C18 (4.6×150 mm, 3.5 μm)	90% 9:1 methanol:10mM ammonium acetate with 0.1% acid 10% 9:1 10mM ammonium acetate with 0.1% acid:methanol	50	1.0	210
C_{14}-BAC	Eclipse XDB-C18 (4.6×150 mm, 3.5 μm)	95% 9:1 methanol:10mM ammonium acetate with 0.1% acid 5% 9:1 10mM ammonium acetate with 0.1% acid:methanol	50	1.0	210
BZT	Eclipse XDB-C18 (4.6×150 mm, 3.5 μm)	90% 9:1 methanol:10mM ammonium acetate with 0.1% acid 10% 9:1 10mM ammonium acetate with 0.1% acid:methanol	50	1.0	210
pCBA	Eclipse XDB-C18 (4.6×150 mm, 3.5 μm)	45% acetonitrile 55% 10mM pH3 phosphate buffer with 10% acetonitrile	40	1.0	238
PNAP	Eclipse XDB-C18 (4.6×150 mm, 3.5 μm)	65% acetonitrile 35% 10 mM pH 3 phosphate buffer with 10% acetonitrile	35	1.0	220
FFA	Eclipse XDB-C18 (4.6×150 mm, 3.5 μm)	10% acetonitrile 90% 10mM pH3 phosphate buffer with 10% acetonitrile	35	1.0	219

[a]Columns were at room temperature (~20 °C)
[b]All mobile phases were isocratic

B.1.2 Photochemical experiments: simulated and outdoor photolysis in river water

Table B-4. Rooftop experiment dates and times

Date	Time out	Time in	Cumulative Hours
6/28/18	12:04 PM	5:00 PM	4.9
6/29/18	10:09 AM	3:40 PM	10.5
7/2/18	10:00 AM	3:50 PM	16.3
7/5/18	12:00 PM	5:00 PM	21.3
7/6/18	11:30 AM	5:00 PM	26.8

Table B-5. SMARTS inputs

Parameter	Value	Units
Site pressure	Calculated from latitude and altitude	
Latitude	44.975	decimal degrees (DD)
Altitude	0.262128	km
Height	0	
Default atmosphere	Mid-latitude summer	
Water vapor	Calculated from reference atmosphere and altitude	
Ozone abundance[a]	0.3125	atm-cm
Ozone column altitude correction	Vertical profile correction	
Gaseous absorption	Light pollution	
Carbon dioxide[b]	Mauna Loa daily or weekly averages	ppm
Extraterrestrial spectrum	1366.1	Wm^{-2}
Aerosol model	Shettle and Fenn rural	
Aerosol optical depth at 500 nm	0.1	
Albedo	Light soil	
Tilt	30	degrees
Surface azimuth	218	degrees SW
Solar constant	1361	Wm^{-2}
Longitude	-93.233611	DD

[a]Average value from Apell and McNeill (2019)[207] for June and September at 40° N and 50° N (converted from Dobson units)
[b]https://www.esrl.noaa.gov/gmd/ccgg/trends/graph.html

B.2 Results and Discussion

B.2.1 Reactivity of QACs with hydroxyl radical from hydrogen peroxide sensitizer experiments

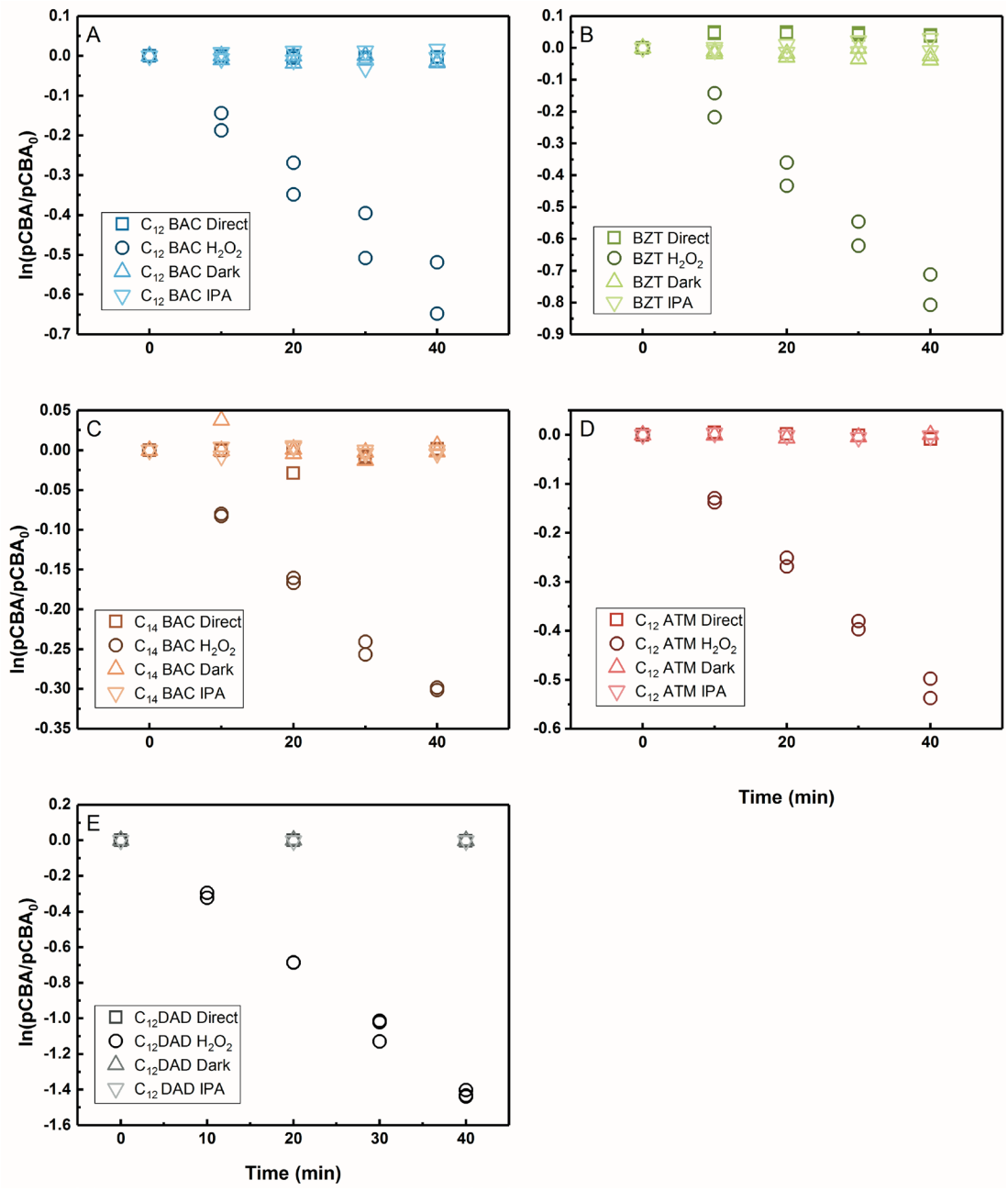

Figure B-2. Log plot of pCBA concentration over time in H_2O_2 sensitizer experiments for: A) C_{12}-BAC, B) BZT, C) C_{14}-BAC, D) C_{12}-ATMA, E) C_{12}-DADMA. Squares are direct photolysis controls, circles are hydrogen peroxide, triangles are dark controls, and upside down triangles are IPA quenched controls.

Table B-6. Steady-state hydroxyl radical concentrations in experiments with hydrogen peroxide.[a]

QAC	$[^{\bullet}OH]_{ss}$ (M)
C_{12}-DADMA	$(1.17 \pm 0.03) \times 10^{-13}$
C_{12}-BAC	$(5.0 \pm 0.5) \times 10^{-14}$
C_{14}-BAC	$(2.6 \pm 0.2) \times 10^{-14}$
BZT	$(6.4 \pm 0.2) \times 10^{-14}$
C_{12}-ATMA	$(4.3 \pm 0.1) \times 10^{-14}$
[a]Errors represent 95% confidence intervals	

B.2.2 Assessing reactivity with other PPRIs

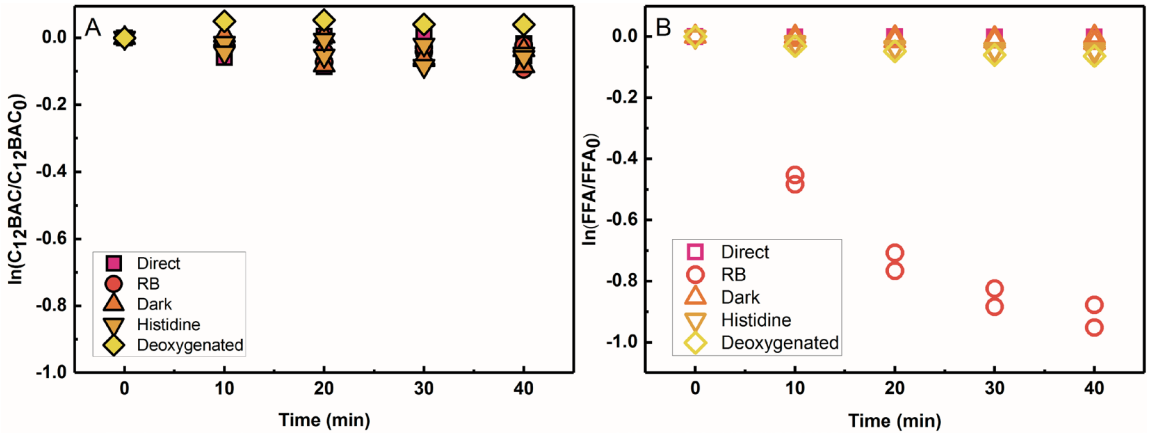

Figure B-3. Log-concentration over time of: C_{12}-BAC (A) and FFA (B) under simulated sunlight in phosphate buffer (Direct, pink squares), with rose bengal (RB, red circles), dark control (orange triangle), histidine quenched control (light orange upside down triangle), deoxygenated control (yellow diamond).

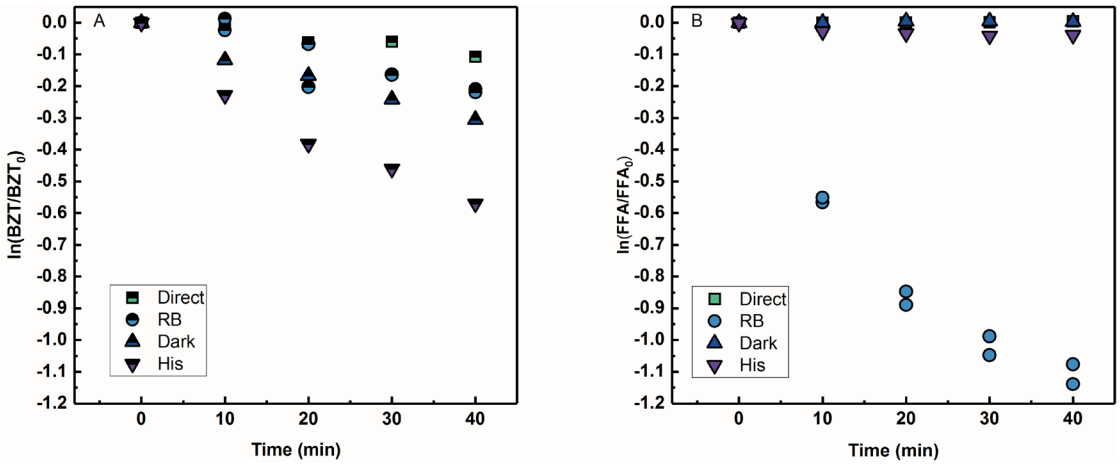

Figure B-4. Log-concentrations over time of: BZT (A) and furfuryl alcohol (B) under simulated sunlight in phosphate buffer (Direct, green squares), with rose bengal (RB, light blue circles), dark control (Dark, dark blue triangle), histidine quenched control (His, purple upside down triangle).

Additional experiments in which 10 μM BZT was spiked into 6 mL buffer and then BZT and 2 μM of RB were spiked into 6 mL buffer and 6 mL river water and wrapped in foil and kept on the bench top under ambient conditions. These tests showed 2% decrease in BZT concentration over 5 days alone in buffer, 20% decrease in buffer with rose bengal, and 18% decrease in river water with rose bengal.

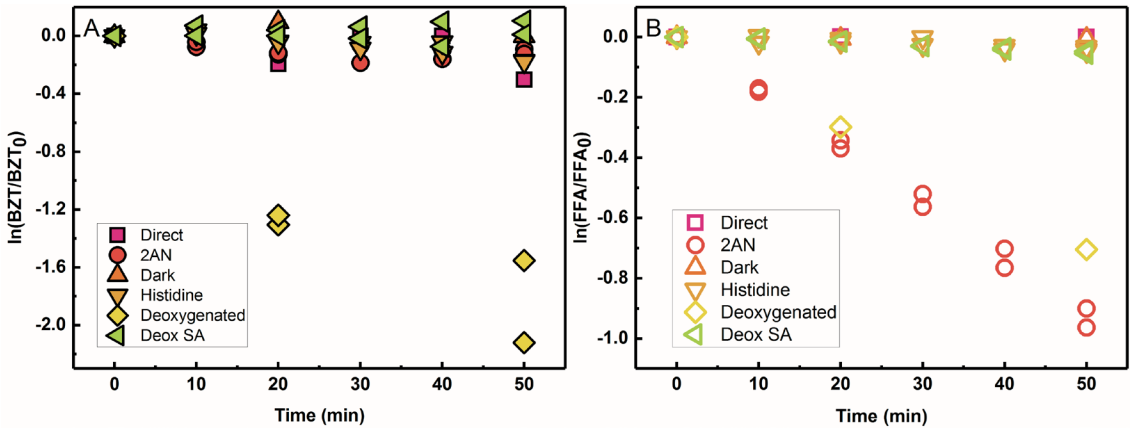

Figure B-5. Log-concentration over time of: BZT (A) and FFA (B) under simulated sunlight in phosphate buffer (Direct, pink squares), with 2-acetylnaphthalene (2AN, red circles), dark control (orange triangle), histidine quenched control (light orange upside down triangle), deoxygenated control (yellow diamond), and sorbic acid quenched deoxygenated control (green left triangle).

Table B-7. Pseudo-first-order rate constants, k_{obs} (s^{-1}), for FFA irradiated under simulated sunlight in singlet oxygen sensitizer experiments and singlet oxygen steady-state concentrations, $[^1O_2]_{ss}$ (M)[a]

	FFA with BZT		FFA with C_{12}-BAC	
Sample	**k_{obs}**	**$[^1O_2]_{ss}$**	**k_{obs}**	**$[^1O_2]_{ss}$**
Direct	N/A	N/A	$(1.2 \pm 0.5) \times 10^{-6}$	$(10 \pm 4) \times 10^{-15}$
2-acetylnaphthalene	$(3.06 \pm 0.08) \times 10^{-4}$	$(2.62 \pm 0.05) \times 10^{-12}$	N/A	N/A
Rose Bengal	N/A	N/A	$(4.5 \pm 0.8) \times 10^{-4}$	$(3.9 \pm 1.2) \times 10^{-12}$
Dark	$(0.2 \pm 0.3) \times 10^{-6}$	$(2 \pm 2) \times 10^{-14}$	$(5 \pm 3) \times 10^{-6}$	$(4 \pm 3) \times 10^{-14}$
Histidine	$(1.2 \pm 0.3) \times 10^{-5}$	$(1.1 \pm 0.3) \times 10^{-13}$	$(2.3 \pm 0.3) \times 10^{-5}$	$(2.0 \pm 0.3) \times 10^{-13}$
Deoxygenated	$(2.4 \pm 0.1) \times 10^{-4}$	$(2.03 \pm 0.05) \times 10^{-12}$	$(3.1 \pm 0.8) \times 10^{-5}$	$(2.7 \pm 0.7) \times 10^{-13}$
Deoxygenated with sorbic acid	$(1.6 \pm 0.1) \times 10^{-5}$	$(1.4 \pm 0.1) \times 10^{-13}$	N/A	N/A

[a]Error bars represent 95% confidence intervals

B.2.2 Photochemical transformation of BACs & BZT in river water under simulated and natural sunlight

Table B-8. Pseudo-first-order rate constants, k_{obs} (h^{-1}) [a], for QACs irradiated under simulated sunlight

	BZT	C_{12}-BAC	C_{14}-BAC
MRW	$(9.7 \pm 0.3) \times 10^{-2}$	$(2.9 \pm 0.4) \times 10^{-2}$	$(2.8 \pm 0.6) \times 10^{-2}$
MRW_{corr}	$(2.0 \pm 0.3) \times 10^{-2}$	-	-
Direct	$(7.2 \pm 0.7) \times 10^{-2}$	$(2 \pm 1) \times 10^{-3}$	$(-6 \pm 3) \times 10^{-3}$
IPA	$(7.7 \pm 0.4) \times 10^{-2}$	$(1.7 \pm 0.3) \times 10^{-3}$	$(5 \pm 3) \times 10^{-3}$
Dark	$(6 \pm 2) \times 10^{-2}$	$(-2 \pm 3) \times 10^{-3}$	$(3 \pm 3) \times 10^{-3}$

[a]Error bars represent 95% confidence intervals

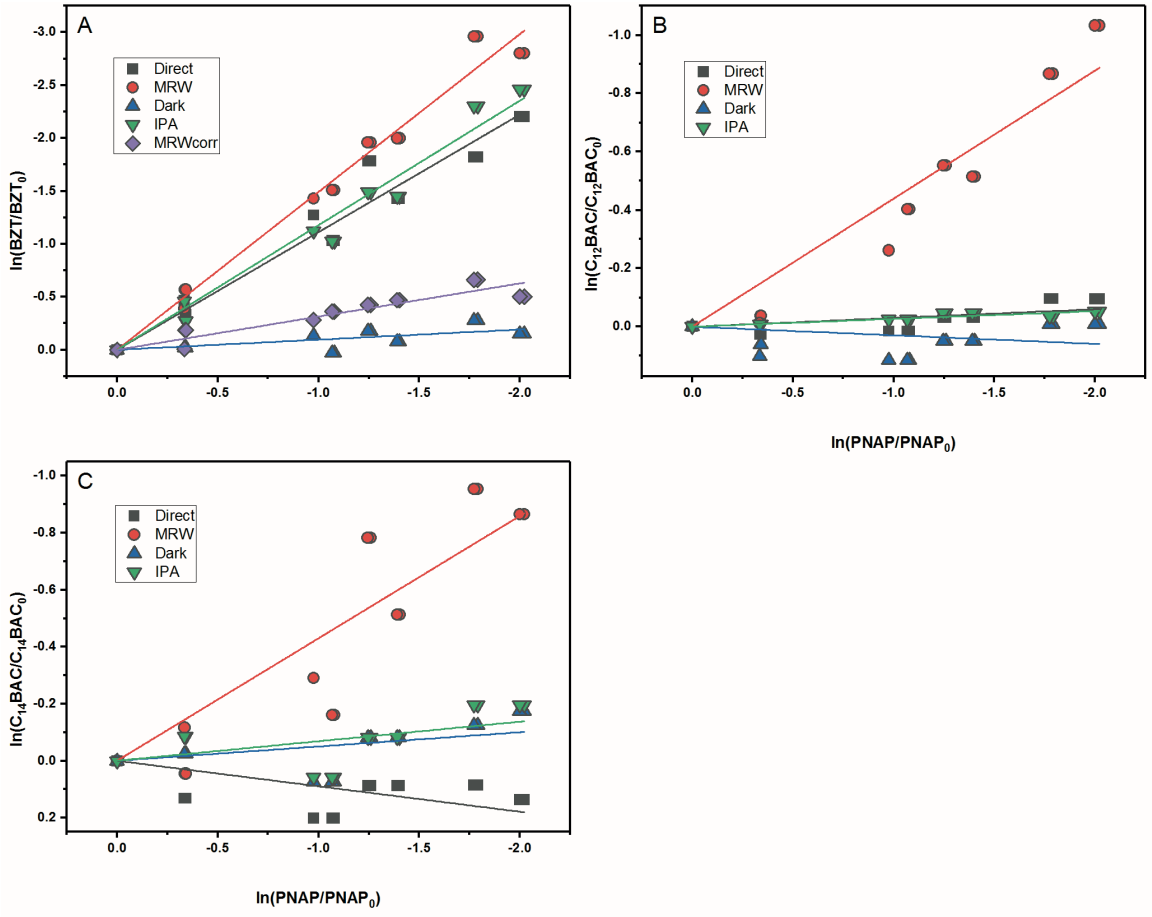

Figure B-6. Logarithmic plots of BZT (A), C_{12}-BAC (B), and C_{14}-BAC (C) solar simulator photolysis versus actinometer loss in phosphate buffer (Direct, black squares), Mississippi River water (MRW, red circles), MRW dark controls (Dark, blue diamonds), and MRW with 1% isopropanol (IPA, green upside down triangles). Purple diamonds are MRW time points corrected for direct photolysis to show BZT indirect photochemical loss in MRW (MRW_{corr}). Solid lines represent linear regressions.

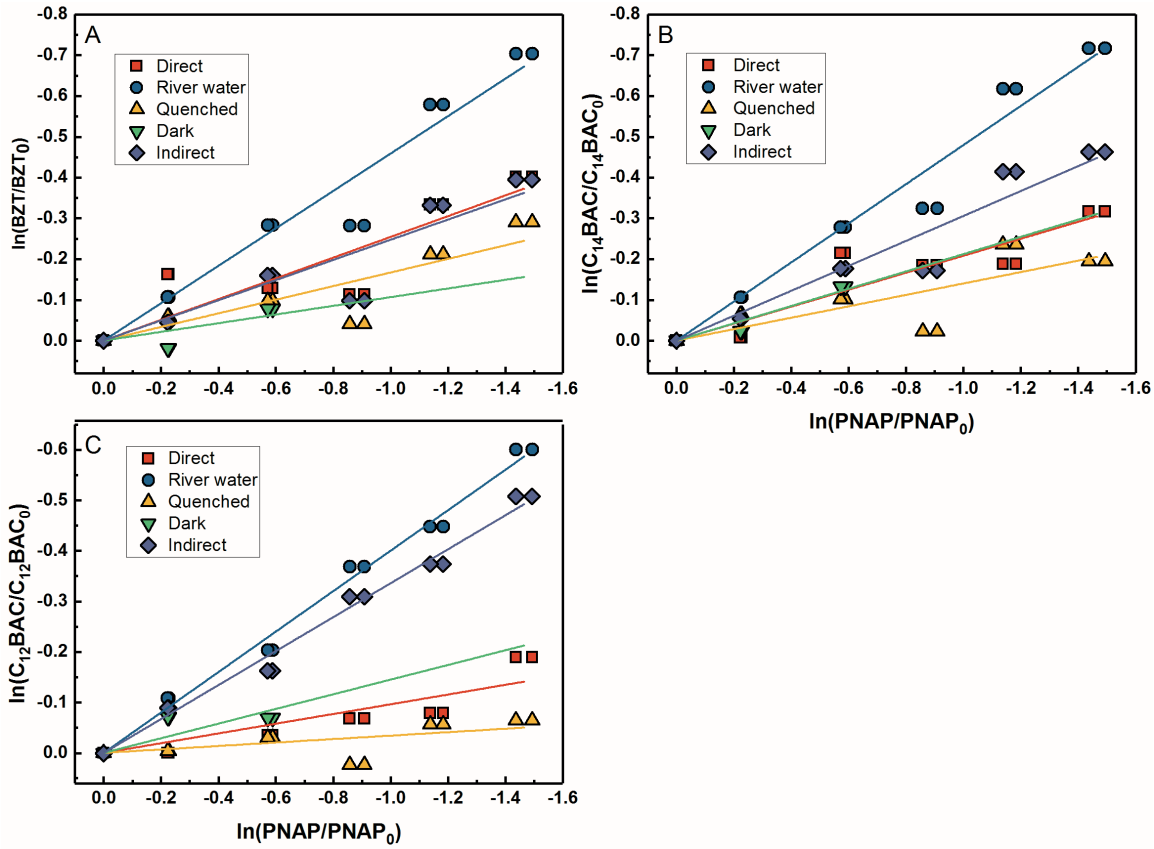

Figure B-7. Logarithmic plots of BZT (A), C_{14}-BAC (B), and C_{12}-BAC (C) natural sunlight photodegradation versus actinometer loss in phosphate buffer (Direct, red squares), Mississippi River water (River water, blue circles), river water with 1% isopropanol (Quenched, yellow triangles), river water dark controls (Dark, green upside down triangles), total photochemical loss in river water minus other abiotic losses (Indirect, purple diamonds). Solid lines represent linear regressions.

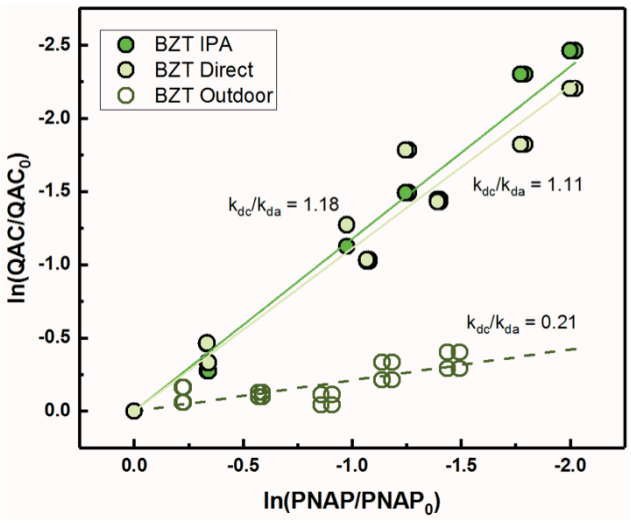

Figure B-8. Log-log plot of BZT versus PNAP for solar simulator (solid symbols) and natural sunlight (open symbols) quantum yield determinations in river water. Solid and dashed lines represent linear regressions for solar simulator and natural sunlight experiments, respectively.

B.3 Additional tables and figures

B.3.1 Photochemical transformation of BACs & BZT in river water under simulated and natural sunlight

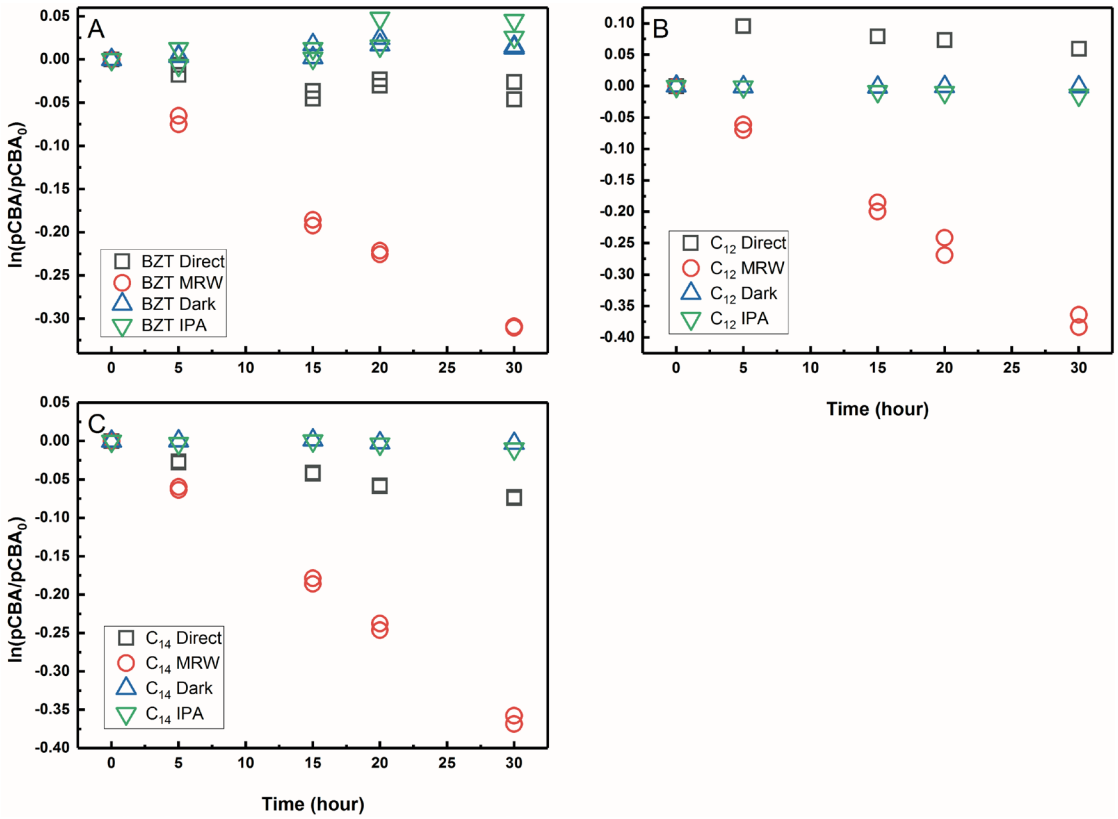

Figure B-9. Logarithmic plot of pCBA loss over time in river water solar simulator experiments for: A) BZT, B) C_{12}-BAC, and C) C_{14}-BAC. Black squares are direct photolysis controls, red circles are river water samples, blue triangles are dark controls, and green triangles are IPA quenched controls.

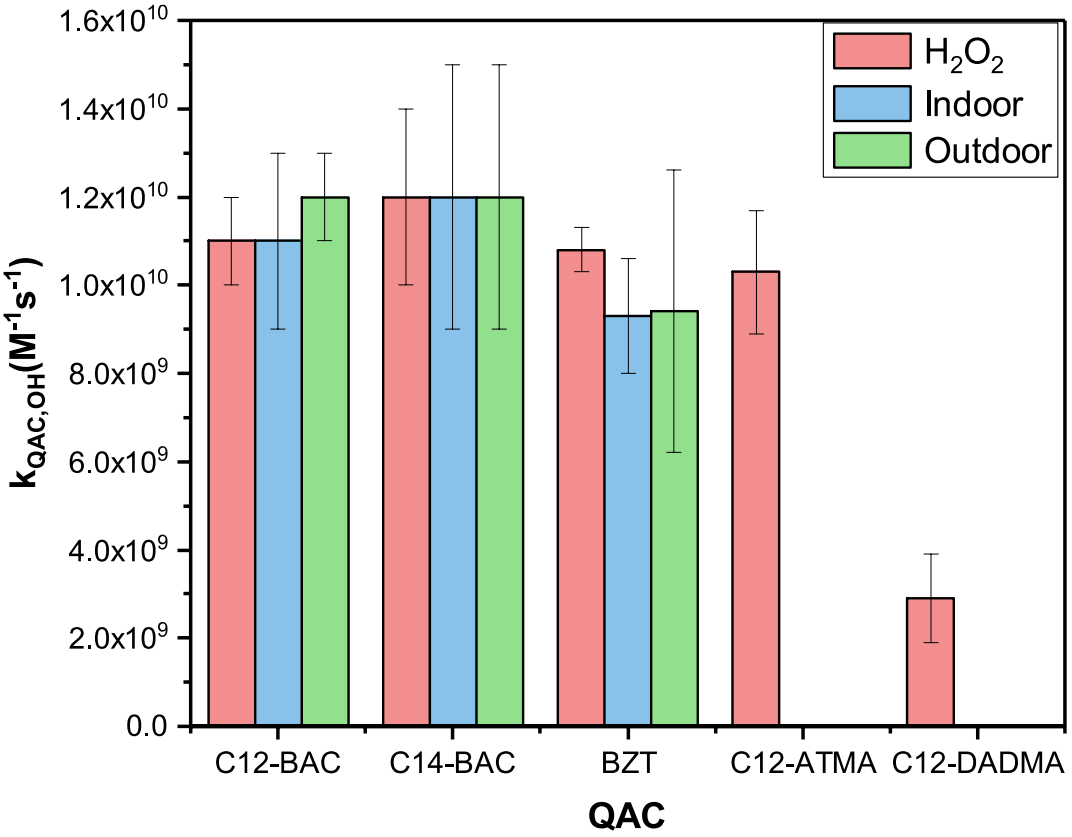

Figure B-10. Bar chart of bimolecular reaction rate constants for QACs and hydroxyl radical.

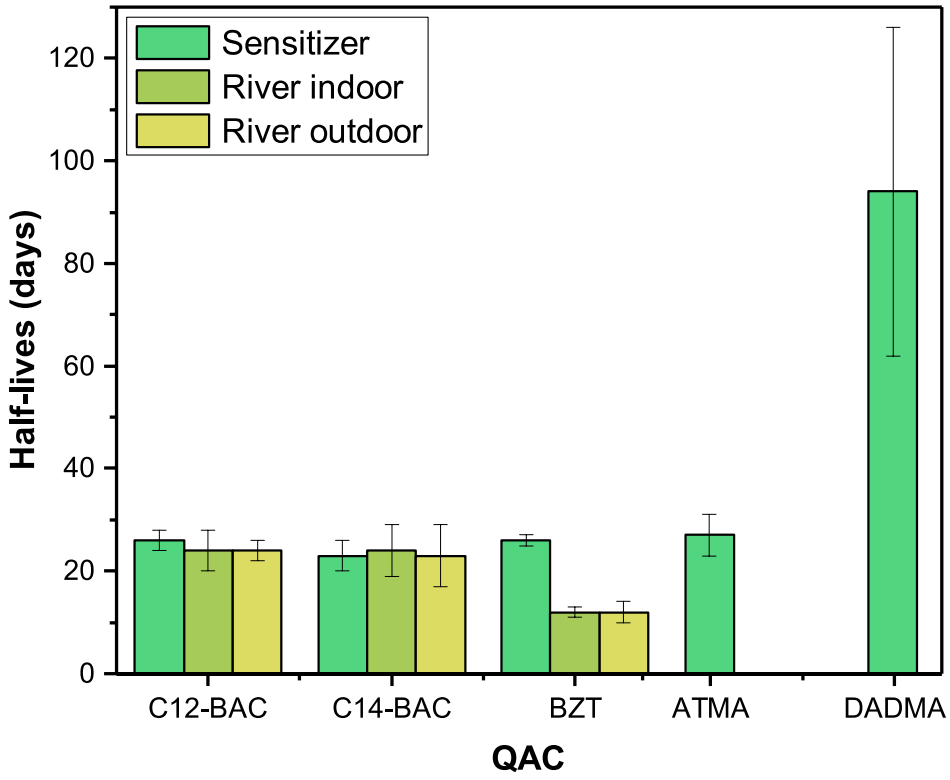

Figure B-11. Bar chart of QAC half-lives.

B.3.2 Half-life estimate

$$k_c = 2.303\Phi_c \sum_{\lambda}(\varepsilon_{\lambda,c} I_{\lambda}) \quad (26)$$

$$t_{1/2} = \frac{ln(2)}{k_c} \quad (27)$$

Appendix C. Supplementary Information for Chapter 4

C.1 Water Quality

Mississippi River water had an initial dissolved organic carbon of 9.85 ± 0.08 mg-C/L and pH of 8.10 ± 0.02 (error bars represent one standard deviation of the average of duplicate measurements).

C.2 Taxonomy

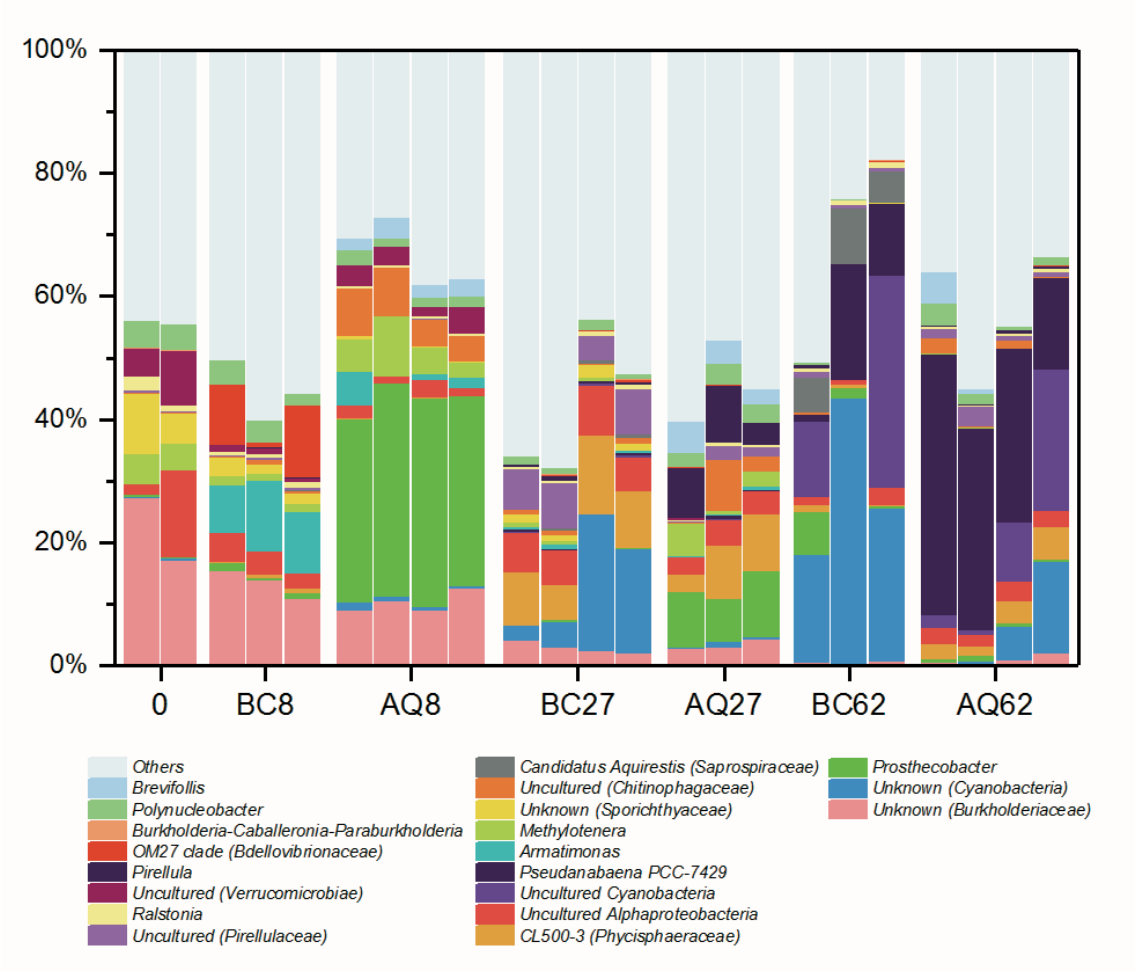

Figure C-1. Taxonomic bar chart showing the genus level shifts with (AQ) and without (BC) QAC amendment over 62 days.

The predominant genera in the river water and in amended (AQ) and bottle control (BC) microcosms are shown in the figure above. The dominant population (17 –

27%) in the river water was an unknown *Burkholderiaceae*-like ASV. After 8 days, the amended microcosms saw an increase in *Prosthecobacter* (30 – 35%). *Prosthecobacter* have been reported to thrive in low-nutrient environments, cannot utilize methanol as a carbon source, and ammonium can be used as the sole nitrogen source if appropriate vitamins and an organic carbon source are provided.[208,209] Over time, cyanobacteria were enriched in the microcosms. At day 27, *Prosthecobacter* appeared to outcompete unknown Cyanobacteria. Later *Pseudanabaena* PCC-7429, another cyanobacteria that are obligate photoautotrophs and lack N_2-fixing ability, became dominant.

C.3 Beta diversity

Table C-1. Spearman's rank correlation coefficient (rho) of Mantel tests between beta diversity distance matrices and the dissimilarity matrix of experimental parameters

Beta Diversity	Reactor type (AQ, BC)	*P*-value[1]
Bray-Curtis	0.4212	**0.002**
Weighted UniFrac	0.4212	**0.001**

[1]Levels of statistical significance based on 999 free permutations.

Table C-2. Spearman's rank correlation coefficient (rho) of Mantel tests between beta diversity distance matrices for BC and the dissimilarity matrix of experimental parameters

Beta Diversity	"Temperature"	*P*-value[1]	"Sample operating day"	*P*-value[1]
Bray-Curtis	0.539	**0.005**	0.9271	**0.002**
Weighted UniFrac	0.4926	**0.018**	0.9344	**0.001**

[1]Levels of statistical significance based on 999 free permutations.

Table C-3. Results of PERMANOVA (Adonis) to test statistical significance of amendment and date on microbial community beta diversity

	"Reactor Type" (i.e. AQ or BC)			"Sample operating day"		
Distance matrix	R^2_{adonis}	P_{adonis}[1]	$P_{betadisp}$[1]	R^2_{adonis}	P_{adonis}[1]	$P_{betadisp}$[1]
Bray-Curtis	0.18443	**0.001**	0.986	0.21639	**0.001**	0.651
Weighted UniFrac	0.18443	**0.001**	0.989	0.21639	**0.001**	0.66

[1]Levels of statistical significance based on 999 free permutations.

Table C-4. Results of PERMANOVA (Adonis) to test statistical significance of amendment concentration, temperature, and date on AQ microbial community beta diversity

	"QAC concentration"			"Temperature"			"Sample operating day"		
Distance matrix	R^2_{adonis}	P_{adonis}[1]	$P_{betadisp}$[1]	R^2_{adonis}	P_{adonis}[1]	$P_{betadisp}$[1]	R^2_{adonis}	P_{adonis}[1]	$P_{betadisp}$[1]
Bray-Curtis	0.37994	**0.001**	**0.009**	0.23228	**0.035**	**0.01**	0.21639	**0.001**	**0.017**
Weighted UniFrac	0.62345	**0.002**	0.077	0.18145	0.183	0.083	0.64753	**0.001**	0.087

[1]Levels of statistical significance based on 999 free permutations.

Table C-5. Post hoc pairwise comparisons (Adonis) to test statistical significance of "Reactor Type" (i.e. AQ vs. BC) on microbial community beta diversity

Distance matrix	R^2_{adonis}	P_{adonis}[1]	$P_{adjusted}$[1]
Bray-Curtis	0.2305451	0.001	**0.001**
Weighted UniFrac	0.2305451	0.001	**0.001**

[1]Levels of statistical significance based on 999 free permutations.

Table C-6. Post hoc pairwise comparisons (Adonis) to test statistical significance of "Sample operating day" on microbial community beta diversity for AQ and BC

Post hoc comparisons	*Bray-Curtis*			Weighted UniFrac		
Pairwise comparisons	R^2_{adonis}	P_{adonis}[1]	$P_{adjusted}$[1]	R^2_{adonis}	P_{adonis}[1]	$P_{adjusted}$[1]
63 vs. 8	0.4648773	0.002	**0.012**	0.4648773	0.007	**0.042**
63 vs. 27	0.2909020	0.015	0.090	0.2909020	0.019	0.114
63 vs. 62	0.5311901	0.037	0.222	0.5311901	0.029	0.174
8 vs. 27	0.2761345	0.011	0.066	0.2761345	0.012	0.072
8 vs. 62	0.5793083	0.005	**0.030**	0.5793083	0.009	0.054
27 vs. 62	0.4137114	0.005	**0.030**	0.4137114	0.007	**0.042**

[1]Levels of statistical significance based on 999 free permutations.

C.4 Differentially Enriched Taxa

Comparing the amended and bottle control microcosms overall, several phyla saw an increase in abundance (Figure C-2). In particular, Proteobacteria of the genus *Methylophilus*, Verrucomicrobia of the genus *Prosthecobacter*, Cyanobacteria of the genus *Pseudanabaena* PCC-7429, Planctomycetes of the genus *SM1A02*, as well as uncharacterized Proteobacteria and Verrucomicrobia.

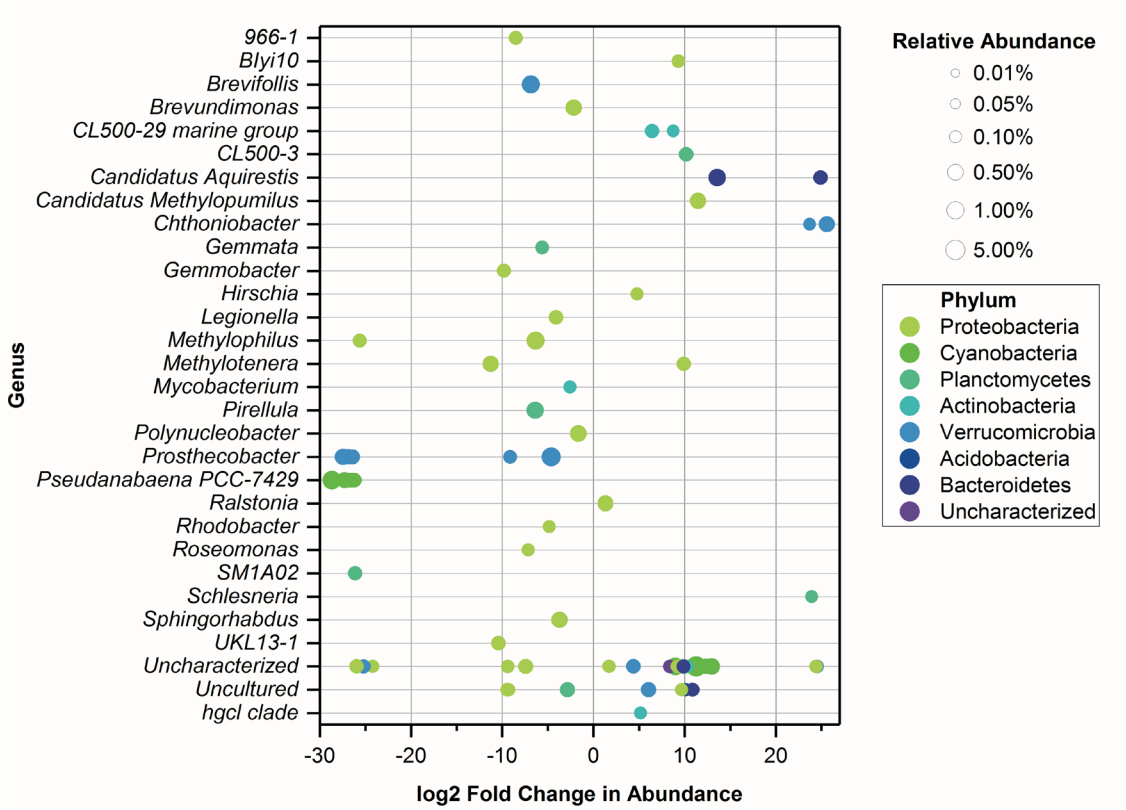

Figure C-2. Differentially enriched taxa comparing between bottle control and amended microcosms over the entirety of the experiment